Numerical Study on the Regularity of the Navier-Stokes Equations

Mark Dowker

School of Mathematics and Statistics
University of Sheffield

Thesis submitted for the Degree of Doctor of Philosophy at the
University of Sheffield
· July 2012 ·

Abstract

This thesis is mainly focused on the regularity problem for the three-dimensional Navier-Stokes equations.

The three-dimensional freely decaying Navier-Stokes and Burgers equations are compared via direct numerical simulations, starting from identical *incompressible* initial conditions, with the same kinematic viscosity. From previous work by Kiselev and Ladyzenskaya (1957), the Burgers equations are known to be globally regular thanks to a maximum principle.

In this comparison, the Burgers equations are split via Helmholtz decomposition with consequence that the potential part dominates over the solenoidal part. The nonlocal term $-\boldsymbol{u}\cdot\nabla p$ invalidates the maximum principle in the Navier-Stokes equations. Its probability distribution function and joint probability distribution functions with both energy and enstrophy are essentially symmetric with random fluctuations, which are temporally correlated in all three cases.

We then evaluate nonlinearity depletion quantitatively in the enstrophy growth bound via the exponent α in the power-law $\frac{dQ}{dt} + 2\nu P \propto (Q^a P^b)^\alpha$, where Q is enstrophy, P is palinstrophy and a and b are determined by calculus inequalities.

Caffarelli-Kohn-Nirenberg theory defines a local Reynolds number over parabolic cylinder Q_r as $\delta(r) = 1/(\nu r)\int_{Q_r} |\nabla \boldsymbol{u}|^2\, d\boldsymbol{x}\, dt$. From this we determine a cross-over scale $r_* \propto L\left(\frac{\overline{\|\nabla \boldsymbol{u}\|_{L^2}^2}}{\|\nabla \boldsymbol{u}\|_{L^\infty}^2}\right)^{1/3}$, corresponding to the change in scaling behavior of $\delta(r)$. Following the assumption that $E(k) \propto k^{-q}$ $(1 < q < 3)$, it is shown that $r_* \propto \nu^a$ where $a = \frac{4}{3(3-q)} - 1$.

Direct numerical simulations of isotropic turbulence with $R_\lambda \approx 100$ and random initial data result in the scaling $\delta(r) \propto r^4$, which extends *throughout the inertial range*. This follows from the smallness of the intermittency parameter $a \approx 0.26$. From this value, the β-model predicts a dissipation correlation exponent $\mu = \frac{4a}{1+a} \approx 0.8$ which is much larger than the experimental observations of $0.2 - 0.4$. This suggests that the β-model is valid qualitatively but not quantitatively. The scale r_* gives a practical method for estimating intermittency.

By studying the steadily propagating shock wave solutions of the one-dimensional Burgers equation with passive scalar, we determine a relationship between the dissipation rate ϵ_θ of passive scalar and Prandtl number P_r as $\epsilon_\theta \propto 1/\sqrt{P_r}$ for large P_r. The profile of the passive scalar manifests as a sum of $\tanh^{2n+1} x$ for suitably scaled x when $\nu \to 0$, implying that we must distinguish between different orders of the Heaviside function H and H^n. If we do not account for this, we obtain the incorrect relationship $\epsilon_\theta \propto 1/P_r$. The correct evaluation of this dissipation anomaly therefore requires Colombeau's theory for multiplication of distributions.

Contents

List of Figures

List of Tables

Acknowledgments

This work has been supported by an EPSRC grant EP/F009267/1.

The work in Chapter 2 was presented as a poster at 'The Analysis of Incompressible Fluids, Turbulence and Mixing', in honor of Peter Constantin's 60th birthday, October 2011, Carnegie Mellon University. We are grateful to A. Biswas, P. Constantin, C. Foias and A. Larios for useful comments.

I would like to thank my supervisor Professor Koji Ohkitani for his continual support and guidance throughout my PhD studies. I am very grateful to all the members of the applied mathematics department for their help, encouragement and friendship. I would also like to thank the other students with whom I have shared the postgraduate experience for making the past few years so enjoyable. Finally, I would like to thank my parents, in particular my father, whose help at A-level laid the foundation for my mathematical achievements.

Preface

The greater part of the contents of this Thesis is the Author's original work.

- Chapter 1 contains introductory material and a brief literature review.
- Chapter 2 is based on a piece of published work, conducted in collaboration with K. Ohkitani, which was published in Phys. Fluids in 2012 [1].
- Chapter 3 is based on a piece of work, conducted in collaboration with K. Ohkitani, which is a preprint [2].
- Chapter 4 is based on a piece of published work, conducted in collaboration with K. Ohkitani, which was published in J. Math. Phys. in 2010 [3].
- Chapter 5 is dedicated to summary and conclusions.

Chapter 1

Introduction

1.1 Equations and definitions

The Navier-Stokes equations, along with the continuity equation describe the motion of viscous incompressible fluids. They are derived via physical conservation laws and the application of Newton's laws of motion to a continuous distribution of fluid. These equations can be extended to d spatial dimensions, but the physically relevant cases are those of two and three dimensions. We mostly (unless otherwise stated) consider here the case with unit density in three dimensions:

$$\frac{\partial \boldsymbol{u}}{\partial t} + (\boldsymbol{u} \cdot \nabla)\boldsymbol{u} = -\nabla p + \nu \nabla^2 \boldsymbol{u} + \boldsymbol{F}, \tag{1.1}$$

$$\nabla \cdot \boldsymbol{u} = 0, \tag{1.2}$$

where $\boldsymbol{u} = \boldsymbol{u}(\boldsymbol{x}, t)$ denotes the fluid velocity, $p = p(\boldsymbol{x}, t)$ is the pressure, ν the kinematic viscosity and $\boldsymbol{F} = \boldsymbol{F}(\boldsymbol{x}, t)$ the external body force, with $\boldsymbol{x} = (x, y, z)$ for the case of three dimensions. Depending on the physical situation, appropriate initial and boundary conditions may also be applied. In the incompressible case, we are dealing with velocities which are small in comparison to the speed of sound in the fluid. We also assume homogenity (constant density) throughout the fluid. The terms, from left to right are widely known as; the time derivative, incompressible/advection term, nonlocal pressure gradient, viscous/diffusion term and the forcing term.

Another important quantity is the vorticity, which is physically twice the local angular velocity of a fluid element, and is defined as:

$$\boldsymbol{\omega} = \nabla \times \boldsymbol{u}, \tag{1.3}$$

which clearly also satisfies the incompressibility condition.

We define the physical quantities energy $E(t)$, enstrophy $Q(t)$ and palinstrophy $P(t)$, given by spatial integrals as follows

$$E(t) = \frac{1}{2}\int |\boldsymbol{u}|^2 \, d\boldsymbol{x}, \; Q(t) = \frac{1}{2}\int |\boldsymbol{\omega}|^2 \, d\boldsymbol{x}, \; P(t) = \frac{1}{2}\int |\nabla \times \boldsymbol{\omega}|^2 \, d\boldsymbol{x}. \tag{1.4}$$

These will be important later in the thesis.

1.2 Kolmogorov Theory

We briefly summarize Kolmogorov's theory (K41), to which we make reference several times throughout the thesis.

For fully-developed statistically-steady turbulent flow, energy is added to the system at large scales becoming kinetic energy in the fluid. This kinetic energy is then transferred from large scale (low wavenumber) turbulent structures to small scale (high wavenumber) ones and is eventually converted into heat. This is called the 'energy cascade', and it is assumed that at each stage, the eddies 'space-fill', meaning that as smaller eddies are formed, these eddies occupy the space left by the breakdown of their 'parent' eddies. Here, eddies are loosely defined as localized turbulent structures of a certain size.

To begin with we must make some physical assumptions. Firstly, the external energy injected into the system is transferred to smaller and smaller scales with negligible loss of energy between scales until it is dissipated to heat at the final stage. The quantity ϵ can therefore be defined as either the rate of injection, transfer, or dissipation of energy. We also assume statistical isotropy at small scales, thus these small scale flows are essentially uniform, and because of the physics involved in the cascade, depend only on the energy injection/transfer/dissipation rate ϵ and the kinematic viscosity ν. The inertial scale motions are also essentially uniform, depending only on ϵ, as no dissipation is present in this range.

A set of length scales $l_n = l_0/2^n$ ($\sim 1/k_n$), are defined. Here l_0 represents the largest length scales at which the energy is supplied to the system, l_n and k_n are the length scale and wavenumber after n generations, respectively, taken throughout the range, defined for successively smaller eddies as the integer n increases. Eddies of this size/wavenumber have kinetic energy per unit mass given by

$$E_n = \int_{k_n}^{k_{n+1}} E(k) \, dk \sim v_n^2,$$

where v_n is defined as the change in velocity over l_n. The time scale, known as 'eddy turnover time' can now be formulated as $t_n \sim l_n/v_n$, which means that the energy transfer rate (which we have assumed to be independent of length scale) is given by $\epsilon \sim E_n/t_n \sim v_n^3/l_n$.

We concern ourselves with three main transitory periods, characterized by three length scales; the integral or "production" range, the inertial range, and the dissipation range.

The integral (production) range is the largest length scale, containing most of the energy in the system. This is the scale at which energy is introduced to the system. Eddies typically spend almost all of their lifetime in this range, thus the dissipation to heat occurs relatively quickly. This range corresponds to the integral length scale l_0, the size of the largest eddies in the flow.

Throughout the intermediate stages, known as the inertial range, the nonlinear term dominates, no energy is being injected and negligible dissipation of energy occurs. The only mechanism present is the transfer of energy from larger to smaller scales represented by l_n. Using the above definitions, we can redefine $v_n \sim \epsilon^{1/3} l_n^{1/3}$, $t_n \sim \epsilon^{-1/3} l_n^{2/3}$ and $E_n \sim \epsilon^{2/3} k_n^{-2/3}$, and so the Kolmogorov spectrum is defined as

$$E(k) = C\epsilon^{2/3} k^{-5/3}, \tag{1.5}$$

where k is the wavenumber and C is known as the Kolmogorov constant. At the shorter end of this scale lies the Taylor microscale λ at which viscosity begins to take effect.

As we continue to smaller scales, the viscous term dominates, this is the dissipative range. The time scale in this case is $t_n^d \sim l_n^2/\nu$, which when equated with the previous definition of t_n produces the Kolmogorov length scale $\eta \sim (\nu^3/\epsilon)^{1/4}$, this scale corresponds to the final stage of the process, indicating the size of the smallest eddies in the flow. Most of the actual dissipation takes place at scales larger than the Kolmogorov length, but smaller than those of the inertial subrange.

So in summary the mechanism is as follows: Energy enters the system at large scales, producing turbulence in the form of large eddies, which break up and transfer their kinetic energy to smaller eddies, which break up again, transferring their kinetic energy to still smaller eddies and so on until the flow is smooth enough for the viscosity to dissipate the kinetic energy, converting it into heat. This means that (by conservation of energy assumption) the rate of dissipation of energy ϵ at the smallest scales is dependent on the rate of energy injection into the system at the

largest scales [4, 5, 6, 7].

1.3 The Beta Model for Intermittency

For the case of fully-developed turbulence with intermittency, assuming space filling at the largest scale, eddies fill progressively less space as the energy cascade propagates to smaller scales. Here we use the same notation as in the previous section, this time corresponding only to regions which are occupied by eddies. At each stage, let an eddy of size l_n produce an average of N smaller eddies of size l_{n+1}. Thus, after n progressions, the fraction of the total space occupied by turbulent motions is

$$\beta_n = \left(\frac{N}{2^3}\right)^n = 2^{-n(3-D)} = \left(\frac{l_n}{l_0}\right)^{3-D}, \qquad \text{where} \quad \frac{N}{2^3} \leq 1 \tag{1.6}$$

with $N = 2^D$ where D is the self-similarity (or fractal) dimension. We can now redefine the quantities for the intermittent case ($t_n \sim l_n/v_n$ as before);

$$\begin{aligned} E_n &\sim \beta_n v_n^2, \\ \epsilon &\sim \beta_n v_n^3/l_n, \\ v_n &\sim \epsilon^{1/3} l_n^{1/3} (l_n/l_0)^{-(3-D)/3}, \\ t_n &\sim \epsilon^{-1/3} l_n^{2/3} (l_n/l_0)^{(3-D)/3}, \\ E_n &\sim \epsilon^{2/3} l_n^{2/3} (l_n/l_0)^{(3-D)/3}. \end{aligned}$$

Thus, the energy spectrum, corrected for intermittency is

$$E(k) \sim \epsilon^{\frac{2}{3}} l_0^{-\frac{3-D}{3}} k^{-(\frac{5}{3}+\frac{3-D}{3})} \sim \epsilon^{\frac{2}{3}} l_0^{-\frac{\mu}{3}} k^{-\frac{1}{3}(5+\mu)}, \tag{1.7}$$

where $\mu = 3 - D$. We will later see that (as $D \geq 0$) the k-dependence is steeper than that of the Kolmogorov energy spectrum (1.5). Physically, we would expect that the velocity difference v_n across smaller and smaller eddies would decrease with eddy size. In this case we should expect that $D > 2$ [7, 8].

1.4 Colombeau Theory for Multiplication of Distributions

For certain mathematical distributions, such as the Heaviside function H, macroscopic changes occur over microscopic intervals. In classical distribution theory, these points of discontinuity are usually neglected.

For some problems in physics, however, certain systems require us to evaluate terms involving products of these discontinuous distributions, for example of the form $H\delta$, where δ is a Dirac delta function (which it can be shown is the derivative of H). These products are clearly meaningless at the points of discontinuity within the functions.

Colombeau's non-classical theory allows for this microscopic behavior by generalizing the classical concept of equality of distributions '=' into the less strict case of association '$\sim$' defined below.

For generalized functions, which have essentially the same properties as C^∞ functions, we say that the functions G_1 and G_2 are associated if

$$\int G_1(x)\psi(x)\,dx = \int G_2(x)\psi(x)\,dx, \tag{1.8}$$

for any C^∞ test function ψ. This association is usually written as $G_1 \sim G_2$. Due to the nature of integration by parts, we see that $G_1' \sim G_2'$. In contrast with the equality, however, we cannot simply multiply functions on both sides of the association; i.e. $GG_1 \sim GG_2$ does not follow from $G_1 \sim G_2$. So, for an illustrative example of this contrast, from (1.8) we can say that

$$G^n \sim G$$

differentiating gives

$$G^{n-1}G' \sim \frac{1}{n}G' \tag{1.9}$$

multiplying by G

$$G^nG' \sim \frac{1}{n}GG'$$

from (1.9) $G^nG' \sim \frac{1}{n+1}G'$ and $GG' \sim \frac{1}{2}G'$ so that

$$\frac{1}{n+1}G' \sim \frac{1}{2n}G'. \tag{1.10}$$

However, if we follow the same calculation through assuming that $G^n = G$, instead of (1.10) we would have

$$\frac{1}{n+1}G' = \frac{1}{2n}G'. \tag{1.11}$$

This is clearly valid only if $n = 1$, for example if we try $n = 2$, we would have

$$\frac{1}{3}G' = \frac{1}{4}G' \quad \rightarrow \quad \frac{1}{3} = \frac{1}{4}.$$

Therefore, we conclude that $G^n \neq G$ for $n \neq 1$.

This powerful method can be applied to specific physical systems in which microscopic behavior occurs, allowing for analysis of discontinuities subject to their particular physical environment. Colombeau theory is of particular interest to our cause in the case of shock waves, a microscopic behavior found in solutions of the 1D Burgers equation (see Chapter 4). A typical shock wave solution of this type is of the form

$$u(x,t) = \Delta u H(x - vt) + u_l, \quad \Delta u = u_r - u_l,$$

where v is the wave speed and u_l and u_r are the velocities to the left and right of the shock, respectively [9, 10, 11, 12].

1.5 Regularity of the Navier-Stokes Equations

The Navier-Stokes equations are used in a wide range of applications to describe both laminar and turbulent flows, and sometimes regularity is taken for granted in physical applications. This is not however guaranteed, in fact the question of whether the 3D Navier-Stokes equations are regular for all times is one of the most pertinent unsolved problems in mathematics, justifying an entire subject area within research, and boasting an extremely large number of publications to that effect. In spite of all of these attempts, none has yet been able to prove that the 3D Navier-Stokes equations have unique smooth regular (classical) solutions for all time and space. This is of more significance than just that of mathematical technicality. If these equations do not in fact admit classical solutions then this calls into question the validity of the small-scale physical assumptions used in their derivation. In this case, by applying the Navier-Stokes model we would be "glossing over" some of the fundamental physical properties of the real fluid. There are several standard approaches of guaranteeing global regularity of the Navier-Stokes equations. These include bounding either the velocity (or its gradient $|\nabla \boldsymbol{u}|$), energy or enstrophy of the equations, or constructed solutions to the equations, for all time and space, and proving the non-existence of singular solutions (discussed later).

First we briefly explore some of the attempts to bound the relevant quantities mentioned above. This has been solved for the two-dimensional case, proving regularity for all time by showing that the enstrophy and velocity gradient norms are bounded for all time if they are initially. We can transform the Navier-Stokes equa-

tions in terms of $\boldsymbol{\omega}$. First we rewrite (1.1), neglecting the forcing term, as

$$\frac{\partial \boldsymbol{u}}{\partial t} + \nabla \left(\frac{1}{2} |\boldsymbol{u}|^2 + p \right) - \boldsymbol{u} \times (\nabla \times \boldsymbol{u}) = \nu \nabla^2 \boldsymbol{u}, \tag{1.12}$$

where we have rewritten the nonlinear term using a standard vector identity. Taking the curl

$$\frac{\partial \boldsymbol{\omega}}{\partial t} - \nabla \times (\boldsymbol{u} \times \boldsymbol{\omega}) = \nu \nabla^2 \boldsymbol{\omega}, \tag{1.13}$$

using another identity with the incompressibility condition, we obtain the vorticity equation

$$\frac{\partial \boldsymbol{\omega}}{\partial t} + (\boldsymbol{u} \cdot \nabla)\boldsymbol{\omega} = (\boldsymbol{\omega} \cdot \nabla)\boldsymbol{u} + \nu \nabla^2 \boldsymbol{\omega}. \tag{1.14}$$

Identifying the terms from left to right, we have; the time derivative, nonlinear term, vortex stretching term, and viscous/diffusion term. The reason that global regularity can be guaranteed in the 2D case is that vortex-stretching term disappears in lower than three dimensions (shown below).

If we define a 2D velocity field $\boldsymbol{u}(x, y, t) = (u_1(x, y, t), u_2(x, y, t), 0)$, so that $\boldsymbol{\omega} = \left(0, 0, \frac{\partial \boldsymbol{u}_2}{\partial x} - \frac{\partial \boldsymbol{u}_1}{\partial y}\right)$, the vortex-stretching term is calculated as

$$(\boldsymbol{\omega}.\nabla)\boldsymbol{u} = \left(\frac{\partial \boldsymbol{u}_2}{\partial x} - \frac{\partial \boldsymbol{u}_1}{\partial y} \right) \frac{\partial \boldsymbol{u}}{\partial z} \equiv 0.$$

The presence of the vortex-stretching term in the 3D case has the consequence that regularity cannot be guaranteed for all time. Bounds can guarantee regularity only for short time intervals, assuming that the initial conditions of the flow are sufficiently smooth.

The rate of change of enstrophy can be bounded in terms of the enstrophy itself, by taking the scalar product of $\boldsymbol{\omega}$ with (1.14) and integrating over the spatial range (note: throughout this derivation, c denotes a positive constant that is not neccessarily the same in each step).

$$\frac{1}{2} \int \frac{\partial |\boldsymbol{\omega}|^2}{\partial t} \, d\boldsymbol{x} = \int \boldsymbol{\omega} \cdot (\boldsymbol{\omega} \cdot \nabla)\boldsymbol{u} \, d\boldsymbol{x} - \int \boldsymbol{\omega} \cdot (\boldsymbol{u} \cdot \nabla)\boldsymbol{\omega} \, d\boldsymbol{x} + \nu \int \boldsymbol{\omega} \cdot \nabla^2 \boldsymbol{\omega} \, d\boldsymbol{x}. \tag{1.15}$$

The intergration (by parts) in the third term gives

$$\int \boldsymbol{\omega} \cdot (\boldsymbol{u} \cdot \nabla)\boldsymbol{\omega} \, d\boldsymbol{x} = \frac{1}{2} \int (\boldsymbol{u} \cdot \nabla) |\boldsymbol{\omega}|^2 \, d\boldsymbol{x} = 0,$$

where we have made use of incompressibility and boundary conditions. For the final term, after applying some vector identities along with Gauss' theorem, (1.15) becomes

$$\frac{dQ}{dt} = \int \boldsymbol{\omega} \cdot (\nabla \boldsymbol{u}) \cdot \boldsymbol{\omega} \, d\boldsymbol{x} - \nu \int |\nabla \times \boldsymbol{\omega}|^2 \, d\boldsymbol{x}, \tag{1.16}$$

in which the definition of enstrophy in (1.4) is used. We now transform the second term - first using the Cauchy-Schwartz inequality, so that

$$\int \boldsymbol{\omega} \cdot (\nabla \boldsymbol{u}) \cdot \boldsymbol{\omega} \leq \left(\int |\boldsymbol{\omega}|^4 \, d\boldsymbol{x} \right)^{1/2} \left(\int |\nabla \boldsymbol{u}|^2 \, d\boldsymbol{x} \right)^{1/2},$$

and then, by the Gagliardo-Nirenberg inequality, which is in integral form

$$\int |D^j f|^p \, d\boldsymbol{x} \leq c \left(\int |D^m f|^r \, d\boldsymbol{x} \right)^{pa/r} \left(\int |f|^q \, d\boldsymbol{x} \right)^{p(1-a)/q}.$$

where

$$\frac{1}{p} = \frac{j}{d} + a\left(\frac{1}{r} - \frac{m}{d}\right) + \frac{1-a}{q}, \qquad 1 \leq q,\ r \leq \infty,\ 0 \leq j < m,\ j, m \in \mathbb{Z}, \text{ and } \frac{j}{m} \leq a < 1,$$

if $m - j - d/j$ is an non-negative integer then, then a is restricted to j/m.
Therefore, taking $p = 4$, $q = r = 2$, $j = 0$, $d = 3$, $a = 3/4$ and $m = 1$, we obtain

$$\int \boldsymbol{\omega} \cdot (\nabla \boldsymbol{u}) \cdot \boldsymbol{\omega} \leq c \left(\int |\nabla \times \boldsymbol{\omega}|^2 \, d\boldsymbol{x} \right)^{3/4} \left(\int |\boldsymbol{\omega}|^2 \, d\boldsymbol{x} \right)^{1/4} \left(\int |\nabla \boldsymbol{u}|^2 \, d\boldsymbol{x} \right)^{1/2}.$$

Then (1.16) can be re-written using (1.4) as

$$\frac{dQ}{dt} \leq cQ^{3/4}P^{3/4} - 2\nu P. \tag{1.17}$$

We can transform still further to eliminate P via the inequality

$$a^p b^q \leq pa + qb, \qquad \text{with } a, b > 0,\ \ 0 < p, q < 1 \text{ and } p + q = 1,$$

so that

$$cQ^{3/4}P^{3/4} = (c^4\nu^{-3}Q^3)^{1/4}(\nu P)^{3/4} \leq \frac{c^4}{4}\nu^{-3}Q^3 + \frac{3}{4}\nu P$$

and apply the Cauchy-Schwartz inequality again to the make $Q^2 \leq EP$ so $P \geq Q^2/E \geq Q^2/E(0)$, and finally

$$\frac{dQ}{dt} \leq \frac{c}{4}\nu^{-3}Q^3 - \frac{5}{4}\nu\frac{Q^2}{E(0)}, \tag{1.18}$$

where c^4 has been renamed as c. The inequalities (1.17) and (1.18) are alternate forms of the so-called enstrophy bound for the 3D Navier-Stokes equations. The latter form involves only energy and enstrophy, which are physical quantities more frequently associated with the question of regularity.

A related but simpler system is that of the 3D Burgers equations, which are known to possess globally regular solutions, thanks to a maximum principle.

$$\frac{\partial \boldsymbol{v}}{\partial t} + (\boldsymbol{v} \cdot \nabla)\boldsymbol{v} = \nu \nabla^2 \boldsymbol{v}, \tag{1.19}$$

where the velocity $\boldsymbol{v} = \boldsymbol{v}(\boldsymbol{x}, t)$ is compressible. The difference with respect to the Navier-Stokes equations (1.1) is clearly that these equations lack the nonlocal pressure gradient, which plays a significant role in the question of regularity of the Navier-Stokes equations. Taking the dot product of $\boldsymbol{u}$ with (1.19) produces the *local* energy density equation

$$\left(\frac{\partial}{\partial t} + \boldsymbol{v} \cdot \nabla\right) \frac{|\boldsymbol{v}|^2}{2} = \nu \boldsymbol{v} \nabla^2 \boldsymbol{v} = -\nu |\nabla \boldsymbol{v}|^2 + \nu \nabla^2 \frac{|\boldsymbol{v}|^2}{2}, \tag{1.20}$$

The second term on the left vanishes because the velocity gradient is zero at local maxima of energy density, and the first term on the right is negative definite, so we obtain the inequality

$$\frac{\partial}{\partial t} \frac{|\boldsymbol{v}|^2}{2} \leq \nu \nabla^2 \frac{|\boldsymbol{v}|^2}{2}. \tag{1.21}$$

From this, global-in-time regularity of Burgers equations is proven by a maximum principle of the form

$$\max_{\boldsymbol{x}} |\boldsymbol{v}(\boldsymbol{x}, t)| \leq \max_{\boldsymbol{x}} |\boldsymbol{v}(\boldsymbol{x}, 0)|,$$

which guarantees that the magnitude velocity field at time t never exceeds that of the initial velocity field, hence if we have a finite initial velocity field it will remain finite for all time [13].

For the Navier-Stokes equations we seek a similar proof of conservation of energy: The equation of local energy density can be calculated by taking the scalar product of $\boldsymbol{u}$ with (1.1) to give (see Chapter 2 for derivation):

$$\frac{\partial}{\partial t} \frac{|\boldsymbol{u}|^2}{2} \leq -\boldsymbol{u} \cdot \nabla p + \nu \triangle \frac{|\boldsymbol{u}|^2}{2}. \tag{1.22}$$

The second term on the right hand side is positive definite, so if we did not have the nonlocal pressure term, which may be unboundedly positive or negative, the maximum principle would apply as in the case of the Burgers equations and we would have global regularity.

The first attempt at a global regularity proof was that of Leray [14], who introduced the idea of a weak (or "turbulent") solution. Weak solutions for a partial differential equation are obtained by taking the dot product of the equation with a

smooth test function and then integrating by parts, taking into account the periodic boundary conditions, so that the derivatives in each term are transferred onto the test function (which is smooth by definition). Solutions to this new equation are known as weak solutions to the original equation. In the case of Navier-Stokes equations, the derivatives are transferred so that the velocity vector is not differentiated. The consequence of this is that the spatial derivatives of the velocity field need not be regular (or even exist) for weak solutions to exist. Once weak solutions have been shown to exist for a partial differential equation, the equation can be shown to be regular if the weak solution is in fact smooth. Unfortunately in the case of the Navier-Stokes equations, this can only be guaranteed for a finite time [15].

Leray succeeded in proving global existence of weak solutions but could only guarantee the existence of classical solutions for a finite time, dependent on the initial conditions. These results hold for any viscosity. For the special case of sufficiently large viscosity (or sufficiently small initial velocity), however, a classical solution exists globally. Leray also predicted possibility of finite time singularities (singularity meaning, in this context, unbounded velocity), but was unable to specify any examples of this behavior. However, he was able to show that if these singularities did indeed occur, they were restricted to a temporal set of measure zero. Hopf [16] reworked these ideas from the perspective of a Galerkin approximation of the Navier-Stokes equations. Since Leray and Hopf, there has been little progress made in proving regularity via the construction of solutions, and another strategies have been implemented. The idea behind these methods is to discount the possibility of singularities in the 3D Navier-Stokes equations, in both space and time. This approach was used by Scheffer [17], who showed that the Hausdorff dimension of the possible singular sets of solutions in (3+1) dimensional space-time cannot be greater than 5/3. Later, Caffarelli, Kohn and Nirenberg (CKN) [18] refined Scheffer's result and showed that the Hausdorff dimension does not in fact exceed 1. CKN theory states that: For a suitable weak solution of the Navier-Stokes equation, if there is a positive dimensionless constant ϵ_{CKN} such that

$$\delta(r) = \frac{1}{\nu r} \int_{Q_r(\boldsymbol{x},t)} |\nabla \boldsymbol{u}|^2 \, d\boldsymbol{x} \, dt \leq \epsilon_{CKN}, \tag{1.23}$$

where Q_r is a parabolic cylinder within $\mathbb{R}^3 \times \mathbb{R}$, then $(\boldsymbol{x}, t)$ is a regular point.

To calculate the Hausdorff dimension (and measure) of the singular set, it must first be acknowledged that for a point $(\boldsymbol{x}, t) \in S$, where S represents the singular

set (in space-time) of solutions to the Navier-Stokes equations,

$$\delta(r) = \frac{1}{\nu r} \int_{Q_r(\boldsymbol{x},t)} |\nabla \boldsymbol{u}|^2 \, d\boldsymbol{x} \, dt > \epsilon_{CKN}, \tag{1.24}$$

Before proceeding, some definitions are required:

Vitali covering lemma: A Vitali covering of a real set A is a set B of closed balls (elements) of arbitrarily small radius, whose union contains all points in A. Therefore pairwise disjoint elements of B can be chosen which cover almost all A.

Hausdorff measure and dimension: The Hausdorff α-measure of real set P is defined as the infimum over all countable covers C_δ of P by closed sets Q with diameter $d_Q \leq \delta$, taken in the limit $\delta \to 0$, written mathematically as

$$\mu_\alpha(P) = \lim_{\delta \to 0} \inf_{C_\delta} \sum_{Q \in C_\delta} d_Q^\alpha, \tag{1.25}$$

with:

$$\mu_\alpha(P) = \begin{cases} \infty & \alpha < \alpha_c, \\ 0 & \alpha > \alpha_c, \end{cases} \tag{1.26}$$

where $\mu_{\alpha_c}(P)$ is the Hausdorff measure and $\alpha_c(P) \geq 0$ is the Hausdorff dimension of P. *Note:* The Hausdorff dimension of a smooth n-dimensional surface is n.

Using Vitali's covering lemma (above) one sees that the singular set, S in can be covered by a family of parabolic cylinders Q_{r_i} such that $r_i < \delta$, for any $\delta > 0$. Rewriting (1.24) in these terms,

$$\frac{1}{\nu r_i} \int_{Q_{r_i}(\boldsymbol{x},t)} |\nabla \boldsymbol{u}|^2 \, d\boldsymbol{x} \, dt > \epsilon_{CKN}, \tag{1.27}$$

and rearranging

$$\sum_i r_i < \frac{1}{\nu \epsilon_{CKN}} \int_{Q_{r_i}(\boldsymbol{x},t)} |\nabla \boldsymbol{u}|^2 \, d\boldsymbol{x} \, dt, \tag{1.28}$$

So, as $\delta \to 0$, the Hausdorff dimension of the singular set is restricted to $\alpha_c(S) \leq 1$, with measure zero. [18, 19].

These results suggest that the Navier-Stokes equations are, for the most part, regular, and that if singularities do occur, they do so very rarely at infrequent locations within the space-time region. Although, to date, there is no evidence for a singularity, the possibility cannot be ruled out.

The subject of intermittency is concerned with situations when the velocity gradient at a particular spatial and/or temporal location suffers a sudden large deviation from the spatial average. These deviations occur rather sporadically, and may also, in the case of singularities, become infinite. Intermittency is growing area of study, with many publications on the subject, most notably for this work is that of Frisch, Sulem and Nelkin [7] who extended Kolmogorov's theory to develop the so called "β-model", which incorporates intermittency into the dynamics of fully developed turbulence. See also [20, 21, 22].

We now proceed to the main body of the thesis. In Chapter 2 we compare the Navier-Stokes and Burgers equations. In Chapter 3 we calculate the CKN local Reynolds number and formulate a new cross-over scale where it's exponent changes. In Chapter 4 we study dissipation anomaly in Burgers equation with passive scalar. Chapter 5 is dedicated to summary and conclusion.

Chapter 2

Numerical study on comparison of Navier-Stokes and Burgers equations

Abstract

We compare freely decaying evolution of the Navier-Stokes equations with that of the 3D Burgers equations with the same kinematic viscosity and the same *incompressible* initial data by using direct numerical simulations. The Burgers equations are well-known to be regular by a maximum principle [Kiselev and Ladyzenskaya (1957)] unlike the Navier-Stokes equations.

It is found in the Burgers equations that the potential part of velocity becomes large in comparison with the solenoidal part which decays more quickly. The probability distribution of the nonlocal term $-\boldsymbol{u}\cdot\nabla p$, which spoils the maximum principle, in the local energy budget is studied in detail. It is basically symmetric, i.e. it can be either positive or negative with fluctuations. Its joint probability density functions with $\frac{1}{2}|\boldsymbol{u}|^2$ and with $\frac{1}{2}|\boldsymbol{\omega}|^2$ are also found to be symmetric, fluctuating at the same times as the probability density function of $-\boldsymbol{u}\cdot\nabla p$.

A power-law relationship is found in the mathematical bound for the enstrophy growth $\dfrac{dQ}{dt}+2\nu P \propto \left(Q^a P^b\right)^\alpha$, where Q and P denote the enstrophy and the palinstrophy, respectively and the exponents a and b are determined by calculus inequalities. We propose to quantify nonlinearity depletion by the exponent α on this basis.

2.1 Introduction

The regularity of the 3D Navier-Stokes equations is a well-known open problem despite lots of progress made in recent years. The mathematical literature are undoubtedly too numerous to cite them all here and we only quote [19, 23, 24, 25, 26, 27, 28, 29, 30, 31, 15] and references cited therein. In the areas of physical and engineering sciences, the regularity is more or less taken for granted. Nevertheless, the problem itself is also regarded as important in physical areas because the regularity is controlled by enstrophy, a physically important quantity closely related with turbulence. Indeed there are publications in this spirit [6, 32, 33, 34, 35, 36, 37].

In mathematical fluid mechanics, proofs of global regularity are obtained in a rather sporadic fashion. It is well known that the incompressible 2D Euler equations are regular for all time. The proof is based on conservation of scalar vorticity, which is a special property of the equations and no other proofs are known which do not depend on it.

As a related but simpler system, the 3D Burgers equations are known to possess globally regular solutions [13, 38]. In this case, because the nonlocal pressure term is absent, the maximum principle is valid and we conclude that the velocity is bounded at any time, if it is so initially. On the other hand, for the 3D Navier-Stokes equations, the possible formation of finite time singularities has not been ruled out, where a singularity means unbounded velocity. Nonetheless, the solutions of the Burgers equations are more singular than those of the Navier-Stokes equations in the sense that the width of shock waves $\propto \nu$ is thinner than the Kolmogorov dissipative scale $\propto \nu^{3/4}$ in Navier-Stokes turbulence. Furthermore the inviscid Burgers equations are known to have solutions that blow up in finite time, whereas for the Euler equations this is not known. For the Burgers equations, see also [39, 40, 41, 42]. Thus it makes sense to give a more detailed comparison of these equations.

The purpose of this paper is (i) to compare these two equations in some details by numerical experiments and (ii) to characterize the notorious nonlocal effects in the Navier-Stokes equations by observing how the maximum principle actually breaks down. A comparison of probability density functions (PDFs) of the velocity with those of a passive scalar are also made. In Section II, mathematical formulation is given with a summary of known properties of these equations. In Section III, we compare numerically the Navier-Stokes with Burgers equations in detail. In Section IV, dynamics of a passive scalar is studied, centering on how its behavior is

affected by a maximum principle. Performance of the enstrophy bounds are assessed, including the quasi-4D Navier-Stokes equations. Section V is devoted to summary and discussion. All the numerical experiments concerned in this chapter are those of freely decaying simulations.

2.2 Mathematical Formulation

We consider the incompressible 3D Navier-Stokes equations under periodic boundary conditions. With standard notations they read

$$\frac{\partial \boldsymbol{u}}{\partial t} + (\boldsymbol{u} \cdot \nabla)\boldsymbol{u} = -\nabla p + \nu \triangle \boldsymbol{u}, \tag{2.1}$$

$$\nabla \cdot \boldsymbol{u} = 0, \tag{2.2}$$

together with a smooth initial condition

$$\boldsymbol{u}(\boldsymbol{x}, t = 0) = \boldsymbol{u}_0(\boldsymbol{x}). \tag{2.3}$$

We can rewrite them equivalently as

$$\begin{aligned} \frac{\partial \boldsymbol{u}}{\partial t} &= \boldsymbol{u} \times \boldsymbol{\omega} - \nabla \left(p + \frac{|\boldsymbol{u}|^2}{2} \right) + \nu \triangle \boldsymbol{u} \\ &= \boldsymbol{P}(\boldsymbol{u} \times \boldsymbol{\omega}) + \nu \triangle \boldsymbol{u}, \end{aligned} \tag{2.4}$$

where $\boldsymbol{P}$ denotes a solenoidal projection.

We also consider the 3D Burgers equations

$$\frac{\partial \boldsymbol{v}}{\partial t} + (\boldsymbol{v} \cdot \nabla)\boldsymbol{v} = \nu \triangle \boldsymbol{v}, \tag{2.5}$$

which are valid in any d-dimensions ($d = 1, 2, 3, \ldots$). Because the velocity $\boldsymbol{v}$ is not incompressible in general $\nabla \cdot \boldsymbol{v} \neq 0$, the energy budget equation takes the form

$$\frac{d}{dt} \int \frac{|\boldsymbol{v}|^2}{2} \, \boldsymbol{dx} + \int (\boldsymbol{v} \cdot \nabla) \frac{|\boldsymbol{v}|^2}{2} \, \boldsymbol{dx} = -\nu \int |\nabla \boldsymbol{v}|^2 \, \boldsymbol{dx}. \tag{2.6}$$

Unlike the Navier-Stokes equations, the second term on the left does not vanish because of the compressible character of the velocity when $d \geq 2$. That is, we have no energy inequality for $d \geq 2$. However, for the 3D Burgers equations a maximum principle of the form

$$\max_{\boldsymbol{x}} |\boldsymbol{v}(\boldsymbol{x}, t)| \leq \max_{\boldsymbol{x}} |\boldsymbol{v}(\boldsymbol{x}, 0)|$$

is valid, which guarantees global-in-time regularity [13]. See Appendix A for first integrals in the inviscid case.

It is a bit ironic that global regularity is known for the Burgers equations because of the maximum principle, even though we cannot establish the existence of weak solutions by the method of energy inequality as in the case of the Navier-Stokes equations.

A sketch of the argument is as follows. The local energy budget for the Navier-Stokes equations reads

$$\begin{aligned}\left(\frac{\partial}{\partial t}+\boldsymbol{u}\cdot\nabla\right)\frac{|\boldsymbol{u}|^2}{2} &= -\boldsymbol{u}\cdot\nabla p+\nu\boldsymbol{u}\triangle\boldsymbol{u}\\ &= -\boldsymbol{u}\cdot\nabla p-\nu|\nabla\boldsymbol{u}|^2+\nu\triangle\frac{|\boldsymbol{u}|^2}{2}\end{aligned}$$

It follows that, because the advection term is zero at local maxima of the energy density,

$$\frac{\partial}{\partial t}\frac{|\boldsymbol{u}|^2}{2}\leq -\boldsymbol{u}\cdot\nabla p+\nu\triangle\frac{|\boldsymbol{u}|^2}{2}. \tag{2.7}$$

Because of the pressure term, we do not have a maximum principle unlike the case of the Burgers equations, e.g. [43]. For the Navier-Stokes equations, global regularity is obtained only for sufficiently large viscosity, or for sufficiently small initial data. With arbitrary viscosity and initial data, only the local existence of classical solutions has been established.

We consider the Helmholtz-Hodge decomposition for the Burgers equations taking a constant term to be zero,

$$\boldsymbol{v}=\boldsymbol{v}^{\perp}+\boldsymbol{v}^{\parallel}, \tag{2.8}$$

where $\boldsymbol{v}^{\perp}$ and $\boldsymbol{v}^{\parallel}$ denote solenoidal and compressible components, respectively, and

$$\nabla\cdot\boldsymbol{v}^{\perp}=0,\ \nabla\times\boldsymbol{v}^{\parallel}=0. \tag{2.9}$$

The solenoidal component can be written as

$$\boldsymbol{v}^{\perp}=\nabla\times\boldsymbol{A}\ \text{ with }\ \nabla\cdot\boldsymbol{A}=0, \tag{2.10}$$

whereas the potential component as

$$\boldsymbol{v}^{\parallel}=\nabla\phi. \tag{2.11}$$

Only when $\boldsymbol{v}^\perp = 0$ can the Cole-Hopf transform

$$\boldsymbol{v} = -2\nu\nabla \log \psi$$

be applied to yield [44]

$$\boldsymbol{v}_t + \boldsymbol{v}\cdot\nabla\boldsymbol{v} - \nu\triangle\boldsymbol{v} = -2\nu\nabla\left(\frac{\psi_t - \nu\triangle\psi}{\psi}\right), \tag{2.12}$$

which reduces (2.5) to a heat diffusion equation. Needless to mention, global regularity is obvious in this case.

The governing equations for each component can be derived as follows. By a well-known identity $\nabla\frac{|\boldsymbol{v}|^2}{2} = \boldsymbol{v}\cdot\nabla\boldsymbol{v} + \boldsymbol{v}\times\boldsymbol{\omega}$, we recast (2.5) as

$$\frac{\partial\boldsymbol{v}}{\partial t} = \boldsymbol{v}\times\boldsymbol{\omega} - \nabla\frac{|\boldsymbol{v}|^2}{2} + \nu\triangle\boldsymbol{v}.$$

Writing $\boldsymbol{v}\times\boldsymbol{\omega} = \boldsymbol{P}(\boldsymbol{v}\times\boldsymbol{\omega}) + (\boldsymbol{I}-\boldsymbol{P})(\boldsymbol{v}\times\boldsymbol{\omega}) = \nabla\times\boldsymbol{B} + \nabla\psi$ with $\boldsymbol{B} \equiv -\triangle^{-1}\nabla\times(\boldsymbol{v}\times\boldsymbol{\omega})$ and $\psi = \triangle^{-1}\nabla\cdot(\boldsymbol{v}\times\boldsymbol{\omega})$, we find

$$\begin{cases} \dfrac{\partial\boldsymbol{v}^\perp}{\partial t} = \boldsymbol{P}(\boldsymbol{v}^\perp\times\boldsymbol{\omega}) + \nu\triangle\boldsymbol{v}^\perp + \boldsymbol{P}(\boldsymbol{v}^\parallel\times\boldsymbol{\omega}), \\ \dfrac{\partial\boldsymbol{v}^\parallel}{\partial t} = -\nabla\dfrac{|\boldsymbol{v}|^2}{2} + (\boldsymbol{I}-\boldsymbol{P})(\boldsymbol{v}\times\boldsymbol{\omega}) + \nu\triangle\boldsymbol{v}^\parallel, \end{cases} \tag{2.13}$$

where $\boldsymbol{I}$ is the identity matrix.

Note that the first equation of (2.13) reduces to the 3D Navier-Stokes equations *if* we ignore the final term on the right-hand-side of it. If we use the impulse formalism we may choose a gauge where the solenoidal component solves the Navier-Stokes equations and the potential component the Burgers equations (see Appendix B).

For more quantitative comparison we define some norms. The total energy may also be split in two parts:

$$\frac{1}{2}\left\langle|\boldsymbol{v}|^2\right\rangle = \frac{1}{2}\left\langle|\boldsymbol{v}^\perp|^2\right\rangle + \frac{1}{2}\left\langle|\boldsymbol{v}^\parallel|^2\right\rangle, \tag{2.14}$$

which may be written $e(t) = e^\perp(t) + e^\parallel(t)$. Here the brackets denote a spatial average $\langle\rangle = \frac{1}{(2\pi)^3}\int d\boldsymbol{x}$. We also have

$$\frac{1}{2}\left\langle|\nabla\boldsymbol{v}|^2\right\rangle = \frac{1}{2}\left\langle|\nabla\boldsymbol{v}^\perp|^2\right\rangle + \frac{1}{2}\left\langle|\nabla\boldsymbol{v}^\parallel|^2\right\rangle, \tag{2.15}$$

which can be written $q(t) = q^\perp(t) + q^\parallel(t)$.

An overall comparison between the Navier-Stokes equations and the Burgers equations is summarized in Table 2.1. Some, but not all, of the features listed

Table 2.1: Navier-Stokes and Burgers equations (for $\nu \ll 1$). In each category, features emphasized in bold represent more singular nature than the other.

	Navier-Stokes	Burgers
Energy inequality	Yes	**No** ($n \geq 2$)
Global weak solutions	Yes	**No**
Energy spectrum $E(k)$	$\boldsymbol{k^{-5/3}}$	k^{-2}
Smallest scale	$\nu^{3/4}$	$\boldsymbol{\nu}$
Maximum principle	**No**	Yes
Global strong solutions	**Unknown**	Known
Blowup of ideal cases	Unknown	**Known**

above suggest that the Burgers equations are more singular than the Navier-Stokes equations. It makes sense to take a closer look at the comparison in order to better understand the role played by the pressure term associated with incompressibility in maintaining the regularity.

2.3 Comparative experiments to the Burgers equations

For this purpose we set up the following experiment: *Assume that we solve the 3D Navier-Stokes equations and the 3D Burgers equations starting from identical incompressible initial data and with the same viscosity. What will happen to the two components* $\boldsymbol{v}^{\perp}$ *and* $\boldsymbol{v}^{\parallel}$ *in the Helmholtz decomposition of the Burgers solution ?* We will consider more specific questions below.

Direct numerical simulations of the Navier-Stokes equations are done under periodic boundary conditions in double-precision arithmetic, using a standard Fourier pseudo-spectral method. The time-marching is done by the fourth-order Runge-Kutta method. Typically we use 256^3 grid points with aliasing errors removed by the so-called 2/3-rule.

We consider for the most part Navier-Stokes flows starting from random initial conditions. The initial conditions are generated to have the energy spectrum

$$E(k) = ck^2 \exp(-k^2), \tag{2.16}$$

where the phases of Fourier components are randomized by pseudo-random numbers and the prefactor c is determined to give unit enstrophy. Here we define the energy spectrum by

$$E(k) = \frac{1}{2} \sum_{k \le |\boldsymbol{k}| < k+1} |\boldsymbol{u}(\boldsymbol{k})|^2, \tag{2.17}$$

where $\boldsymbol{u}(\boldsymbol{k})$ is the Fourier coefficient of the velocity. The values of kinematic viscosity used are $\nu = 0.005$ and $\nu = 0.01$. We mainly discuss the case with $\nu = 0.005$ (used in all the figures) and $\nu = 0.01$ is used to check numerical accuracy. The typical time increment is $\Delta t = 2 \times 10^{-3}$.

We consider freely-decaying flows only, mostly those developing from random initial conditions and also the Taylor-Green initial condition at the end of this paper. We consider the decomposition $\boldsymbol{v} = \boldsymbol{v}^{\perp} + \boldsymbol{v}^{\parallel}$ for the solution of the Burgers equation, assuming initially that $\boldsymbol{v}^{\parallel}(0) = 0$ (due to the incompressible initial data), and feed the Navier-Stokes equations the same initial data $\boldsymbol{u}(0) = \boldsymbol{v}^{\perp}(0)$. We begin confirming that our numerical experiments have some standard properties known for these flows.

2.3.1 Energy and enstrophy

We study what happens to the decomposition of the Burgers equations. In Fig.2.1a, we show how each component of the energy evolves in the Burgers equations together with the energy in the Navier-Stokes equations. For the Burgers equations, the incompressible component $e^{\perp}(t)$ decays rapidly while the compressible part $e^{\parallel}(t)$ grows rapidly from zero, reaching a maximum just before $t = 2$. Both components keep decaying and become comparable later. For the Navier-Stokes equations, the decay of energy takes place but more slowly than the sum of the two components of the Burgers equations. In Fig.2.1b, we show a similar comparison in terms of the enstrophy. The compressible part rapidly increases from zero to attain a maximum around $t = 2$, which is twice as large as the peak value of the incompressible part. The peak value of the total enstrophy of the Burgers equations is larger than that of the Navier-Stokes equations by a factor of 3 and a mild maximum is attained for the Navier-Stokes equations later around $t = 6$. These results are consistent with a view that the Burgers equations are more singular than the Navier-Stokes equations.

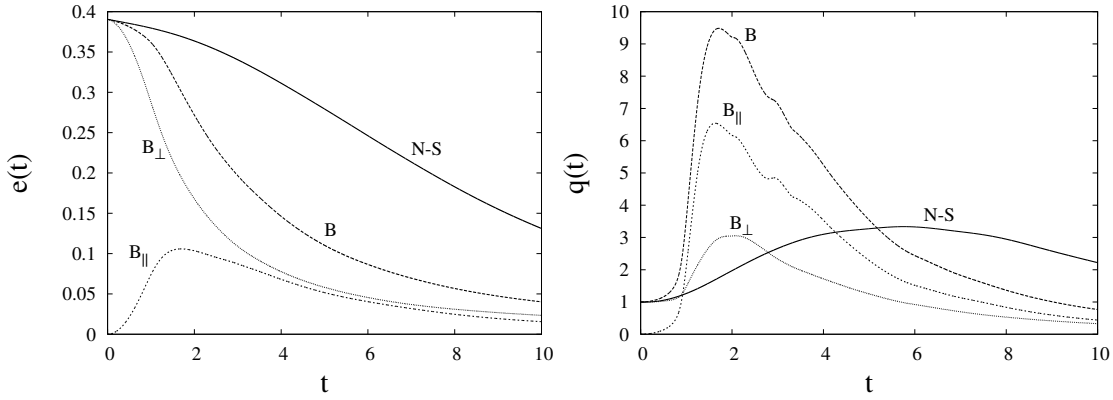

Figure 2.1: Comparison of norms for the Navier-Stokes and Burgers equations: (a) the energy (left) and (b) the enstrophy (right). Here N-S stands for the Navier-Stokes equations, B for the Burgers equations, with $B_\perp$ and $B_\parallel$ representing the solenoidal and potential components of the Burgers equations respectively.

2.3.2 Energy spectra

Now we examine the difference by studying the energy spectra. In Fig.2.2, we show each component of the Fourier energy spectra

$$E(k) = E^\perp(k) + E^\parallel(k) \tag{2.18}$$

for the Burgers equations together with that of the Navier-Stokes equations. They are taken at the same time $t = 5$. For the Navier-Stokes equations the higher wave number part decays rapidly, while the Burgers equations have much more excitations in that range, which is marginally resolved. In the lower wave number range, we observe power-law behaviors close to k^{-2} in both $E^\parallel(k)$ and $E^\perp(k)$. For the Navier-Stokes equations, it is not clear if the flow displays $k^{-5/3}$ or not, because the viscosity $\nu = 0.005$ is not sufficiently small. Note that using the Navier-Stokes equations at a smaller value of viscosity and with a forcing term we may generate a power-law range consistent with $E(k) \propto k^{-5/3}$ (not shown). Actually, even at the current spatial resolution of 256^3 we can choose a smaller $\nu = 0.0025$ for the Navier-Stokes equations, but not for the Burgers equations because of truncation errors (see Appendix C). Judging from the excitations at higher wavenumbers we observe that the Burgers equations are far more singular than the Navier-Stokes equations.

A few remarks regarding numerical accuracy for the computations are in order. We fit the energy spectrum as $E(k) = A(t)k^{n(t)}\exp(-\mu(t)k)$, where $A(t), n(t)$ and $\mu(t)$ are determined by the least-squares method. At $t = 2$, which is the least-

resolved instant of time, the flow is somewhat under-resolved with $\mu(t = 2) = 2.25 \times 10^{-2} < \frac{2\pi}{N} = 2.45 \times 10^{-2}$(mesh size) where $N = 256$. The flow is found to be better resolved at other times. We have conducted the same computation with 512^3 grid points to double-check that the evolution of the enstrophy in each component is independent of spatial resolutions (figure omitted). We have also confirmed that the dominance of the potential part over the the solenoidal part is seen in a well-resolved computation with $\nu = 0.01$. We conclude that the properties of the Burgers equations obtained here are genuine, not numerical artifacts.

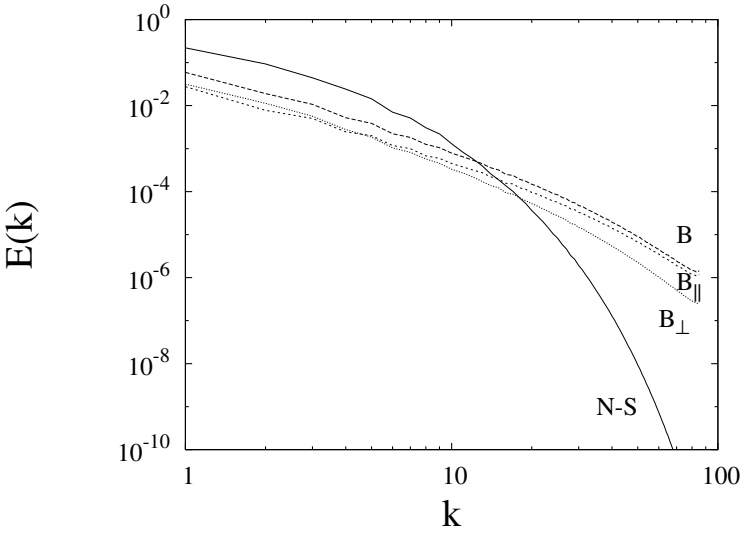

Figure 2.2: Energy spectra $E(k)$ of the Navier-Stokes equations at $t = 5$ (solid), with corresponding $E(k)$ (dashed), $E(k)^{\|}$ (short-dashed) and $E(k)^{\perp}$ (dotted) for the Burgers equations at the same time. Symbols have the same meaning as in Fig.1.

2.3.3 Probability density function (PDF) of velocity

Now we consider how the absence of a maximum principle affects the dynamics of Navier-Stokes equations. It is well-known that the one-point PDF of a velocity component is close to a Gaussian distribution for Navier-Stokes turbulence. Fig.2.3a shows the time evolution of the PDF of the velocity, which is normalized to have unit variance. As time goes on, the tail parts spread out toward larger amplitudes, getting closer to the normal Gaussian distribution. In contrast, for the Burgers equations the PDF behaves differently. That is, their wings remain restricted close to the initial

profile (Fig.2.3b). This can be explained because the maximum principle precludes excitations at large amplitudes. Similar observations were made, for example, in [45] in a different context. We note that the PDFs of the velocity gradients distinguish the two equations more clearly; the Burgers equations are more intermittent than those of the Navier-Stokes equations (not shown here). We only consider the PDFs of velocity gradients because we are interested in the presence or absence of the maximum principle.

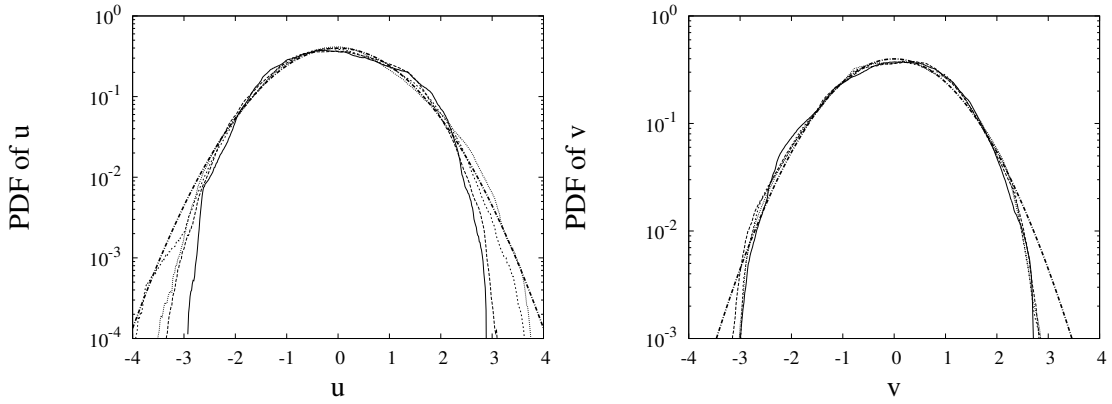

Figure 2.3: PDFs of velocity field for a) the Navier-Stokes (left) and b) the Burgers (right) equations. Both are normalized to have unit variance: Plotted at $t = 2$ (solid), 5 (dashed), 8 (short-dashed) and 10 (dotted). The thicker dot-dashed lines denote the standard normal distribution $N(0, 1)$.

2.3.4 Nonlocal Term $-(\boldsymbol{u} \cdot \nabla)p$

It is this term which is responsible for the breakdown of the maximum principle for the Navier-Stokes equations. Therefore it makes sense to study the behaviors of the quantity in some detail. First, we show the PDF of $-(\boldsymbol{u} \cdot \nabla)p$ in Fig.2.4.

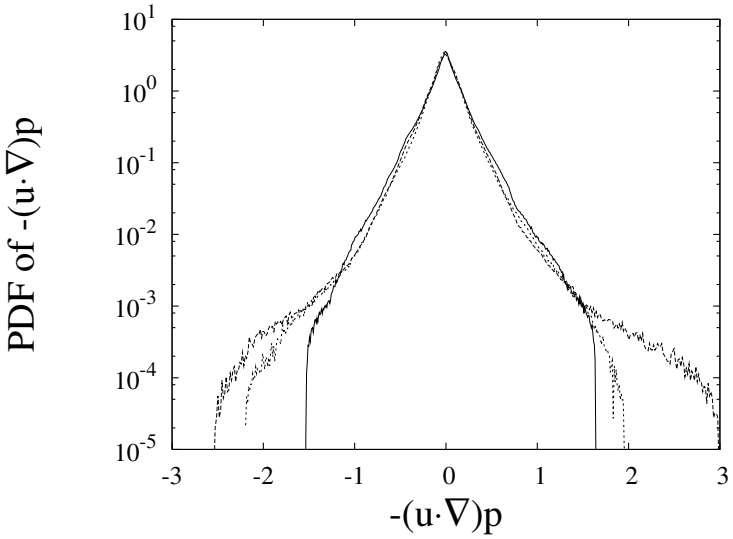

Figure 2.4: The PDF of $-(\boldsymbol{u}\cdot\nabla)p$ at $t = 2$ (solid), $t = 4$ (dashed) and $t = 5$ (dotted), for the Navier-Stokes equations. Skewness correlates with the local maxima mentioned above and shown in Fig.2.6b. The quantity $-(\boldsymbol{u}\cdot\nabla)p$ is not normalized.

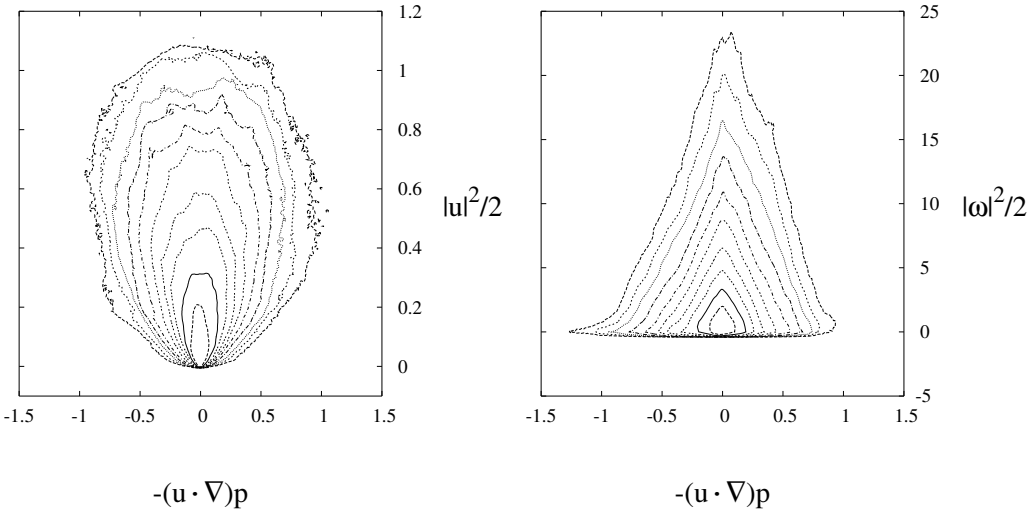

Figure 2.5: Joint PDFs: (a) $-(\boldsymbol{u}\cdot\nabla)p$ and $\frac{1}{2}|\boldsymbol{u}|^2$ (left) and (b) $-(\boldsymbol{u}\cdot\nabla)p$ and $\frac{1}{2}|\boldsymbol{\omega}|^2$ (right) for the Navier-Stokes equations. The quantities are not normalized. Contour levels are set at $a(t)/2^n$, for $n = 0, 1, 2, ..., 10$, where $a(t)$ is the maximum value of the PDF at the time instant (in this case $t = 4$).

We see that it is basically symmetric, that is, no preference is observed for positive or negative values. However, if we examine $-(\boldsymbol{u}\cdot\nabla)p$ at several different times in more detail, we see some fluctuations from time to time, occasionally making it skewed positively, e.g. at $t = 4$ (this point is to be examined below).

We study a possible correlation of these fluctuations with large energy or enstrophy, both of which are related with extreme events in Navier-Stokes equations. Shown in Fig.2.5a is a joint PDF between $-(\boldsymbol{u}\cdot\nabla)p$ and the local energy density $\frac{1}{2}|\boldsymbol{u}|^2$. There is no systematic trend of the sign of $-(\boldsymbol{u}\cdot\nabla)p$ correlated with large or small energy density. In fact, average of the local energy or enstrophy density conditioned on the sign of $-(\boldsymbol{u}\cdot\nabla)p$ is 1:1 to within relative error of 1 %. A similar joint PDF with the local enstrophy density $\frac{1}{2}|\boldsymbol{\omega}|^2$ is given in Fig.2.5b. Again, there is no overall trend to be correlated with large or small enstrophy density, although a small negative fluctuation is seen for small values of $|\boldsymbol{\omega}|^2$ at $t = 4$. We have analyzed the data at other times and the slight fluctuations occur rarely and do not seem to follow any particular pattern. We conclude that the term $-(\boldsymbol{u}\cdot\nabla)p$ neither contributes to the formation of a singularity, nor to avoid it; it simply makes the maximum principle invalid.

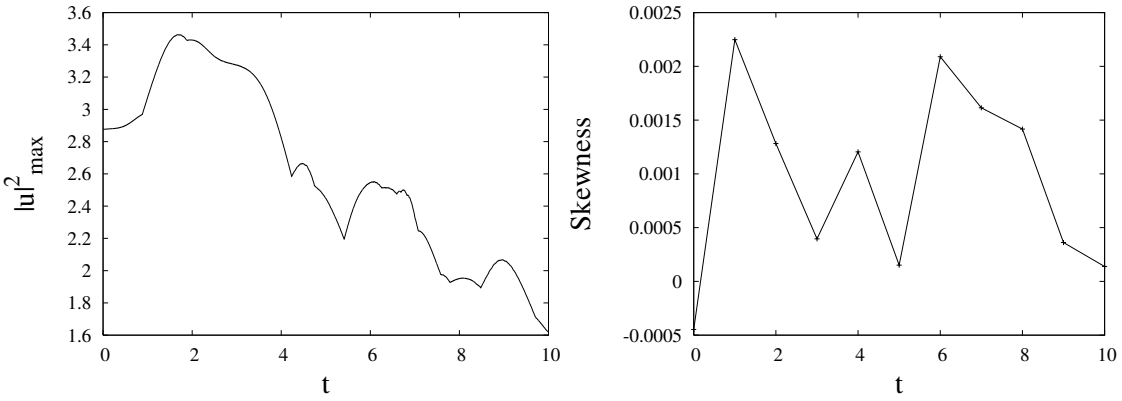

Figure 2.6: Time evolution of (a) $\max|\boldsymbol{u}|^2$ (left) and (b) the skewness factor of $-(\boldsymbol{u}\cdot\nabla)p$ (right) for the Navier-Stokes equations.

In Fig.2.6a we plot the time evolution $|\boldsymbol{u}|^2_{\max}$, which sometimes exceeds its initial value. In Fig.2.6b we plot the skewness of $-(\boldsymbol{u}\cdot\nabla)p$. It should be noted that local maxima of $|\boldsymbol{u}|^2_{\max}$ at $t \approx 2, 4, 6$ are just preceded by those of the skewness factor. This means that fluctuations of the skewness factor correlate with local increase (or decrease) of the energy. If $-(\boldsymbol{u}\cdot\nabla)p$ is positively skewed instantaneously, it pumps up the energy at that time, as this term represents the inviscid contribution of the

Lagrangian time derivative of local energy density.

2.4 Passive scalar as quasi-4D Navier-Stokes flow

2.4.1 Passive scalar

We will consider a passive scalar field $\theta(\boldsymbol{x}, t)$ subject to the velocity in this section. The motivation is two-fold: 1) because differences between the Navier-Stokes and Burgers equations stem from the nonlocal pressure term, it makes sense to take a detailed look at the effect of nonlocality and 2) to quantify numerically, in several spatial dimensions, the performance of the enstrophy bounds available mathematically. It should be kept in mind that the pressure has both nonlocal and nonlinear characters, as is clear from its definition

$$p = -\triangle^{-1} \left(\frac{\partial u_i}{\partial x_j} \frac{\partial u_j}{\partial x_i} \right).$$

The equation for the passive scalar is given by

$$\frac{\partial \theta}{\partial t} + (\boldsymbol{u} \cdot \nabla)\theta = \nu \triangle \theta, \tag{2.19}$$

where θ is a passive scalar, $\boldsymbol{u}$ is the solution of the 3D Navier-Stokes equations.

We take the diffusivity at the same value as the viscosity (unit Prandtl number) to make the comparison as parallel as possible. We initialize a passive scalar by $\theta(\boldsymbol{x}, 0) = u_1(\boldsymbol{x}, 0)$. Therefore any differences that may arise in the subsequent evolution between $u_1(\boldsymbol{x}, t)$ and $\theta(\boldsymbol{x}, t)$ for $t > 0$ should be attributed to the pressure gradient term [46]. In particular, by tracing the subsequent deviation we may monitor how the maximum principle breaks down for a component of velocity.

In Fig.2.7, we compare evolution of the enstrophy $q(t)$ with the spatial average of the square of passive scalar gradient

$$q_\theta(t) = \frac{1}{2} \left\langle |\nabla \theta|^2 \right\rangle. \tag{2.20}$$

We note that $q_\theta(t)$ attains a maximum around $t = 3$ earlier than that of the enstrophy $q(t)$ at $t = 7$. Peak values are comparable. In Fig.2.8, we show energy spectra $E(k)$ and passive scalar spectrum $E_\theta(k)$ at several different times.

$$E_\theta(k) = \frac{1}{2} \sum_{k \le |\boldsymbol{k}| < k+1} |\boldsymbol{\theta}(\boldsymbol{k})|^2. \tag{2.21}$$

We observe that the slope of $E_\theta(k)$ is shallower than that of $E(k)$.

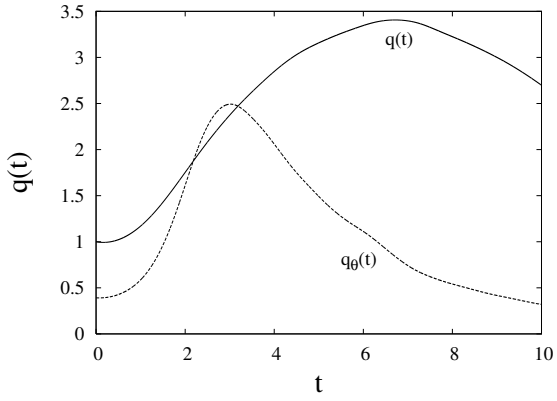

Figure 2.7: Time evolution of $q(t)$ and $q_\theta(t)$ for the Navier-Stokes and passive scalar equations.

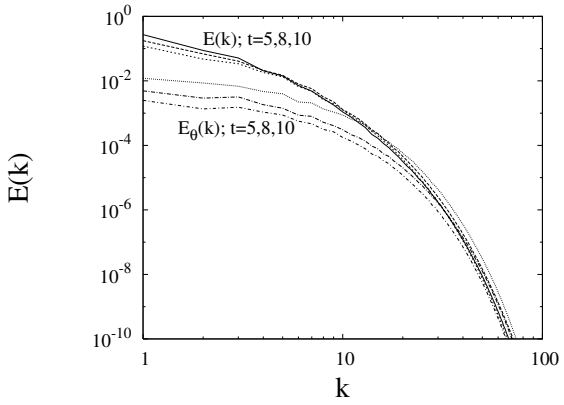

Figure 2.8: Time evolution of energy spectra $E(k)$ and $E_\theta(k)$ of the Navier-Stokes and passive scalar equations at $t = 5, 8$ and 10, respectively (in descending order from the top line).

In order to study the difference in behavior of θ^2 and u_1^2, we show in Fig.2.9 the time evolution of their maximum values. It should be noted that u_1^2 increases in the early stage in contrast to a monotonic decay of θ^2, the latter behavior of course comes from the maximum principle. In Fig.2.10 we also show the time evolution of $\langle (u_1 - \theta)^2 \rangle$.

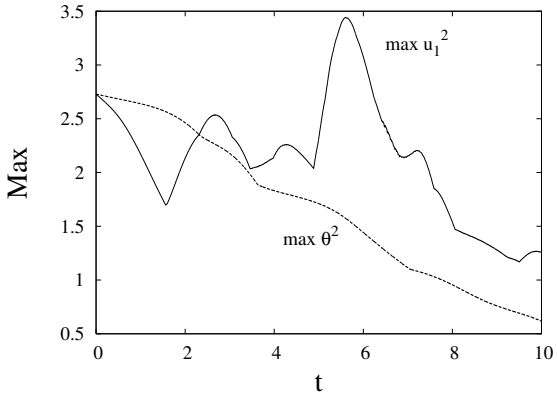

Figure 2.9: Time evolution of $\max u_1^2$ and $\max \theta^2$ for the Navier-Stokes and passive scalar equations.

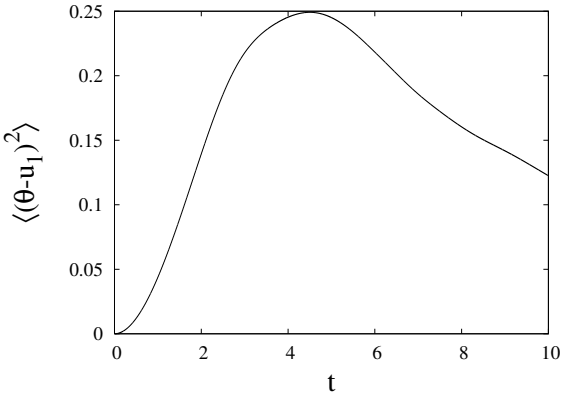

Figure 2.10: Time evolution of $\langle (u_1 - \theta)^2 \rangle$ for the Navier-Stokes and passive scalar equations.

Because of the initialization of θ, this is 0 at $t = 0$, and then grows in time

because of the non-local effects. It attains a maximum around $t = 4$, which is between the times of maxima in $q(t)$ and $q_\theta(t)$. This suggests the nonlocal pressure term is intimately connected with the stretching of the vorticity and of the passive scalar gradient.

In Fig.2.11 we show iso-surface plots of $(u_1 - \theta)^2$, together with those of enstrophy. The large deviations and high enstrophy are correlated not only temporally but spatially. This indicates that the maximum principle breaks down in the vicinity of near-singular structure associated with large enstrophy, see also [45, 47]. In Fig. 2.12, we compare the PDFs of the velocity and passive scalar. The tails of the PDF of the passive scalar spread out, because of a faster decay of its variance than the kinetic energy.

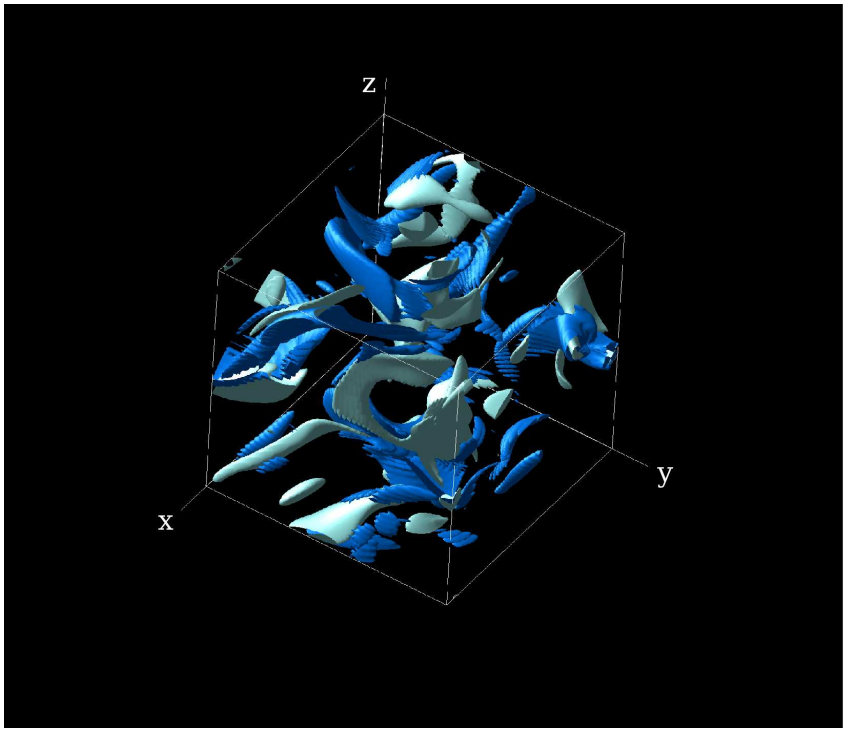

Figure 2.11: Iso-surfaces of $|\boldsymbol{\omega}|^2$ (grey, blue in color copies) and $(\theta - u_1)^2$ (white), for the Navier-Stokes and passive scalar equations. The threshold is chosen as $|\boldsymbol{\omega}|^2 = 4\left\langle |\boldsymbol{\omega}|^2 \right\rangle$ and $(\theta - u_1)^2 = 4\left\langle (\theta - u_1)^2 \right\rangle$.

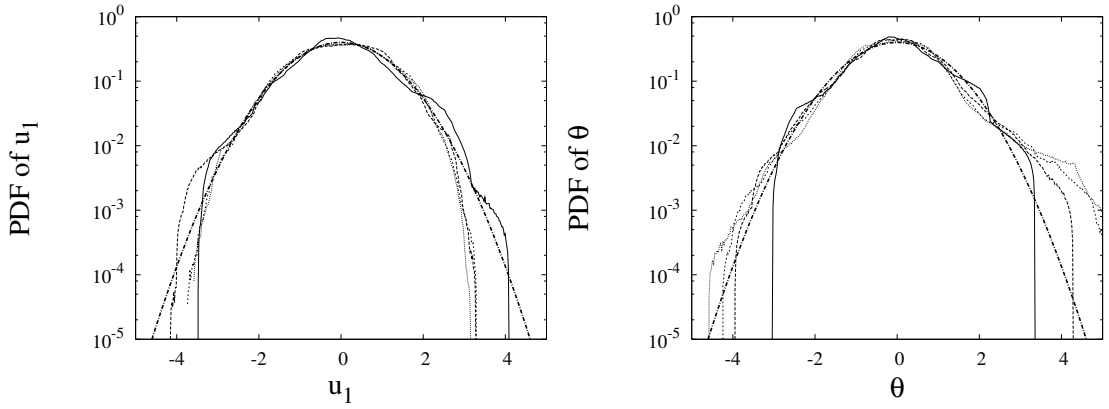

Figure 2.12: PDFs of a) the velocity component u_1 of the Navier-Stokes equations (left) and b) the passive scalar θ subject to the Navier-Stokes equations (right). Both are normalized to have unit variance: plotted at $t = 2$ (solid), 5 (dashed), 8 (short-dashed) and 10 (dotted). The thicker dot-dashed lines denote the standard normal distribution $N(0, 1)$.

2.4.2 Performance of enstrophy bounds

Here, we will consider the existing mathematical bounds for enstrophy growth. We will study their performance numerically, thereby quantifying the so-called depletion of nonlinearity. We define spatial integrals, which are *not* averaged by volume, as follows

$$E(t) = \frac{1}{2}\int |\boldsymbol{u}|^2 d\boldsymbol{x},\ Q(t) = \frac{1}{2}\int |\boldsymbol{\omega}|^2 d\boldsymbol{x} \text{ and } P(t) = \frac{1}{2}\int |\nabla \times \boldsymbol{\omega}|^2 d\boldsymbol{x}. \tag{2.22}$$

They correspond to squared L_2, H_1 and H_2 norms of the velocity, respectively.

It follows from the vorticity equation

$$\frac{\partial \boldsymbol{\omega}}{\partial t} + (\boldsymbol{u}\cdot\nabla)\boldsymbol{\omega} = (\boldsymbol{\omega}\cdot\nabla)\boldsymbol{u} + \nu\triangle\boldsymbol{\omega} \tag{2.23}$$

that

$$\frac{dQ}{dt} = \int \boldsymbol{\omega}\cdot(\nabla\boldsymbol{u})\cdot\boldsymbol{\omega} d\boldsymbol{x} - \nu\int |\nabla\times\boldsymbol{\omega}|^2 d\boldsymbol{x}. \tag{2.24}$$

By standard procedures we can derive an enstrophy bound [48]

$$\frac{dQ}{dt} \leq cQ^{3/4}P^{3/4} - 2\nu P \tag{2.25}$$

$$\leq \frac{c}{4}\nu^{-3}Q^3 - \frac{5}{4}\nu\frac{Q^2}{E(0)}. \tag{2.26}$$

(In inequalities in this chapter c denotes positive constants, which may be different from each other.) This is done in two steps: 1) applications of the Cauchy-Schwartz

and Gagliardo-Nirenberg inequalities to get (2.25) and 2) that of the Hölder inequality to get (2.26). The details may be found in, e.g. [25, 48] and here we recall step 2 only.

We have $a^p b^q \leq pa+qb$ for $a, b > 0$ with $0 < p, q < 1, p+q = 1$ by a version of the Hölder inequality. Thus we find $cQ^{3/4}P^{3/4} = (c^4\nu^{-3}Q^3)^{1/4}(\nu P)^{3/4} \leq \frac{c^4}{4}\nu^{-3}Q^3 + \frac{3}{4}\nu P$. By the Cauchy-Schwartz inequality, we have $Q^2 \leq EP$ or $P \geq \frac{Q^2}{E} \geq \frac{Q^2}{E(0)}$. Renaming c^4 as c, we obtain (2.26). This procedure breaks down in the four dimensional case $d = 4$ (see below) because we cannot take p or q to be equal to 1.

The well-known bound (2.26) has been discussed numerically in the literature, e.g. [48, 49, 50, 51, 52]. We note also that in the one-dimensional case we have

$$\frac{dQ}{dt} \leq c\nu^{-1/3}Q^{5/3} - 2\nu P, \tag{2.27}$$

which was studied in [42] and [48].

To study how the performance of mathematical estimates depend on the governing equations and the spatial dimensions they are defined in, we also consider the so-called quasi-4D (sometimes called 3.5D) Navier-Stokes equations. This class is defined by the following principle:
If $\boldsymbol{u}$ solves the 3D Navier-Stokes equations and θ is the passive scalar subject to it, then by setting

$$\boldsymbol{u}_{4D} = \begin{pmatrix} \boldsymbol{u}(x_1, x_2, x_3, t) \\ \theta(x_1, x_2, x_3, t) \end{pmatrix}, \tag{2.28}$$

$\boldsymbol{u}_{4D}$ solves the 4D Navier-Stokes equations because $\frac{\partial p}{\partial x_4} = 0$ [53]. It is a very special class of higher-dimensional Navier-Stokes flows, yet is physically relevant because the fourth component is a passive scalar. Care should be taken that genuine 4D Navier-Stokes flows cannot be formed by this construction. With this reservation, it is still of interest what scaling behaviors the 3.5D Navier-Stokes flows exhibit. More general 4D Navier-Stokes equations have been discussed in a number of different contexts, see [54, 55, 56, 57, 58, 59, 60, 61].

We note that Q has $[L^d T^{-2}]$ and ν has $[L^2 T^{-1}]$ as physical dimensions, where L, T denote length and time, respectively. We thus find on dimensional grounds in d-dimensions as a counterpart to (2.26),

$$\frac{dQ}{dt} \leq c\nu^{-\frac{d}{4-d}}Q(t)^{\frac{6-d}{4-d}}, \tag{2.29}$$

for $d < 4$ we kept the contribution from the nonlinear term only. Thus, as known

in the folklore of mathematical fluid dynamics, at $d = 4$ the exponent $\frac{6-d}{4-d}$ becomes divergent and the bound becomes useless [62].

However, step 1 yields a bound in d-dimensions

$$\frac{dQ}{dt} + 2\nu P \leq cQ^{\frac{6-d}{4}} P^{\frac{d}{4}}, \tag{2.30}$$

which is still valid at $d = 4$. For the 4D Navier-Stokes equations, we have for the enstrophy bound

$$\frac{dQ}{dt} \leq cQ^{1/2}P - 2\nu P.$$

The mathematical results are summarized in the second column of Table 2.2. We understand that in one dimension we redefine $E(t), Q(t)$ and $P(t)$, respectively by

$$E(t) = \frac{1}{2}\int u^2 dx,\ Q(t) = \frac{1}{2}\int (\partial_x u)^2 dx, \text{ and } P(t) = \frac{1}{2}\int (\partial_x^2 u)^2 dx. \tag{2.31}$$

Also, in four dimensions we replace $E(t)$ by $2\pi\left(E(t) + \frac{1}{2}\int |\theta|^2 \boldsymbol{dx}\right)$, $Q(t)$ by $2\pi\left(Q(t) + \frac{1}{2}\int |\nabla\theta|^2 \boldsymbol{dx}\right)$ and $P(t)$ by $2\pi\left(P(t) + \frac{1}{2}\int |\triangle\theta|^2 \boldsymbol{dx}\right)$, respectively. We examine performance of those bounds by numerical simulations.

We begin with the 1D Burgers equation under periodic boundary conditions

$$\frac{\partial u}{\partial t} + u\frac{\partial u}{\partial x} = \nu\frac{\partial^2 u}{\partial x^2} \tag{2.32}$$

with an initial condition

$$u(x, 0) = -\sin x \tag{2.33}$$

and viscosity $\nu = 5 \times 10^{-3}$. In view of

$$\frac{dQ}{dt} + 2\nu P \leq cQ^{5/4}P^{1/4}, \tag{2.34}$$

we plot in Fig.2.13 $\frac{dQ}{dt} + 2\nu P$ against $Q^{5/4}P^{1/4}$. Here we have estimated $\frac{dQ}{dt}$ by a finite-difference scheme in time. It shows a clear linear behavior with a slope close to 1 and also with a prefactor close to 1. In this sense, the inequality (2.34) is in fact very close to an *equality*, that is, it is doing a good job. (See Appendix D for a result for other initial data).

We show a similar plot in Fig.2.14 for the 3D Navier-Stokes equations. Unlike the 1D Burgers equation, no linear behavior is observed.

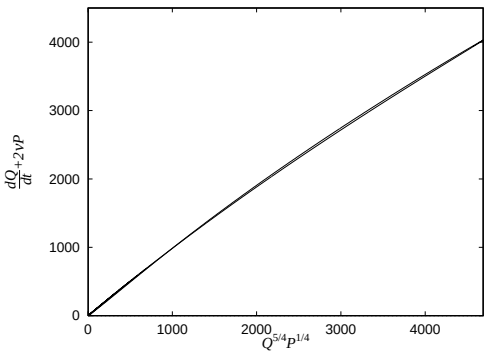

Figure 2.13: Enstrophy growth for the 1D Burgers equation.

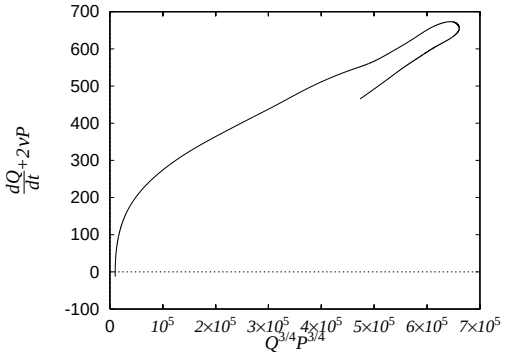

Figure 2.14: Enstrophy growth for the 3D Navier-Stokes equations.

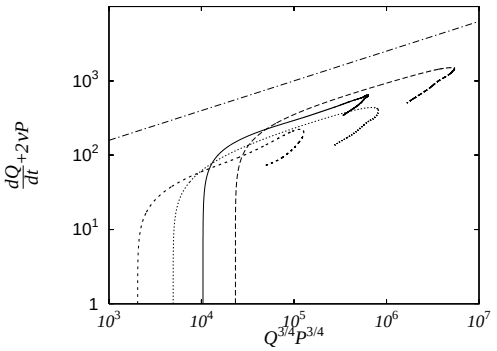

Figure 2.15: Enstrophy growth for the 3D (solid) and quasi-4D (dashed) Navier-Stokes equations. The straight line denotes a slope 0.4. Also included are enstrophy growth for the 3D (dotted) and quasi-4D (short-dashed) for the Taylor-Green initial condition (see the text for further discussion).

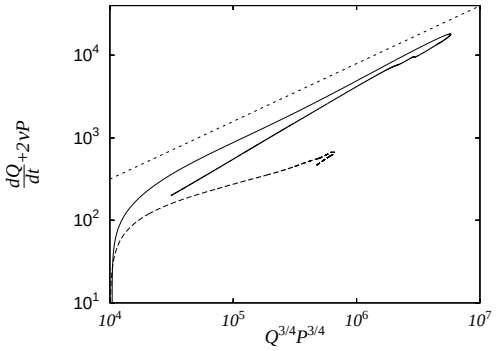

Figure 2.16: Enstrophy growth for the 3D Burgers equations (solid) and the 3D Navier-Stokes equations (dashed). The straight line denotes a slope 0.7.

In Fig.2.15 we try an alternative presentation, where $\frac{dQ}{dt} + 2\nu P$ is presented against $Q^{3/4}P^{3/4}$ in a log-log plot. It is noted that here we have a clear straight line behavior with a slope of about 0.4. In fact, the same scaling with the exponent is obtained even if we change the pseudo-random number sequences in the initial conditions (figures omitted).

In the same figure, a corresponding plot is made for the quasi-4D Navier-Stokes equations as well. It also shows a power-law with exponent 0.4. These power-law

behaviors imply that the bounds over-estimate the enstrophy growth excessively. Moreover, we can quantify the excess by determining the exponent, which may be regarded as a characterization of nonlinearity depletion. It is noted that the quasi-4D Navier-Stokes equations share the same exponent 0.4 with the 3D Navier-Stokes equations. One explanation for this is that the quasi-4D Navier-Stokes equations are essentially three-dimensional in character. We expect that if we do the same experiment using the genuine 4D Navier-Stokes equations they would show more depletion, with exponent < 0.7.

In Fig.2.16 we compare the 3D Navier-Stokes with the 3D Burgers equations, using a similar log-log plot. The 3D Burgers equations show a similar power law behavior, but with an exponent 0.7 which is closer to 1 than that of 3D Navier-Stokes equations. This implies that while the bound over-estimates the enstrophy growth in 3D Burgers equations as well, the excess is not large in comparison with the 3D Navier-Stokes equations. In Fig.2.17, we put all the cases in one figure, where we can grasp the excesses of the mathematical bounds for different cases intuitively. Basically, as the graph is shifted to the right and the slope becomes shallower, the bounds over estimate the reality drastically.

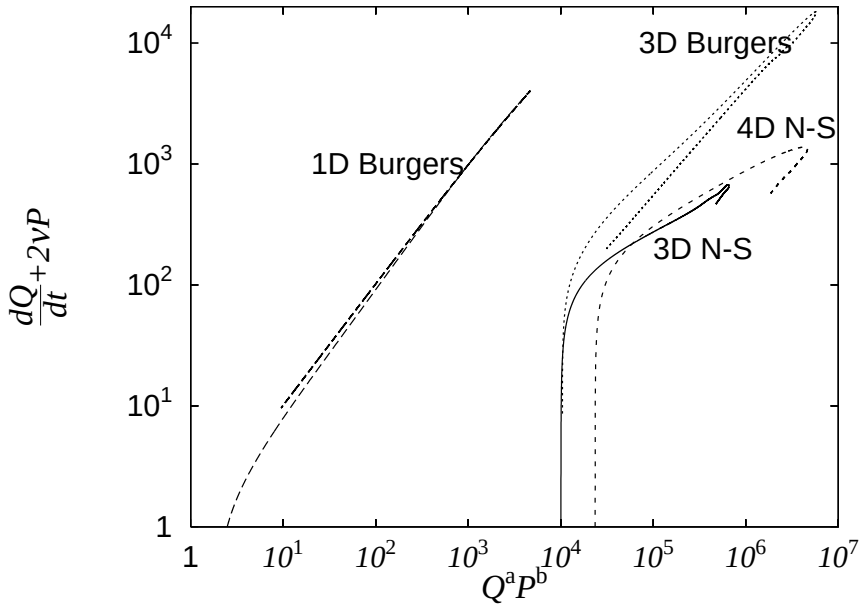

Figure 2.17: Enstrophy growth for the 1D and 3D Burgers equations and for the 3D and quasi-4D Navier-Stokes equations.

Finally, we show a result of comparison of the 3D Navier-Stokes with Burgers

Table 2.2: Navier-Stokes and Burgers equations

Equations	Mathematical bounds	Numerics	Verdict
1D Burgers	$\frac{dQ}{dt} + 2\nu P \leq cQ^{5/4}P^{1/4}$	$\frac{dQ}{dt} + 2\nu P \approx Q^{5/4}P^{1/4}$	Good
3D Navier-Stokes	$\frac{dQ}{dt} + 2\nu P \leq cQ^{3/4}P^{3/4}$	$\frac{dQ}{dt} + 2\nu P \propto \left(Q^{3/4}P^{3/4}\right)^{0.4}$	Over-estimate
3D Burgers	$\frac{dQ}{dt} + 2\nu P \leq cQ^{3/4}P^{3/4}$	$\frac{dQ}{dt} + 2\nu P \propto \left(Q^{3/4}P^{3/4}\right)^{0.7}$	Intermediate
Quasi-4D Navier-Stokes	$\frac{dQ}{dt} + 2\nu P \leq cQ^{1/2}P$	$\frac{dQ}{dt} + 2\nu P \propto \left(Q^{1/2}P\right)^{0.4}$	Over-estimate

equations using another initial condition (the Taylor-Green vortex). This is defined as follows

$$\begin{cases} u_1 = \cos x \sin y \sin z, \\ u_2 = -\sin x \cos y \sin z, \\ u_3 = 0. \end{cases} \tag{2.35}$$

In Fig.2.18a we compare energy norms. We see that the solenoidal component decays very quickly to zero. At late times, the entire flow field is dominated by the potential part. In terms of the enstrophy, the solenoidal part does not increase at all, but it monotonically decreases to zero (Fig.2.18b). For the Navier-Stokes equations, the enstrophy attains its peak later and the peak value is lower than that of the Burgers equations. The dominance of the potential component is even more prominent in the case of Taylor-Green initial condition.

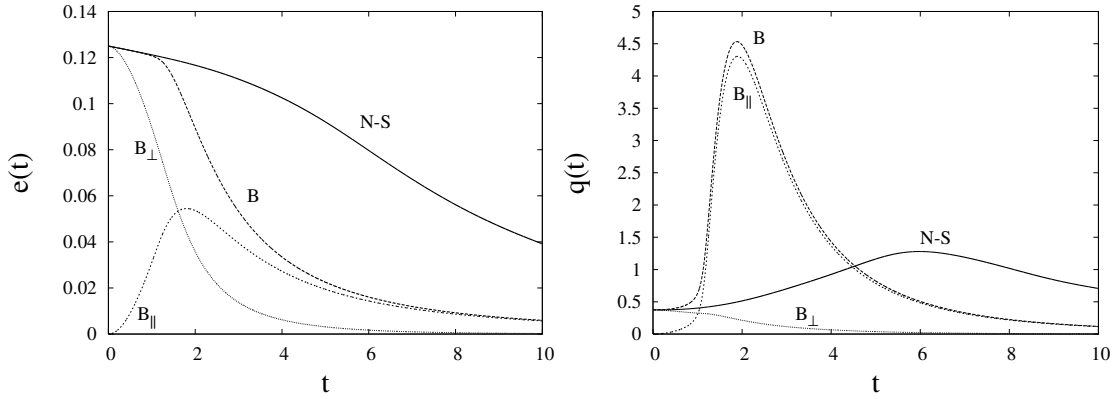

Figure 2.18: Comparison of the norms for the Navier-Stokes and Burgers equations for the Taylor-Green vortex: (a) the energy (left) and (b) the enstrophy (right). Labels are as in Fig.2.1.

To conclude this section we comment on robustness of the power-laws found here. We have already mentioned that for different random initial conditions we observe the same power-laws. We point out that the power-law behavior (with $\alpha = 0.4$) is

also observed for the Taylor-Green vortex, both with 3D and quasi-4D Navier-Stokes equations where we take $\theta = u_1$ initially, see Fig.2.15. Because it is a flow developing from a completely different initial condition, this indicates that such a power-law holds for a wider class of initial data. More work needs to be done to investigate how robust the scaling is.

2.5 Summary and Discussion

In this chapter we have compared the Navier-Stokes equations with the Burgers equations and that of a passive scalar, centering on the effect of the absence or presence of the maximum principle.

In the PDF of the velocity, the Burgers equations have limited excitations at large amplitude, whereas the Navier-Stokes equations' wings are spread close to a Gaussian distribution. Breakdown of a maximum principle for the Navier-Stokes equations is due to the term $-\boldsymbol{u} \cdot \nabla p$ in the energy budget. Its PDF is basically symmetric, so are the joint PDFs of $-\boldsymbol{u} \cdot \nabla p$ with $\frac{1}{2}|\boldsymbol{u}|^2$ and $\frac{1}{2}|\boldsymbol{\omega}|^2$. This term neither contributes to enhance nor to avoid singularity formations, but simply makes the maximum principle invalid.

We have studied a passive scalar by initializing it as one component of the velocity, again to see the effect of the pressure term. Their deviation is maximized in the L^2-norm, at a time between the peak times of the enstrophy and the average of the squared passive scalar gradient.

Finally, we have introduced a method for estimating performance of the enstrophy bounds (that is, a log-log plot at step 1) and tested it against numerical experiments. This includes the quasi-4D Navier-Stokes equations using the passive scalar as the fourth component. In contrast to the 1D Burgers equation, for the 3D Burgers equations the bound over-estimates the enstrophy growth to some degree. In the 3D and 4D Navier-Stokes equations, the excess is more significant. Thus the bounds are less sharp in higher dimensions and under the incompressible condition.

Let us consider an analogy. In [8] it was shown that if $\tilde{E}(k) \propto k^{-n}, n > \frac{8}{3}$ then the energy spectral flux $\Pi(k) \to 0$ as $k \to \infty$ using flows with finite total kinetic energy. Here $\tilde{E}(k)$ denotes the energy spectrum based on the total energy. Indeed, if we use the total kinetic energy for dimensional analysis we would get [8]

$$\tilde{E}(k) \propto \tilde{\epsilon}^{2/3} k^{-8/3} \tag{2.36}$$

for the energy spectrum, where $\tilde{\epsilon}$ is the dissipation rate of total kinetic energy. Note that here $\tilde{E}(k)$ is an extensive variable, that is, it grows in proportion to its volume. This scaling is also consistent with global weak solutions of the Navier-Stokes equations, see [63].

Later, in connection with Onsager conjecture, a $r^{1/3}$-behavior was derived in [64] using Besov space techniques (see also [65]). This of course is consistent with the Kolmogorov scaling

$$E(k) \propto \epsilon^{2/3} k^{-5/3}, \tag{2.37}$$

if we use energy and energy dissipation rate per unit volume, which are intensive variables themselves.

Standard mathematical analyses use extensive variables, such as the total enstrophy $Q(t)$ to find

$$\frac{dQ}{dt} \leq c\frac{Q^3}{\nu^3}, \tag{2.38}$$

However, if we use instead the enstrophy $q(t)$ per unit volume, we find

$$\frac{dq}{dt} \leq cq^{3/2} \tag{2.39}$$

in *any* spatial dimensions. Note that we may derive the above using the Karman-Howarth equation under the assumption of constancy of the skewness factor (see e.g. [51]). This suggests a possibility that using an intensive variable may improve the situation. Indeed, an envelope of volume averaged enstrophy follows (2.39), see [51]. Pursuing this line of analysis looks interesting, although it is yet to be justified.

Chapter 3

Intermittency and local Reynolds number in Navier-Stokes turbulence: a cross-over scale in the Caffarelli-Kohn-Nirenberg integral

Abstract

We study space-time integrals which appear in Caffarelli-Kohn-Nirenberg (CKN) theory for the Navier-Stokes equations analytically and numerically. The key quantity is written in standard notations $\delta(r) = 1/(\nu r)\int_{Q_r} |\nabla \boldsymbol{u}|^2 \, d\boldsymbol{x}\, dt$, which can be regarded as a local Reynolds number over a parabolic cylinder Q_r.

First, by re-examining the CKN integral we identify a cross-over scale $r_* \propto L\left(\frac{\overline{\|\nabla \boldsymbol{u}\|_{L^2}^2}}{\|\nabla \boldsymbol{u}\|_{L^\infty}^2}\right)^{1/3}$, at which the CKN Reynolds number $\delta(r)$ changes its scaling behavior. This reproduces a result on the minimum scale $r_{\min}$ in turbulence: $r_{\min}^2 \|\nabla \boldsymbol{u}\|_\infty \propto \nu$, consistent with a result of Henshaw *et al.* (1989). For the energy spectrum $E(k) \propto k^{-q}$ $(1 < q < 3)$, we show that $r_* \propto \nu^a$ with $a = \frac{4}{3(3-q)} - 1$. Parametric representations are then obtained as $\|\nabla \boldsymbol{u}\|_\infty \propto \nu^{-(1+3a)/2}$ and $r_{\min} \propto \nu^{3(a+1)/4}$. By the assumptions of the regularity and finite energy dissipation rate in the inviscid limit, we derive $\lim_{p\to\infty} \frac{\zeta_p}{p} = 1 - \zeta_2$ for any phenomenological models on intermittency, where ζ_p is the exponent of p-th order (longitudinal) velocity structure function. It follows that $\zeta_p \le (1-\zeta_2)(p-3) + 1$ for any $p \ge 3$ *without* invoking fractal energy cascade.

Second, we determine the scaling behavior of $\delta(r)$ in direct numerical simulations of the Navier-Stokes equations. In isotropic turbulence around $R_\lambda = 100$ starting from random initial conditions, we have found that $\delta(r) \propto r^4$ *throughout the inertial range*. This can be explained by the smallness of $a \approx 0.26$. If the β-model is perfectly correct, the intermittency parameter a is related to the dissipation correlation exponent μ as $\mu = \frac{4a}{1+a} \approx 0.8$ which is larger than the observed $\mu \approx 0.20$. Corresponding integrals are studied using the Burgers vortex and the Burgers equations. The scale r_* offers a practical method of estimating intermittency.

This paper also sorts out a number of existing mathematical bounds and phenomenological models on the basis of the CKN Reynolds number.

3.1 Introduction

The question of regularity of the three-dimensional Navier-Stokes equations is one of the most prominent unsolved problems in mathematics. The relevance of this issue exceeds that of pure mathematics, as the equations themselves represent an important physical process of turbulence. The integrity of this model, and our interpretation of the related physics involved, thus rests on whether the equations do admit unique classical solutions.

It is well-known that in the two-dimensional case the regularity is maintained with unique smooth solutions being defined for all time. This is the case because the quantity $\|\boldsymbol{\omega}\|_{L^2}^2$ is bounded from above for all time. In the case of three dimensions, however, this is known to hold for short time intervals only, assuming sufficiently smooth initial conditions. This cannot be guaranteed for an arbitrary time interval due to the vortex-stretching term, which is absent in two dimensions. At high Reynolds numbers, where turbulence becomes pronounced, the possibility that the Navier-Stokes equations may develop finite time singularities cannot be ruled out [23, 24, 25, 27, 43].

There have been many previous attempts to tackle the regularity problem, notably Leray [14], who first introduced the concept of weak solutions, followed by Hopf [16]. Later Scheffer [17], subsequently refined by Caffarelli, Kohn and Nirenberg (hereafter, CKN) [18], set limits on the dimension of the possible singular set of solutions. Others have produced a range of global weak, and local or particular strong solutions, but the existence of global classical solutions has not yet been established for general smooth initial conditions.

This mathematical problem is connected with the problem of turbulence. A conventional picture of energy cascade in 3D Navier-Stokes turbulence goes as follows. For a flow with huge Reynolds number $Re = UL/\nu > Re_{\rm cr}$, where U, L, ν and Re_{cr} denote the velocity, length scale, kinematic viscosity and critical Reynolds number, respectively, the large-scale disturbances are subject to instability and they generate disturbances with a length scale l_1 and velocity scale v_1. The corresponding Reynolds number $Re_1 = v_1 l_1/\nu$ is still large and first-order disturbances are unstable and break down, resulting in smaller length l_2 and velocity v_2, whose Reynolds number is $Re_2 = v_2 l_2/\nu$. This process continues until $Re_N = v_n l_n/\nu$ becomes $O(1)$, or on the order of $Re_{\rm cr}$. In a nutshell, the regularity can be monitored by watching a suitably defined local Reynolds number. The CKN criterion was originally devel-

oped for testing the regularity of Navier-Stokes flows, but here we will show how useful it is in the characterization of intermittency in turbulence. See also [66] for another approach to intermittency.

In recent years, much progress has been made, both analytically (see in particular [24], [29] and [32]) and numerically. There have been numerous contributions to the field from the latter perspective, of which mention here only a few closely related to the main focus of the present paper. In particular, studies of possible singularities [33, 34, 35] and the monitoring of enstrophy and vorticity growth rates [48, 51]. See also [6, 19, 28, 30, 31, 15, 36, 38, 47, 49, 50, 67, 68] for various aspects of the Navier-Stokes equations.

In Section 3.2 we introduce the equations that will be the main subject of study of the paper. Section 3.3 presents numerical results on the scaling of the CKN integral. Section 3.4 gives examples by exact solutions. Section 3.5 is devoted to a summary and discussion.

3.2 Mathematical Formulation

3.2.1 Caffarelli-Kohn-Nirenberg integrals

The three-dimensional Navier-Stokes equations

$$\frac{\partial \boldsymbol{u}}{\partial t} + (\boldsymbol{u} \cdot \nabla)\boldsymbol{u} = -\nabla p + \nu \nabla^2 \boldsymbol{u} + \boldsymbol{F}, \tag{3.1}$$

together with the continuity equation

$$\nabla \cdot \boldsymbol{u} = 0, \tag{3.2}$$

describe the motion of viscous incompressible fluids, where $\boldsymbol{u}$ denotes the fluid velocity, p the pressure, ν the kinematic viscosity and $\boldsymbol{F}$ the external body force, with appropriate initial and boundary conditions.

These equations can be transformed into vorticity equations

$$\frac{\partial \boldsymbol{\omega}}{\partial t} + (\boldsymbol{u} \cdot \nabla)\boldsymbol{\omega} = (\boldsymbol{\omega} \cdot \nabla)\boldsymbol{u} + \nu \nabla^2 \boldsymbol{\omega} + \nabla \times \boldsymbol{F}, \tag{3.3}$$

where $\boldsymbol{\omega} = \nabla \times \boldsymbol{u}$ is the vorticity.

The function $\delta(r)$ is a local average of $\nabla \boldsymbol{u}$ over a parabolic cylinder. This non-dimensional quantity is defined by the space-time integral

$$\delta(r) = \frac{1}{\nu r} \int_{Q_r} |\nabla \boldsymbol{u}|^2 \, d\boldsymbol{x}\, dt, \tag{3.4}$$

where r is the distance from the center point $\boldsymbol{x}_0$. The integral is taken over the space-time region, a parabolic cylinder,

$$Q_r(\boldsymbol{x},t) = \left\{ (\boldsymbol{x},t) : \, |\boldsymbol{x}-\boldsymbol{x}_0| < r, \, t_0 < t < t_0 + \frac{r^2}{\nu} \right\}, \tag{3.5}$$

where $\boldsymbol{x} = (x,y,z)$, with a center point $\boldsymbol{x}_0 = (x_0,y_0,z_0)$ and reference time t_0.

According to the CKN theory [18, 19, 28], if $\delta(r) \le \epsilon_{CKN}$ near $(\boldsymbol{x}_0,t_0)$, where ϵ_{CKN} is a positive constant, then $(\boldsymbol{x}_0,t_0)$ is a regular point, that is, the velocity must be bounded there. In fact, the CKN theory refines Scheffer's previous estimate [17], to show that the Hausdorff dimension of the possible singular sets of velocity in $(3+1)$-dimensional space-time does not exceed 1. See [69, 70] for more recent works.

We may interpret $\delta(r)$ as the local Reynolds number as follows [28]

$$Re = \frac{r^2}{\nu}\left(\frac{1}{|Q_r|}\int_{Q_r} |\nabla \boldsymbol{u}|^2 \, d\boldsymbol{x}\, dt \right)^{1/2} = \left(\frac{3}{4\pi}\delta(r) \right)^{1/2}. \tag{3.6}$$

We will study the following questions: What kind of scaling behavior do we expect for $\delta(r)$? and in which range are these power-laws observed ?

We consider a theory for the case of $\mathbb{R}^3$ first and then translate the result to the case of $\mathbb{T}^3$ or homogeneous turbulence. Let us consider the total kinetic energy, the enstrophy and the energy dissipation rate

$$E' = \int_{\mathbb{R}^3} \frac{|\boldsymbol{u}|^2}{2} d\boldsymbol{x}, \; Q' = \int_{\mathbb{R}^3} \frac{|\nabla \boldsymbol{u}|^2}{2} d\boldsymbol{x}, \; \epsilon' = \nu \int_{\mathbb{R}^3} |\nabla \boldsymbol{u}|^2 d\boldsymbol{x},$$

where $'$ denotes un-averaged spatial integrals in $\mathbb{R}^3$.

We examine the power-laws for $\delta(r)$ by examining the definition (3.4). The volume of the parabolic cylinder (3.5) is $|Q_r| = 4\pi r^3/3 \cdot r^2/\nu = 4\pi r^5/3\nu$. A normalization of (3.4) over the volume gives

$$\delta(r;\boldsymbol{x}_0,t_0) = \frac{4\pi}{3}\frac{r^4}{\nu^2}\frac{1}{|Q_r|}\int_{Q_r} |\nabla \boldsymbol{u}|^2 \, d\boldsymbol{x}\, dt,$$

which means that in the limit of $r \to 0$ we have

$$\delta(r) \to \frac{4\pi}{3}\frac{r^4}{\nu^2} |\nabla \boldsymbol{u}|^2 (\boldsymbol{x}_0,t_0), \tag{3.7}$$

picking up a point-wise value of the strain rate at $(\boldsymbol{x}_0,t_0)$. On the other hand, in the limit of $r \to \infty$ we have

$$\delta(r) \to \frac{r}{\nu^2}\frac{1}{r^2/\nu}\int_{t_0}^{t_0+r^2/\nu} dt \int_{\mathbb{R}^3} |\nabla \boldsymbol{u}|^2 \, d\boldsymbol{x} = \frac{r}{\nu^2}\overline{\int_{\mathbb{R}^3} |\nabla \boldsymbol{u}|^2 \, d\boldsymbol{x}}, \tag{3.8}$$

where the bar denotes a long time-average. Hence, the function $\delta(r)$ shows two distinctive behaviors and the cross-over takes place at $r = r_*$, where

$$r_* = \left(\frac{3}{4\pi} \frac{\overline{\int_{\mathbb{R}^3} |\nabla \boldsymbol{u}|^2 \, d\boldsymbol{x}}}{\|\nabla \boldsymbol{u}\|_\infty^2} \right)^{1/3} = \left(\frac{3}{4\pi} \frac{\overline{\epsilon'}}{\nu \|\nabla \boldsymbol{u}\|_\infty^2} \right)^{1/3}. \tag{3.9}$$

Here we have taken the point $(\boldsymbol{x}_0, t_0)$ as the point of maximum $|\nabla \boldsymbol{u}|^2$, which is equal to $|\nabla \boldsymbol{u}\|_\infty^2$ [25]. Because small-scale structure of finite-energy turbulence is expected to be not much different from that of homogeneous turbulence [8], the above expression translates to

$$r_* = L \left(\frac{3}{4\pi} \frac{\frac{1}{L^3}\overline{\int_{\mathbb{T}^3} |\nabla \boldsymbol{u}|^2 \, d\boldsymbol{x}}}{\|\nabla \boldsymbol{u}\|_\infty^2} \right)^{1/3} = L \left(\frac{3}{4\pi} \frac{\overline{\epsilon}}{\nu \|\nabla \boldsymbol{u}\|_\infty^2} \right)^{1/3} \tag{3.10}$$

in the case of $\mathbb{T}^3$. Here $\epsilon = \frac{\nu}{L^3} \int_{\mathbb{T}^3} |\nabla \boldsymbol{u}|^2 \, d\boldsymbol{x}$ is the energy dissipation rate averaged over a cube of size L. From the above we can see that as the numerator is the temporal average of the L^2 norm of $|\nabla \boldsymbol{u}|^2$ and the denominator is its L^∞ norm (or maximum value), therefore a smaller r_* implies more intermittency. Solving (3.10) for $\|\nabla \boldsymbol{u}\|_\infty$, we find

$$\|\nabla \boldsymbol{u}\|_\infty \approx \sqrt{\frac{3}{4\pi}} \sqrt{\frac{\overline{\epsilon}}{\nu}} \left(\frac{L}{r_*} \right)^{3/2}. \tag{3.11}$$

Plugging this into (3.7) and assuming that the maximum strain is attained at $\boldsymbol{x}_0$, we find

$$\delta(r) \approx \left(\frac{L}{r_*} \right)^3 \frac{\overline{\epsilon} r^4}{\nu^3} \tag{3.12}$$

for small r. By demanding that $\delta(r_{\min}) = 1$, we determine the smallest scale excited in the flow as

$$r_{\min} \approx \left(\frac{\nu^3}{\overline{\epsilon}} \right)^{1/4} \left(\frac{r_*}{L} \right)^{3/4}. \tag{3.13}$$

Eliminating r_* from (3.11) and (3.13), we obtain a condition

$$r_{\min}^2 \|\nabla \boldsymbol{u}\|_\infty \propto \nu.$$

This is equivalent to a rigorous result on the estimate of the smallest length scale in turbulence [25, 71, 72]

$$r_{\min} \propto \sqrt{\frac{\nu}{\|\nabla \boldsymbol{u}\|_\infty}}.$$

It is defined as a reciprocal of the wavenumber therein, beyond which Fourier coefficients decay exponentially. See also [73] on how the minimum scale is affected by intermittency. In what follows, we will write simply ϵ for $\overline{\epsilon(t)}$ because its temporal fluctuations are not large.

3.2.2 The ν-dependence of r_*

We show that a power-law of r_* follows from that of $E(k)$. The following assumptions are made in the subsequent argument.

1. The energy dissipation rate ϵ and viscosity ν are independent in the inviscid limit.

2. The energy spectrum follows $E(k) \propto k^{-q}$ in the inertial subrange, with $1 < q < 3$.

3. An ensemble and a spatial average are equal (ergodic hypothesis).

4. The velocity gradient is finite for a small, but fixed ν.

We write

$$\frac{r_*}{L} = F(\nu),$$

because if F were independent of ν, we would have non-intermittent turbulence (K41). We have therefore

$$\|\nabla \boldsymbol{u}\|_\infty \propto \sqrt{\frac{\epsilon}{\nu}} F(\nu)^{-3/2} \tag{3.14}$$

and

$$r_{\min} \approx \left(\frac{\nu^3}{\epsilon}\right)^{1/4} F(\nu)^{3/4}. \tag{3.15}$$

By the assumptions 1), 2) and the definition of ϵ

$$\epsilon = 2\nu \int_0^{k_d} k^2 E(k) dk$$

together with $k_d = 1/r_{\min}$, we have

$$\epsilon \approx \frac{2\nu}{3-q} \left(\left(\frac{\nu^3}{\epsilon}\right)^{-\frac{1}{4}} F(\nu)^{-\frac{3}{4}} \right)^{3-q}.$$

It follows that

$$F(\nu) \approx \left(\frac{2}{3-q}\frac{\nu}{\epsilon}\right)^{\frac{4}{3(3-q)}} \left(\frac{\nu^3}{\epsilon}\right)^{-\frac{1}{3}},$$

that is,

$$F(\nu) \propto \nu^a,$$

where

$$a \equiv \frac{4}{3(3-q)} - 1. \tag{3.16}$$

Thus, r_* also has a power-law dependence on ν. Inverting (3.16) we obtain

$$q = \frac{5+9a}{3(1+a)}. \tag{3.17}$$

3.2.3 Parametrization of intermittency via a

By writing

$$\frac{r_*}{L} = \left(\frac{\eta}{L}\right)^{4a/3} \propto \nu^a,$$

where η denotes the Kolmogorov length scale, we find from (3.11) and (3.13)

$$\|\nabla \boldsymbol{u}\|_\infty \approx \sqrt{\frac{3}{4\pi}}\sqrt{\frac{\epsilon}{\nu}}\left(\frac{L}{\eta}\right)^{2a}, \tag{3.18}$$

and

$$r_{\min} \approx \eta\left(\frac{\eta}{L}\right)^a \tag{3.19}$$

as parameterizations of the maximum strain and the minimum scale excited in turbulence. We also note in passing that Kolmogorov velocity (with intermittency effect taken into account) is given by

$$v_{\mathrm{Kol}} \propto (\epsilon\nu)^{1/4}\left(\frac{L}{\eta}\right)^a$$

and acceleration A by

$$A \propto \frac{v_{\mathrm{Kol}}^3}{\nu}.$$

To summarize, in terms of a we have the following parametrizations

$$\|\nabla \boldsymbol{u}\|_\infty \propto \nu^{-\frac{1+3a}{2}},\ r_{\min} \propto \nu^{\frac{3(a+1)}{4}},\ r_* \propto \nu^a. \tag{3.20}$$

Under the assumption of the β-model [7], we can write

$$\|\nabla \boldsymbol{u}\|_\infty \propto \nu^{-\frac{5-D}{1+D}},\ r_{\min} \propto \nu^{\frac{3}{1+D}},\ r_* \propto \nu^{\frac{3-D}{1+D}} \tag{3.21}$$

in terms of the self-similarity dimension D. Equivalently, under the same assumption, using the exponent of dissipation correlation $\mu = 3 - D$, we have

$$\|\nabla \boldsymbol{u}\|_\infty \propto \nu^{-\frac{2+\mu}{4-\mu}},\ r_{\min} \propto \nu^{\frac{3}{4-\mu}},\ r_* \propto \nu^{\frac{\mu}{4-\mu}}. \tag{3.22}$$

Note that the parametrization in terms of a does not require the assumption of fractal cascade. In Table 3.1 we compare some phenomenological models of intermittency [7, 8, 74]. In [74], the distribution of Lyapunov exponents for the Navier-Stokes equations was studied and its behavior was found to change at $\mu = 2/5$ on the basis of the β-model. In [75], a model of intermittency was developed on the basis of log-Poisson statistics of the energy dissipation rate (see Appendix E), which shows agreement with experiments. The relationship $a = \mu/(4 - \mu)$ is depicted in Fig.3.1.

Table 3.1: Comparison of models of intermittency

	General	K41	Ruelle	She-Leveque (SL)	Burgers	Sulem-Frisch (SF)
Intermittency exponent	a	0	1/9	1/5	1/3	3
D	$\frac{3-a}{1+a}$	3	13/5	7/3	2	0
μ	$\frac{4a}{1+a}$	0	2/5	2/3	1	3
$\|\nabla \boldsymbol{u}\|_\infty$	$\nu^{-(1+3a)/2}$	$(\epsilon/\nu)^{1/2}$	$\nu^{-2/3}$	$\nu^{-4/5}$	ν^{-1}	ν^{-5}
$r_{\min}$	$\nu^{3(a+1)/4}$	$\eta = (\nu^3/\epsilon)^{1/4}$	$\nu^{5/6}$	$\nu^{9/10}$	ν	ν^3
v_{Kol}	$\nu^{(1-3a)/4}$	$(\epsilon\nu)^{1/4}$	$\nu^{1/6}$	$\nu^{1/10}$	ν^0	ν^{-2}
Hölder continuity	$C^{\frac{1-3a}{3(1+a)}}$	$C^{1/3}$	$C^{1/5}$	$C^{1/9}$	C^0	$C^{-2/3}$
$E(k) \propto k^{-q}$	$q = \frac{5+9a}{3(1+a)}$	$q = 5/3$	$q = 9/5$	$q \approx 5/3 + 0.03 < 17/9$	$q = 2$	$q = 8/3$

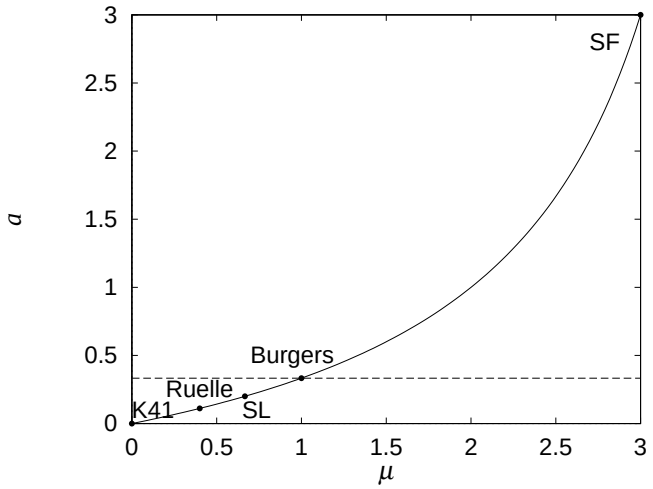

Figure 3.1: The a-μ diagram, with relationship $a = \frac{\mu}{4-\mu}$. The horizontal line denotes $a = 1/3$.

3.2.4 A constraint on the scaling exponents

We derive one constraint on the p-th order scaling exponents ζ_p for the velocity structure function (for theory see [4])

$$\langle (\delta u_r)^p \rangle \propto r^{\zeta_p},$$

where δu_r is the velocity increment between two points separated by r and the angled brackets denote an ensemble average.

Again, by 1),

$$\epsilon = 2\nu \int_0^{k_d} k^2 E(k) dk$$

is independent of ν in the limit $\nu \to 0$. Because k_d is related with the L^∞-norm of the velocity gradient and $E(k)$ with the L^2-norm, it should give a constraint on ζ_p. We will determine what this is.

By the definition

$$\left\langle \left(\frac{\delta u_r}{r} \right)^p \right\rangle^{\frac{1}{p}} \propto r^{\frac{\zeta_p}{p}-1},$$

with [76] we have

$$\|\nabla \boldsymbol{u}\|_{L^p} = \lim_{r \to r_{\min}} \left\langle \left(\frac{\delta u_r}{r} \right)^p \right\rangle^{\frac{1}{p}} \propto \nu^{\frac{3(a+1)}{4}\left(\frac{\zeta_p}{p}-1\right)}$$

and

$$\|\nabla \boldsymbol{u}\|_{L^\infty} = \lim_{p\to\infty} \lim_{r\to r_{\min}} \left\langle \left(\frac{\delta u_r}{r}\right)^p \right\rangle^{\frac{1}{p}} \propto \nu^{\frac{3(a+1)}{4}(\alpha-1)}, \tag{3.23}$$

where $\alpha \equiv \lim_{p\to\infty} \frac{\zeta_p}{p}$ is finite by 2) [77]. Here we essentially make use of the regularity of the Navier-Stokes solutions. An asymptotic linearity of ζ_p follows from the finiteness of α. In fact, we can obtain a more precise expression for the exponents.

By (3.23) and $(3.20)_1$, we find in the limit of $\nu \to 0$

$$\alpha = \frac{1-3a}{3(1+a)}. \tag{3.24}$$

(It is of interest to note that $a = \dfrac{1-3\alpha}{3(1+\alpha)}$, hence the inverse has the same functional form). Because of $E(k) \propto k^{-q}$ and (3.17) and the definition $q = 1 + \zeta_2$, we have

$$\zeta_2 + 1 = \frac{5+9a}{3(1+a)}. \tag{3.25}$$

Eliminating a between (3.24) and (3.25), we obtain

$$\zeta_2 + \lim_{p\to\infty} \frac{\zeta_p}{p} = 1. \tag{3.26}$$

Up to here, fractal energy cascade such as in the β-model is *not* assumed. The condition (3.26) implies

$$\zeta_p = (1-\zeta_2)p + o(p) \tag{3.27}$$

for large p. A super-linear behavior in ζ_p, as in the log-normal model, is thus excluded by finiteness of α. In other words, this argument supports an asymptotic linear behavior of the scaling exponent predicted in the β-model. See [78] for 'asymptotic linearization' of scaling exponents in more general cases.

A simple inequality for ζ_p follows from this. Setting

$$\zeta_p = (1-\zeta_2)p + f_p, \quad \text{with} \quad \lim_{p\to\infty} f_p = 0,$$

we have $f_3 = 1 - 3(1-\zeta_2)$ by $\zeta_3 = 1$. By the convexity $f_p \le f_3$ for $p \ge 3$, we find

$$\zeta_p \le (1-\zeta_2)(p-3) + 1. \tag{3.28}$$

We note that the prediction from the β-model

$$\zeta_p = \frac{p}{3} - \frac{\mu}{3}(p-3)$$

satisfies (3.26) for arbitrary $\mu(>0)$, that is, we cannot fix μ by the 'constraint' (3.26), as it becomes an identity.

If $\zeta_2 = \frac{2}{3}$, (3.28) implies that

$$\zeta_p \leq \frac{p}{3}, \text{ for any } p \geq 3.$$

On the other hand, if $\zeta_2 = \frac{2}{3} + \frac{\mu}{3}$, we would have

$$\zeta_p \leq \frac{p}{3} - \frac{\mu}{3}(p-3),$$

which means (3.28) places the scaling of β-model as an upper-bound of the possible scaling.

It should be noted that all the above results are obtained by balancing powers of ν, hence the arguments are valid only in the limit of $\nu \to 0$. For finite Reynolds number turbulence, (3.28) would not hold as is.

By a rigorous analysis in [63], notations in being the same as those of [63]. As seen above, we have $\|\nabla \boldsymbol{u}\|_\infty \propto Re^{(1+3a)/2}$ for $r_* \propto \nu^a$. It follows that $\langle \kappa_{n,1}^2 \rangle \leq c_n L^{-2} Re^{\frac{3}{2}(a+1)}$, where $Re \propto 1/\nu$. Then we have (in the limit that small constant $\delta = 0$)

$$\begin{aligned} \langle \kappa_n^2 \rangle &\leq Re^{\frac{3}{2}(a+1)\frac{n-1}{n}} Re^{\frac{1}{n}} \\ &= Re^{\frac{3}{2}(a+1) - \frac{3a+1}{2n}}, \end{aligned}$$

in place of (78) and (79) of [63]. Using Lemma 1 of [63], we find

$$L^{2n} \langle \kappa_n^2 \rangle^n \leq c_n Re^{\frac{3}{2}(a+1)n - \frac{3a+1}{2}},$$

or

$$L \langle \kappa_n \rangle \leq c_n Re^{\frac{3}{4}(a+1) - \frac{3a+1}{4n}}.$$

Comparing this with $Re^{\frac{1}{3-q} - \frac{1}{2n}\frac{q-1}{3-q}}$, we get

$$q \leq \frac{5+9a}{3(a+1)} = \frac{5}{3} + \frac{4a}{3(1+a)}$$

for the exponent of the energy spectrum $E(k) \propto k^{-q}$. From this we obtain

$$\zeta_2 + \lim_{p\to\infty} \frac{\zeta_p}{p} \leq 1.$$

It can also be obtained by writing (3.28)

$$1 - \zeta_2 \geq \frac{\zeta_p - 1}{p-3} \text{ for } p \geq 3$$

and passing to the limit $p \to \infty$. See also [20, 21, 79] for mathematical works on intermittency.

3.3 Numerical Experiments

3.3.1 Numerical Methods

The pseudo-spectral method was used for the evaluation of nonlinear terms and the fourth-order Runge-Kutta for time-stepping. The initial data are generated with the energy spectrum

$$E(k) = k^4 e^{-k^2}, \tag{3.29}$$

where the phases of the Fourier coefficients are randomized.

The numerical simulations have been performed for various values of Reynolds number by choosing the number of grid points N, and viscosity ν to ensure that the turbulence is developed and resolved. Results were obtained from a $N = 256$ cubic grid, with mesh size $\Delta x = 2\pi/N$ and time increment $\Delta t = 2 \times 10^{-3}$. Typically, in the case of forced simulations, we have as an estimate of accuracy $k_{\max}\eta \geq 1.5$ for $\nu = 0.005$ and $k_{\max}\eta \geq 1.1$ for $\nu = 0.0025$ throughout the time evolution. For the latter (slightly under-resolved) case a check was performed with a $N = 512$ cubic grid to ensure agreement, and hence that none of our results are numerical artifacts.

The integral $\delta(r)$ is calculated for a sequence of values of r, increasing outwards from the center point $\boldsymbol{x}_0$ of the spatial integration region. The increasing radii of integration are taken as

$$r_j = \frac{2\pi d^{j-1}}{N}, \quad \text{for } j = 1, 2, 3, ..., p, \tag{3.30}$$

to determine the power-law relationship between $\delta(r)$ and r. The fundamental period is 2π, and $d > 1$ is chosen such that the sphere at r_p covers at least 10% of the total spatial range 2π.

By monitoring the time-evolution of the energy and the enstrophy, the lower limit of the time integral t_0 is set after the turbulence reaches a statistically steady state. The time integral is taken over the range $t_0 < t < t_0 + r^2/\nu$. The quantity $\delta(r)$ was calculated for various different center points in order to determine the effect of position. These points were chosen, some at fixed $(0, 0, 0)$, $(\pi, 0, 0)$, $(0, \pi, 0)$, $(\pi, \pi, 0)$, and others at points of local (in space and time) maxima of $|\nabla \boldsymbol{u}|^2$.

Two important quantities are $E(t) = \frac{1}{2}\langle|\boldsymbol{u}|^2\rangle$ and $Q(t) = \frac{1}{2}\langle|\boldsymbol{\omega}|^2\rangle$, which denote the spatial average of kinetic energy and the enstrophy, respectively.

3.3.2 Freely-decaying case

We first study freely-decaying turbulence. In this case we take t_0 after the time corresponding to the peak enstrophy as this is the point at which turbulence begins to decay [19]. The parameter d is chosen to be 1.92.

Because the Reynolds number is not sufficiently large, the energy spectrum does not display the characteristic Kolmogorov power-law for fully-developed turbulence [6, 30] for sufficiently long time to evaluate the space-time integral accurately. This can be seen in Fig.3.2, which shows a log-log plot of the energy spectra as a function of the wavenumber for various times throughout the time range covered by the integral. Figure 3.3 shows the evolution of the enstrophy, for the two values of viscosity throughout this time interval.

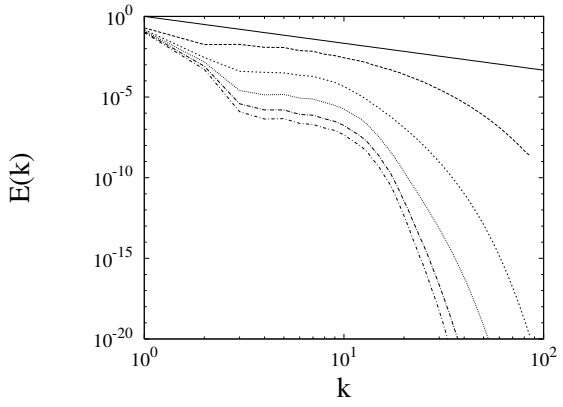

Figure 3.2: The energy spectra for the freely-decaying case with $\nu = 5 \times 10^{-3}$: the upper to lower dashed lines show spectra for $t = 10, 30, 50, 70$ and 86, respectively. The solid line represents a slope $k^{-5/3}$.

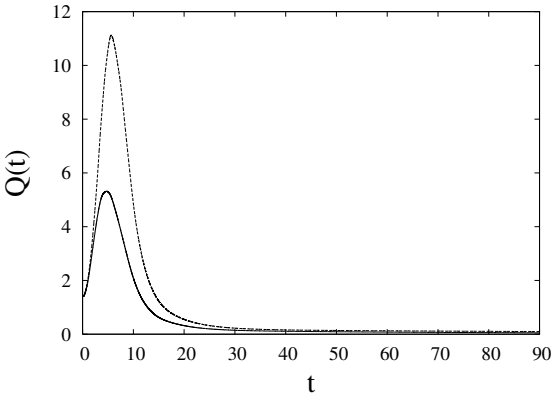

Figure 3.3: Evolution of the enstrophy for the freely-decaying case with $\nu = 5 \times 10^{-3}$ (solid) and $\nu = 2.5 \times 10^{-3}$ (dashed).

In Fig.3.4 we show local Reynolds number $\delta(r)$ against r. Due to the rapid decay of energy mentioned earlier, a clear power-law behavior is not observed. Nevertheless we do observe an r^4 behavior for small r and a shallower power-law for larger r.

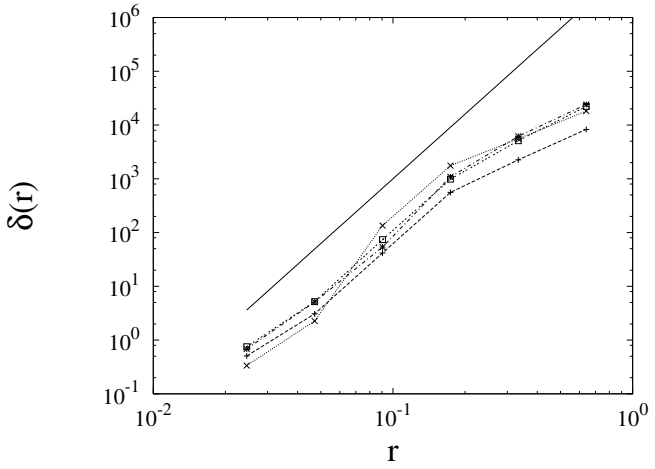

Figure 3.4: The CKN integral $\delta(r)$ against r for various center points, compared with r^4 (solid) for $\nu = 5 \times 10^{-3}$. Line conventions are $\boldsymbol{x}_0 = (0,0,0); +$, $(\pi,0,0); \times$, $(0,\pi,0); *$, $(\pi,\pi,0); \Box$.

3.3.3 Forced Turbulence

To integrate $\delta(r)$ for a sufficiently long time to ensure its convergence, we introduce a forcing term. At every time step, the vorticity components for wavenumber $|\boldsymbol{k}| = 1$, are held fixed at their initial values, effectively injecting energy back into the system and sustaining a statistically steady state of turbulence. As can be seen from Fig.3.5, the energy spectra display a power-law close to $-5/3$, corresponding to the Kolmogorov spectrum in turbulence. This persists throughout the whole time interval required for the evaluation of the space-time integral. Figure 3.6 shows the evolution of enstrophy associated with this forced computation.

At first, we see an increase up to a maximum, it then levels out into a statistically steady state, which fluctuates about an average value. Figure 3.7 is shown to verify that the dissipation rate $\epsilon(t)$ is independent of ν.

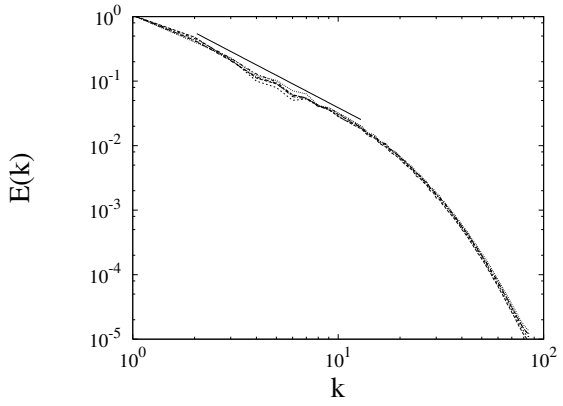

Figure 3.5: Energy spectra for the forced case: $\nu = 2.5\times10^{-3}$ compared with $k^{-5/3}$ (solid), the dashed lines show spectra for times $10, 30, 50, 70$ and 90, respectively.

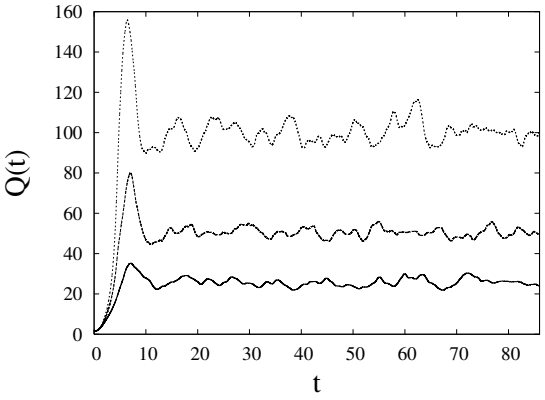

Figure 3.6: Time evolution of the enstrophy for the forced case: $\nu = 1 \times 10^{-2}$ (solid), 5×10^{-3} (dashed) and 2.5×10^{-3} (dotted).

.

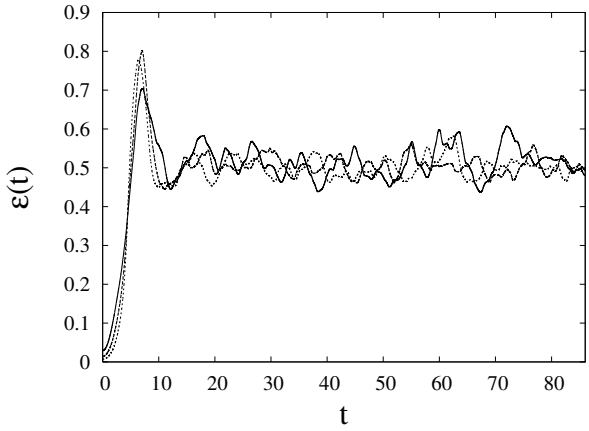

Figure 3.7: Time evolution of the energy dissipation rate for the forced case. The plot shows the independence of $\epsilon(t)$ and ν. Line convention is the same as in Fig 3.6.

We can then calculate a value for the Kolmogorov length scale based on the time average of the enstrophy in each case of viscosity, using $\eta = (\nu^3/\epsilon)^{1/4} = 1/k_d$, where $\epsilon = 2\nu\overline{Q}$ is the time-averaged energy dissipation rate. It is $\eta \approx 2.2 \times 10^{-2}$ for $\nu = 5 \times 10^{-3}$, and $\eta \approx 1.3 \times 10^{-2}$ for $\nu = 2.5 \times 10^{-3}$. The estimates of η, corresponding to the values of viscosity, are indicated by an arrow on Figs.3.8 and 3.9.

This statistically steady state produces a clearer power-law behavior. The integral was evaluated at different center points, for two different values of viscosity and $d = 1.92$. The double-log plots of $\delta(r)$ with r^4 for each viscosity are shown in Figs.3.8 and 3.9.

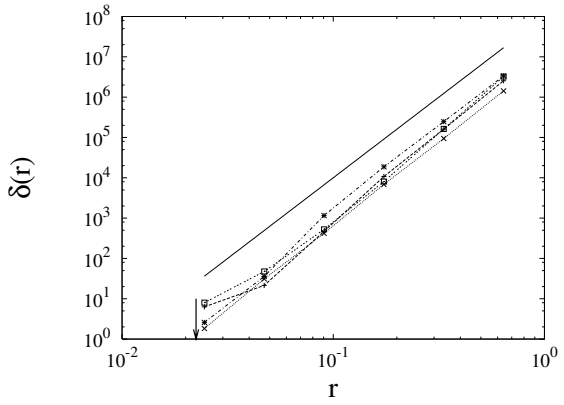

Figure 3.8: The CKN integral $\delta(r)$ vs. r for various center points, compared with r^4 (solid) for $\nu = 5 \times 10^{-3}$. Line convention is the same as in Fig.3.4. The arrow indicates the Kolmogorov length scale η.

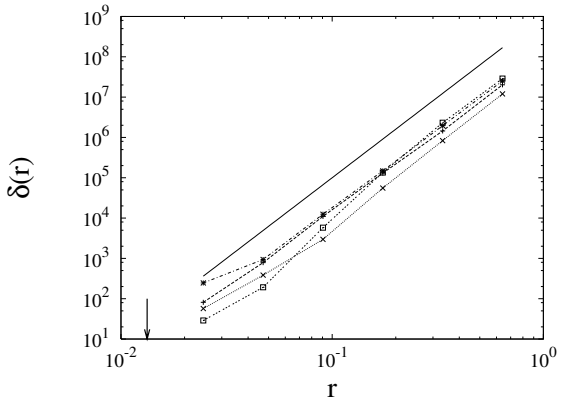

Figure 3.9: The CKN integral $\delta(r)$ vs. r for various center points, compared with r^4 (solid) for $\nu = 2.5 \times 10^{-3}$. Line convention is the same as in Fig.3.4. The arrow indicates the Kolmogorov length scale η.

At least at this moderately high Reynolds number, the function $\delta(r)$ displays a clear power-law $\delta(r) \propto r^4$ throughout the inertial subrange. As noted above this is expected only in the dissipative range.

Then why do we have $\delta(r) \propto r^4$ in the whole the inertial subrange ? To explain this, we compare in Fig.3.10, the time evolution of r_* with those of the Taylor microscale $\lambda(t) = \sqrt{10\nu E(t)/\epsilon(t)}$, and the Kolmogorov scale $\eta(t) = (\nu^3/\epsilon(t))^{1/3}$, where $\epsilon(t) = 2\nu Q(t)$. It is clear that they are very different; r_* takes a value which is a multiple of λ and it is larger than η by almost two orders-of-magnitude. It should be noted that the cross-over scale lies close to the energy-containing range. It makes a marked contrast to the exact solutions of Burgers vortex and equations, where r_* lies in the dissipative scale. (See Section IV below.)

To study its behavior more precisely, we show the time-averaged r_* for various values of ν in Fig.3.11. (The original definition $r_*/L = \overline{\left(\frac{3}{4\pi}\frac{\epsilon(t)}{\nu\|\nabla \boldsymbol{u}\|_\infty}\right)^{1/3}}$ is used for its evaluation here, but no change is observed even if we take time-average $\overline{\epsilon(t)}$ first .)

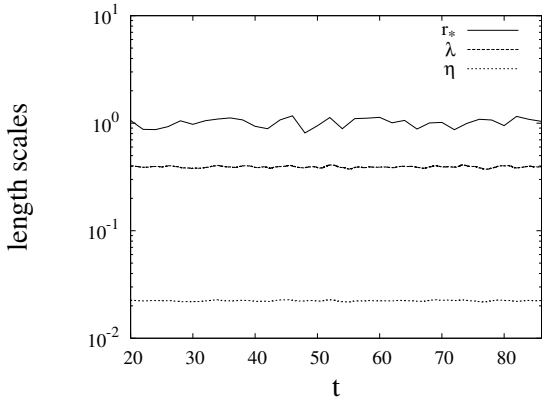

Figure 3.10: Time evolution of r_* (solid) together with that of the Taylor micro-scale $\lambda(t)$ (dashed) and the Kolmogorov length scale $\eta(t)$ (dotted) for $\nu = 0.005$.

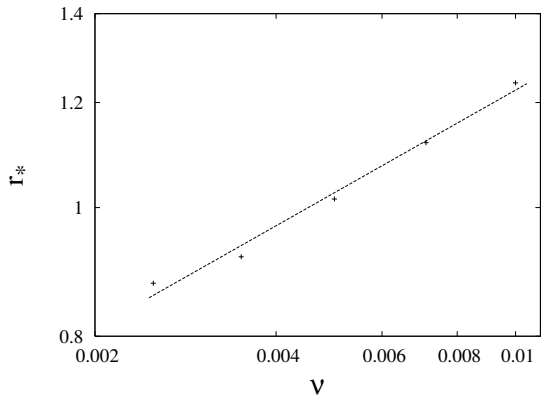

Figure 3.11: The cross-over scale r_* as a function of viscosity: $r_* \propto \nu^a$. The straight line shows a least-squares fit with $a = 0.26$.

It shows that r_* depends weakly on ν, that is, $r_* \propto \nu^a$ with $a \approx 0.26$. More importantly, $r_* = O(1)$ in the energy-containing range for all the values of ν used. This is why we do not observe a transition to $\delta(r) \propto r$ within the inertial subrange.

We have noted above that ζ_p behaves linearly at large p just like the β-model. If the β-model is perfectly correct that would imply the dissipation correlation exponent $\mu(= 3 - D)$ takes $\mu = \frac{4a}{1+a} \approx 0.8$, which is much larger than the experimentally accepted range 0.2-0.4. Indeed, we see in Fig.3.12 that the plot of dissipation correlation against distance r gives $\mu = 0.20$.

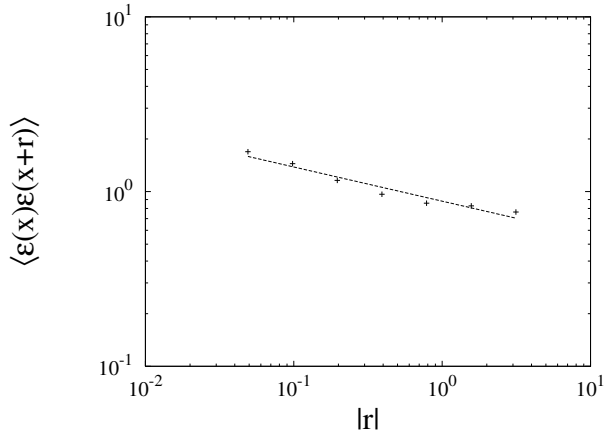

Figure 3.12: The dissipation correlation $\langle \epsilon(\boldsymbol{x})\epsilon(\boldsymbol{x}+\boldsymbol{r})\rangle \propto |\boldsymbol{r}|^{-\mu}$ with a least-squares fit $\mu = 0.20$.

This value of μ is calculated via the same data as for r_* against ν which suggests that as the value of μ lies within the accepted range, our value of a then implies that although the β model may not be quantitatively perfect, it remains valid qualitatively. For experimental works on dissipation correlation and intermittency, see [80, 81, 82] and more recent [83, 84, 85, 86, 87, 88].

3.3.4 Colliding Orthogonal Lamb Dipoles

We now investigate another initial condition of colliding orthogonal Lamb dipoles [52, 89]. It is defined as a solution of the two-dimensional Euler equations. The dipoles travel in a straight path at a constant speed, preserving their structure as they do so. If viscosity is taken into account, they start to diffuse and slow down with time. When two dipoles are set orthogonally and allowed to collide, they interact, producing areas of very high vorticity. It is these areas of the maximum velocity gradient $|\nabla \boldsymbol{u}|^2$ that we are interested in for the evaluation of $\delta(r)$.

The general form of the vorticity is given in polar coordinates, centered on the dipole, by

$$\omega = \begin{cases} -2UK\frac{J_1(Kr)}{J_0(KR)}\sin(\theta-\theta_0) & r < R, \\ 0 & r \geq R. \end{cases} \tag{3.31}$$

The radius, r is given by, for example $r = \sqrt{(x-x_0)^2+(y-y_0)^2}$, with (x_0, y_0) being the dipole's center point. Here, U denotes the travel speed of the dipole, $\theta = \theta_0$ its direction with respect to the separatrix, R its constant outer radius. The parameter K is a constant such that $KR \approx 3.8317$ gives the first positive zero of the Bessel function J_1.

We have taken $U = 0.5$, $R = \pi/4$, and $\nu = 2.5 \times 10^{-3}$. We solve the Navier-Stokes equations subject to this initial condition, until the time of maximum $|\nabla \boldsymbol{u}|^2$ is attained. One dipole is aligned parallel to the z-axis with its center along the line $(\pi, \frac{\pi}{2}, z)$ $(0 \leq z \leq 2\pi)$ and travels in the direction of increasing y. The other is aligned parallel to the x-axis with its center along the line $(x, \frac{3\pi}{2}, \pi)$ $(0 \leq x \leq 2\pi)$, traveling in the direction of decreasing y. As they approach each other they begin to deform, and then collide, interacting via reconnection to produce areas of high vorticity mentioned above. We show in Fig.3.13 the iso-surface plot of $|\nabla \boldsymbol{u}|^2$.

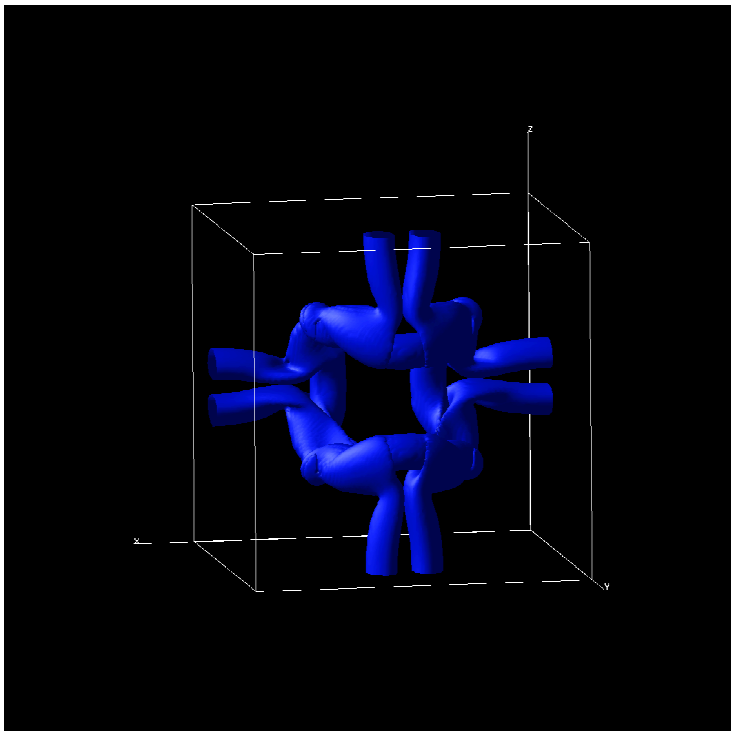

Figure 3.13: Configuration of Lamb dipoles at time of maximum $|\nabla \boldsymbol{u}|^2$, $t = 5.8$. The threshold is $|\nabla \boldsymbol{u}|^2 = 3\,\langle |\nabla \boldsymbol{u}|^2 \rangle$, where $\langle |\nabla \boldsymbol{u}|^2 \rangle = 1.58$. The dipoles have collided and reconnection is occurring at the corners, producing intense vorticity.

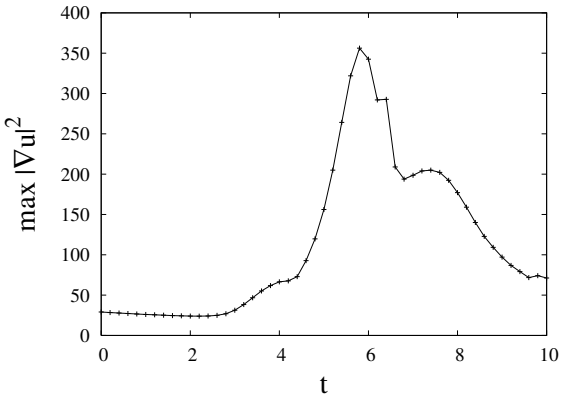

Figure 3.14: Evolution of maximum $|\nabla \boldsymbol{u}|^2$ with Lamb dipole initial conditions, $\nu = 2.5 \times 10^{-3}$.

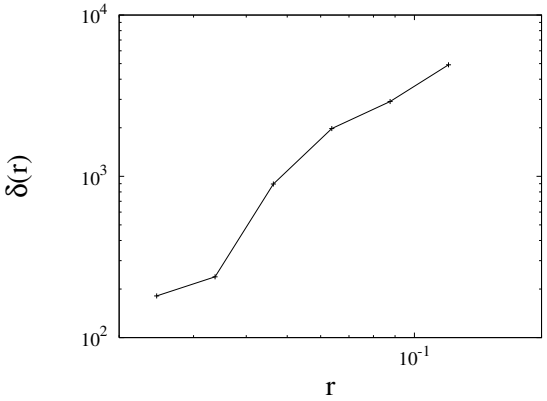

Figure 3.15: $\delta(r)$ vs. r for Lamb dipole.

For the CKN integral, we take the center point $\boldsymbol{x}_0$ at the spatial location of

maximum $|\nabla \boldsymbol{u}|^2$. We choose $d = 1.37$ so that we obtain a sufficient number of points for $\delta(r)$ as we integrate over the time range, taken from $t = 0$ to the time of maximum $|\nabla \boldsymbol{u}|^2$, which can be seen in Fig.3.14. In the situation of moving dipoles, the maximum point does not remain fixed in space for long periods of time. We observe in Fig.3.15 a generic tendency that the exponent of $\delta(r)$ becomes shallower for larger r, in agreement with the above theory.

3.4 Examples by exact solutions

3.4.1 Burgers Vortex

We consider the Burgers vortex, an exact solution of the Navier-Stokes equations subject to a constant straining flow. The velocity for the Burgers vortex tube in cylindrical polar coordinates is given by

$$\begin{cases} u_r = -\alpha r, \\ u_\theta = \frac{\Gamma}{2\pi r}\left(1 - e^{-\frac{\alpha r^2}{2\nu}}\right), \\ u_z = 2\alpha z, \end{cases} \tag{3.32}$$

and the vorticity by

$$\omega = \frac{\alpha\Gamma}{2\pi\nu}\exp\left(-\frac{\alpha r^2}{2\nu}\right).$$

Here, the constant α denotes rate of strain and Γ velocity circulation. It can be shown that

$$|\nabla \boldsymbol{u}|^2 = 6\alpha^2 + \left(\frac{\partial u_\theta}{\partial r}\right)^2 + \left(\frac{u_\theta}{r}\right)^2, \tag{3.33}$$

see e.g. [43]. The definition of $\delta(r)$ is similar to the one in previous section. In this case, the integral to be calculated is

$$\delta(r) = \frac{1}{\nu}\int_{Q_r^{2D}} |\nabla \boldsymbol{u}|^2 \, d\boldsymbol{x}\, dt. \tag{3.34}$$

The bounds of Q_r^{2D} are given by the disc $|\boldsymbol{x} - \boldsymbol{x}_0| < r$ and $|t - t_0| < r^2/\nu$, where $\boldsymbol{x} = (x, y)$. Because this is a steady state solution, the time integral simplifies to a multiplication by r^2/ν [19], we have

$$\delta(r) = \frac{r^2}{\nu^2}\int_{V_r^{2D}} |\nabla \boldsymbol{u}|^2 \, d\boldsymbol{x}, \tag{3.35}$$

where V_r^{2D} denotes a disc of radius r. Noting that as $r \to 0$,

$$\frac{1}{|V_r^{2D}|}\int_{V_r^{2D}} |\nabla \boldsymbol{u}|^2 \, d\boldsymbol{x} \to |\nabla \boldsymbol{u}|^2(\boldsymbol{x}_0),$$

with $|V_r^{2D}| = \pi r^2$, we have

$$\delta(r) \to \begin{cases} \dfrac{\pi r^4}{\nu^2}|\nabla \boldsymbol{u}|^2(\boldsymbol{x}_0) & \text{as } r \to 0, \\ \\ \dfrac{r^2}{\nu^2}\int_{\mathbb{R}^2} |\nabla \boldsymbol{u}|^2 d\boldsymbol{x} & \text{as } r \to \infty. \end{cases} \tag{3.36}$$

The cross-over takes place at $r = r_*$, where

$$\frac{r^4}{\nu^2}|\nabla \boldsymbol{u}|^2(\boldsymbol{x}_0) \approx \frac{r^2}{\nu^2}\int_{\mathbb{R}^2} |\nabla \boldsymbol{u}|^2 d\boldsymbol{x},$$

or,

$$r_* = \left(\frac{\int_{\mathbb{R}^2} |\nabla \boldsymbol{u}|^2 d\boldsymbol{x}}{|\nabla \boldsymbol{u}|^2(\boldsymbol{x}_0)}\right)^{1/2}.$$

Using $|\nabla \boldsymbol{u}|^2 \approx \omega^2 = \left(\frac{\alpha\Gamma}{2\pi\nu}\right)^2$ and $\epsilon = \nu\int_{\mathbb{R}^2} |\nabla \boldsymbol{u}|^2 d\boldsymbol{x} \approx \frac{\alpha\Gamma^2}{4\pi}$, we find

$$r_* \approx \left(\frac{\pi\nu}{\alpha}\right)^{1/2}.$$

This is proportional to the core radius of the Burgers vortex.

We can confirm this result by using the exact solution. In the limit of large Reynolds number, $r/\nu \gg 1$, we may neglect the first term on the right hand side of (3.33). The spatial part of the integral becomes

$$\frac{1}{\nu}\int_0^r |\nabla \boldsymbol{u}|^2 \, 2\pi r \, dr \simeq \frac{2\pi}{\alpha}\left(\frac{\alpha\Gamma}{4\pi\nu}\right)^2 \int_0^{\frac{\alpha r^2}{2\nu}} \left[\left(2e^{-\xi} - \frac{1-e^{-\xi}}{\xi}\right)^2 + \left(\frac{1-e^{-\xi}}{\xi}\right)^2\right] d\xi, \tag{3.37}$$

where $\xi = \alpha r^2/2\nu$ [43]. It follows that

$$\int_0^r |\nabla \boldsymbol{u}|^2 \, 2\pi r \, dr \to \begin{cases} r^2|\nabla \boldsymbol{u}|^2 & \text{for } r \ll \sqrt{\nu/\alpha}, \\ \int_{\mathbb{R}^2} |\nabla \boldsymbol{u}|^2 d\boldsymbol{x} & \text{for } r \gg \sqrt{\nu/\alpha}. \end{cases} \tag{3.38}$$

This confirms the transition at $r \approx \sqrt{\nu/\alpha}$ and we have as $r \to 0$

$$\delta(r) \propto \frac{1}{\pi}\left(\frac{\Gamma}{\nu}\right)^2 \xi^2,$$

which is consistent with the above $\delta(r) \propto r^4$. We note that in this case r_* lies in the dissipation range. Unlike Navier-Stokes turbulence, a typical multi-scale phenomenon, this example has a single scale.

3.4.2 Burgers equation

As another example, we consider the Burgers equation

$$\frac{\partial u}{\partial t} + u\frac{\partial u}{\partial x} = \nu \frac{\partial^2 u}{\partial x^2}. \tag{3.39}$$

As a comparison, we compute $\delta(r)$, which in one dimension is given by;

$$\delta(r) = \frac{r}{\nu}\int_{Q_r^{1D}} \left(\frac{\partial u}{\partial x}\right)^2 dx\, dt, \quad Q_r^{1D}(x,t) = \left\{(x,t):\ |x-x_0| < r,\ t_{\max} - \frac{r^2}{\nu} < t < t_{\max}\right\}. \tag{3.40}$$

The power-law can be worked out by a simple analysis for

$$\delta(r) = \frac{r^3}{\nu^2}\int_{Q_r^{1D}} \left(\frac{\partial u}{\partial x}\right)^2 dx. \tag{3.41}$$

In the limit $r \to 0$ the integral scales as $\propto r(\partial u/\partial x)^2$, and we have

$$\delta(r) \propto \begin{cases} 2\dfrac{r^4}{\nu^2}\left(\dfrac{\partial u}{\partial x}\right)^2 & \text{as} \quad r \to 0, \\ \dfrac{r^3}{\nu^2}\displaystyle\int_{-\infty}^{\infty}\left(\dfrac{\partial u}{\partial x}\right)^2 dx & \text{as} \quad r \to \infty \end{cases} \tag{3.42}$$

The cross-over occurs at

$$r_* = \frac{\displaystyle\int_{-\infty}^{\infty}\left(\frac{\partial u}{\partial x}\right)^2 dx}{2\sup_x\left(\dfrac{\partial u}{\partial x}\right)^2}.$$

An exact steadily traveling wave solution can be written as

$$u = U\tanh\frac{Ux}{2\nu},$$

after a translation. For this solution, we have $\frac{\partial u}{\partial x} = \frac{U^2}{2\nu}\mathrm{sech}^2\frac{Ux}{2\nu}$ and $\int_{-\infty}^{\infty}\left(\frac{\partial u}{\partial x}\right)^2 dx = \frac{2U^3}{3\nu}$, thus we find

$$r_* = \frac{4}{3U}\nu.$$

The cross-over scale is on the order of the width of the shock wave. Again, r_* is in the dissipative range unlike for the Navier-Stokes flows.

We can confirm this by the exact solution. It gives in this case

$$\delta(r) = 4\xi^3\left(\tanh\xi - \frac{1}{3}\tanh^3\xi\right),$$

where $\xi = \frac{Ur}{2\nu}$. It follows that

$$\delta(r) \approx 4\xi^4 \text{ as } \xi \to 0,$$

in agreement with the above analysis.

Finally, a pseudo-spectral calculation is performed in a way analogous to that of the three-dimensional integral, starting from initial data $u_0 = \sin x$, with $x_0 = \pi$ located at the position of shock wave formation for the velocity field. The upper limit $t_{\max}$ (≈ 1.6) is the time of maximum enstrophy, which can be seen in Fig.3.16. We integrate from $t_{\max}$ back in time over successively larger increments as r increases spatially outwards from x_0, with the lower time limit $t = 1$. The radii of integration r_j are given as in (3.30), with the number of grid points N and viscosity ν chosen to ensure that the flow is well-resolved. In this case we have used $N = 4096$, $\nu = 2 \times 10^{-3}$ and $\Delta t = 1 \times 10^{-4}$.

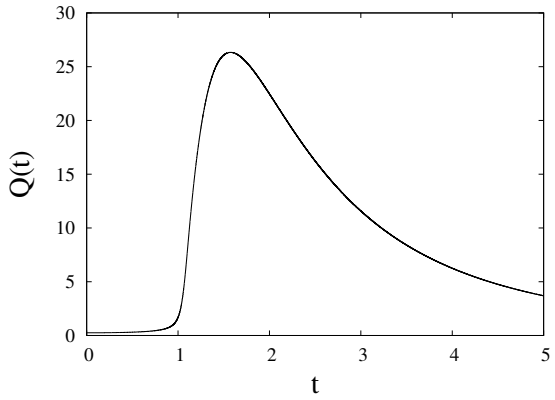

Figure 3.16: Enstrophy evolution for the 1D Burgers equation with viscosity $\nu = 2 \times 10^{-3}$, maximum is at $t = 1.57$.

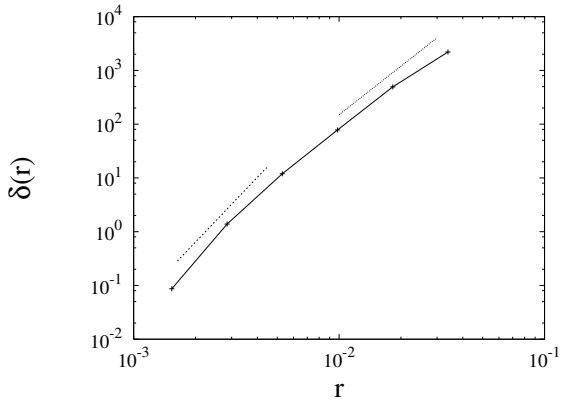

Figure 3.17: $\delta(r)$ vs. r for center point $x_0 = \pi$ (solid), compared with r^4 (dashed) and r^3 (dotted), for viscosity $\nu = 2 \times 10^{-3}$.

We can see in Fig.3.17 that the scaling is close to r^4 for small r. As r increases, it becomes closer to a shallower r^3, consistent with the above argument.

3.5 Summary and discussion

Intermittency in turbulence is related with the mathematical problem of the Navier-Stokes equations in that it is associated with rapid growth of local vorticity. By

using the CKN local Reynolds number, we have developed a systematic method of characterization of intermittency.

First, we have re-examined the CKN integral and identified a cross-over scale r_*, at which the scaling behavior of $\delta(r)$ changes. On this basis, we have introduced the parameter a characterizing intermittency as $r_* \propto \nu^a$. As a by-product we have derived the constraint $\lim_{p\to\infty} \frac{\zeta_p}{p} = 1-\zeta_2$ for the scaling exponents ζ_p of the velocity structure functions in the limit $\nu \to 0$. This in turn implies that $\zeta_p = (1-\zeta_2)p+o(p)$.

Second, we have performed direct numerical simulations of the Navier-Stokes equations at moderately high Reynolds numbers (≈ 100) to examine the behavior of the CKN integral $\delta(r)$. We have found a scaling $\delta(r) \propto r^4$ in the whole inertial range, not only in the dissipative range. We explain the absence of cross-over phenomenon by finding r_* is actually in the energy-containing range. The intermittency parameter a is found to be 0.26. If the β-model is perfectly correct, $a = 0.26$ would imply $\mu = 0.8$ for the dissipation correlation exponent, which is beyond the acceptable range of $0.2 - 0.4$ within which our experimentally determined value lies. We point out that while the β-model may not be quantitatively perfect, its prediction serves as an upper-bound for the scaling exponents. Similar cross-over phenomena have been studied on the basis of exact solutions of the Burgers vortex and the Burgers equation.

All the results obtained here are based on the framework of phenomenology, but we have double-checked their consistency against rigorous mathematical theory, where possible e.g. [63, 72]. It would be interesting to make the present theory solid, say, by applying Besov-space techniques [22, 90, 91]. This will be left for future study.

Chapter 4

Burgers equation with a passive scalar: Dissipation anomaly and Colombeau calculus

Abstract

A connection between dissipation anomaly in fluid dynamics and Colombeau's theory of products of distributions is exemplified by considering Burgers equation with a passive scalar. Besides the well-known viscosity-independent dissipation of energy in the steadily propagating shock wave solution, the lesser known case of passive scalar subject to the shock wave is studied. An exact dependence of the dissipation rate ϵ_θ of the passive scalar on the Prandtl number P_r is given by a simple analysis: we show in particular $\epsilon_\theta \propto 1/\sqrt{P_r}$ for large P_r. The passive scalar profile is shown to have a form of a sum of $\tanh^{2n+1} x$ with suitably scaled x, thereby implying the necessity to distinguish H from H^n when P_r is large, where H is the Heaviside function and n is a positive integer. An incorrect result of $\epsilon_\theta \propto 1/P_r$ would otherwise be obtained. This is a typical example where Colombeau calculus for products of weak solutions is required for a correct interpretation. A Cole-Hopf-like transform is also given for the case of unit Prandtl number.

4.1 Introduction

One of the most important properties of fully-developed turbulence is that the dissipation rate ϵ of the total kinetic energy remains non-zero even in the limit of vanishing viscosity: $\epsilon \to \text{const} \neq 0$, see e.g. [4]. It is called anomaly because in the case of totally inviscid fluid $\nu \equiv 0$, $\epsilon \equiv 0$. This empirical observation is called "dissipation anomaly" and is believed to form the basis for turbulence theory. In the case of the 3D Navier-Stokes equations this is just a conjecture and no mathematical proof is available to support it.

Here we consider a much simpler model of fluid equation to study a similar phenomenon. More precisely we consider the Burgers equation [92, 93] together with a passive scalar:

$$\frac{\partial u}{\partial t} + u\frac{\partial u}{\partial x} = \nu\frac{\partial^2 u}{\partial x^2}, \tag{4.1}$$

$$\frac{\partial \theta}{\partial t} + u\frac{\partial \theta}{\partial x} = \kappa\frac{\partial^2 \theta}{\partial x^2}, \tag{4.2}$$

where u denotes the velocity field, θ the passive scalar field, ν the kinematic viscosity and κ the diffusivity. As boundary conditions, we consider constant values of velocity and scalar at infinity (see below). We note that Burgers equation with a passive scalar has been considered in [94] in connection with its non-Gaussian statistics.

In Section II, we study steadily propagating waves in u and θ and study whether the dissipation rate ϵ_θ of θ is independent of ν or of κ. In Section III we derive an expression ϵ_θ in terms of the Prandtl number $P_r = \nu/\kappa$ and investigate its dependency on P_r. In Section IV, we determine the profile for θ and note that Colombeau calculus for the product of distributions [9, 10, 11] is required to interpret the result. We also discuss a generalization of the so-called Cole-Hopf transform [95, 96, 97] to the case of the passive scalar in Section V. Section VI is devoted to a Summary.

4.2 Steady-State Solutions in a Moving Frame

We consider (4.1) under the boundary conditions $u(x = \pm\infty) = \mp u_1$. If we seek a solution steady in a frame moving with a constant speed U we find using a change of variables $X = x - Ut,\ T = t$ [98];

$$u = U - u_1 \tanh\frac{u_1}{2\nu}(x - Ut + c), \tag{4.3}$$

where c is a constant of integration. The dissipation rate of total kinetic energy

$$\epsilon = \nu \int_{-\infty}^{\infty} \left(\frac{\partial u}{\partial x}\right)^2 dx,$$

is given by

$$\epsilon = \frac{u_1^3}{2} \int_{-\infty}^{\infty} \frac{d\xi}{\cosh^4 \xi},$$

where $\xi = \frac{u_1}{2\nu}(x - Ut + c)$. Because this (convergent) integral no longer involves viscosity, we see that ϵ is independent of ν in the limit $\nu \to 0$ without evaluating the definite integral (actually, $= 4/3$).

Now we consider θ. From (4.2), the steady-state should satisfy

$$(u - U)\frac{d\theta}{dX} = \kappa \frac{d^2\theta}{dX^2}. \tag{4.4}$$

Using (4.3), it follows from (4.4) that

$$\frac{d\theta}{dX} = c' \left[\cosh \frac{u_1}{2\nu}(X + c)\right]^{-2\frac{\nu}{\kappa}}. \tag{4.5}$$

Hence we find that

$$\theta = c_1 \int_0^{\xi} \frac{d\eta}{\cosh^{2P_r} \eta} + c_2, \tag{4.6}$$

where $c_1 = 2\nu c'/u_1$ and c_2 are constants of integration. Under the boundary condition $\theta(x = \pm\infty) - U = \mp\theta_1$ we may fix the constants as $c_1 = -\frac{\theta_1}{I_\alpha(\infty)}$ and $c_2 = U$. Here, for convenience. we have introduced a function $I_\alpha(\xi)$ defined by

$$I_\alpha(\xi) \equiv \int_0^{\xi} \frac{d\eta}{\cosh^{2\alpha} \eta}.$$

4.3 Dissipation Rate of a passive scalar

By (4.5), the dissipation rate of passive scalar variance ϵ_θ is evaluated as follows:

$$\begin{aligned}
\epsilon_\theta &= \kappa \int_{-\infty}^{\infty} \left(\frac{\partial \theta}{\partial x}\right)^2 dx \\
&= \kappa \tilde{c'}^2 \int_{-\infty}^{\infty} \left[\cosh \frac{u_1}{2\nu}(X + c)\right]^{-4P_r} dX \\
&= \kappa \frac{(u_1\theta_1)^2}{4\nu^2 I_{P_r}(\infty)^2} \frac{2\nu}{u_1} \int_{-\infty}^{\infty} \cosh^{-4P_r}(\xi) d\xi,
\end{aligned}$$

thus we find

$$\epsilon_\theta = u_1 \theta_1^2 \frac{1}{P_r} \frac{I_{2P_r}(\infty)}{I_{P_r}(\infty)^2}. \tag{4.7}$$

Because the integral $I_{P_r}(\infty)$ depends on ν and κ through P_r, we must evaluate it in full.

For integer-numbered P_r, say $= n$ we may explicitly carry out the integration in $I_{P_r}(\xi)$. The first two ($n = 1, 2$) are

$$\int_0^\xi \frac{d\eta}{\cosh^2\eta} = \tanh\xi, \quad \int_0^\xi \frac{d\eta}{\cosh^4\eta} = \tanh\xi - \frac{1}{3}\tanh^3\xi.$$

More generally, noting that:

$$\frac{1}{\cosh^{2n}\xi} = \frac{1}{\cosh^2\xi}(1-\tanh^2\xi)^{n-1} = \frac{1}{\cosh^2\xi}\sum_{r=0}^{n-1}(-1)^r\binom{n-1}{r}\tanh^{2r}\xi \qquad (4.8)$$

we find

$$I_n(\xi) = \int_0^\xi \frac{d\eta}{\cosh^{2n}\eta} = \sum_{r=0}^{n-1}(-1)^r\binom{n-1}{r}\frac{\tanh^{2r+1}\xi}{2r+1}$$

and

$$I_n(\infty) = \sum_{r=0}^{n-1}(-1)^r\binom{n-1}{r}\frac{1}{2r+1}.$$

Actually we have [99]

$$I_n(\infty) = \frac{2^{2(n-1)}\{(n-1)!\}^2}{(2n-1)!}.$$

For $P_r = n$ we obtain an exact expression

$$\epsilon_\theta = u_1\theta_1^2\frac{\{(2n)!\}^4}{(4n)!(n!)^4}.$$

(For more general real-valued $P_r = \alpha$, we have $I_\alpha(\infty) = \frac{\sqrt{\pi}}{2}\frac{\Gamma(\alpha)}{\Gamma(\frac{1}{2}+\alpha)}$ and thus $\epsilon_\theta = u_1\theta_1^2\frac{2}{\sqrt{\pi}}\frac{\Gamma(2\alpha)\Gamma(\frac{1}{2}+\alpha)^2}{\alpha\Gamma(\alpha)^2\Gamma(\frac{1}{2}+2\alpha)}$, where $\Gamma(\alpha)$ is the gamma function.)

By Stirling's formula $n! \simeq \sqrt{2\pi n}n^n e^{-n}$ for $n \gg 1$, we deduce that

$$I_{n+1}(\infty) \simeq \frac{1}{2}\sqrt{\frac{\pi}{n}}.$$

Therefore the dissipation rate of θ in the limit of large P_r is

$$\epsilon_\theta \simeq u_1\theta_1^2\sqrt{\frac{2}{\pi P_r}}, \text{ as } P_r \to \infty, \qquad (4.9)$$

which decays as $P_r^{-\frac{1}{2}}$ with P_r. Even in this simple 1D model, the problem of dissipation anomaly is subtle, in that ϵ_θ does depend on P_r in a nontrivial fashion.

On the other hand, it can be checked that

$$\lim_{P_r \to 0} \frac{1}{P_r} \frac{I_{2P_r}(\infty)}{I_{P_r}(\infty)^2} = 1$$

so

$$\epsilon_\theta \to u_1 \theta_1^2, \quad \text{as} \quad P_r \to 0.$$

In the cases $P_r \ll 1$ or $P_r = O(1)$, ϵ_θ remain finite. Thus, there is anomaly in the dissipation ϵ_θ of the passive scalar because it remains non-zero in the limit of $\nu \to 0$, when we take $P_r = \text{const}$ or $P_r \ll 1$.

4.4 Connection to Colombeau calculus

In the case of $\nu \to 0$, care should be taken in the interpretation. Indeed, in the expression

$$\theta(\xi) = -\frac{\theta_1}{I_n(\infty)} \sum_{r=0}^{n-1} (-1)^r \binom{n-1}{r} \frac{\tanh^{2r+1} \xi}{2r+1} + U, \tag{4.10}$$

formally $\tanh \xi \to 2H(\xi) - 1$ as $\nu \to 0$, where H is the Heaviside function, but this does not necessarily mean that $\tanh^{2r+1} \xi \to 2H(\xi) - 1$ for $r(> 0)$.

Colombeau theory has been developed to account for multiplication of distributions to some extent [9, 10, 11], by generalizing Schwartz theory of distributions. For details, see [12, 100, 101]. Later its connection to non-standard analysis has been pointed out [102]. We note that this theory has been applied to the Burgers equation, e.g. [10, 103, 104] but not to the problem with a passive scalar.

A notable feature of Colombeau theory is that it can handle not only H, but also H^n $(n \neq 1)$. In this sense the problem in question is a typical example to which Colombeau theory applies. If we naively identify $\tanh^{2r+1} \xi$ with $\tanh \xi$ in the limit of vanishing viscosity $\nu \to 0$, we would get $I_n(\xi) \approx I_n(\infty) \tanh \xi$, or

$$\theta(\xi) \approx -\theta_1 \tanh \xi + U.$$

It follows that

$$\epsilon_\theta \approx \frac{1}{P_r} u_1 \theta_1^2 \int_0^\infty \frac{d\xi}{\cosh^4 \xi} = u_1 \theta_1^2 \frac{2}{3P_r}, \tag{4.11}$$

or $\epsilon_\theta \propto 1/P_r$ rather than the correct asymptotic dependence $\epsilon_\theta \propto 1/\sqrt{P_r}$. Therefore the above naive identification would lead to a completely wrong dependence on P_r.

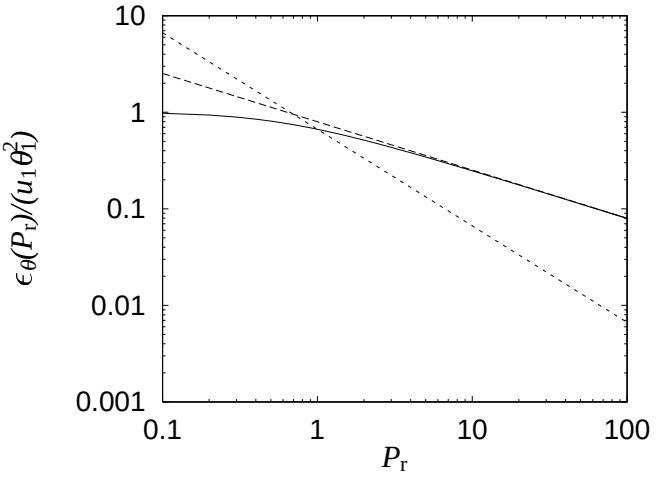

Figure 4.1: Non-dimensionalized dissipation rate of the passive scalar $\frac{\epsilon_\theta(P_r)}{u_1\theta_1^2}$ as a function of P_r (solid line) and the large-P_r asymptotics $\sqrt{\frac{2}{\pi P_r}}$ (dashed line). The dotted line shows the *incorrect* behavior $\frac{2}{3P_r}$ obtained by discarding the subtle differences among $\tanh^n \xi$.

In Fig. 4.1 we plot the dependency of ϵ_θ on P_r as given by (4.7). (For numerical purposes it is convenient to write $I_\alpha(\infty) = \int_0^1 (1-\tau^2)^{\alpha-1}\, d\tau$.) It shows how quickly ϵ_θ asymptotes to (4.9) and that how poor a job the naive (4.11) does.

The above results on dissipation anomaly suggests that Colombeau calculus is required for a correct description of the present problem. In order to check this view we see how jump conditions [10] come out of Colombeau calculus. Below the symbol $\sim$ denotes *association* which is a weaker relationship than equality (=).

Case 1.

We start from

$$u_t + uu_x \sim 0,\ \theta_t + u\theta_x \sim 0,$$

$$u(x,t) = \Delta u H(x - Ut) + U + u_1,$$

$$\theta(x,t) = \Delta\theta K(x - Ut) + U + \theta_1,$$

where $\Delta u = u(\infty) - u(-\infty) = -2u_1$ and $\Delta\theta = \theta(\infty) - \theta(-\infty) = -2\theta_1$. Here H and K are Heaviside step functions. Recall that H and K may not be equal to each other, as Colombeau's theory can handle different Heaviside functions. From the first condition we have

$$-U\Delta u\, H' + (\Delta u)^2 HH' + (U + u_1)\Delta u H' \sim 0.$$

Since $HH' \sim \frac{1}{2}H'$, we obtain

$$\frac{1}{2}\Delta u + u_1 = 0.$$

We have from the second relation

$$-UK' + \Delta u H K' + (U + u_1)K' \sim 0.$$

Because $K' \sim \delta$, the above shows that $HK' \sim A\delta$ with some function $A = A(\Delta u, \Delta\theta, u_1, U)$, we have

$$A\Delta u + u_1 = 0.$$

From these we can fix $A = 1/2$, consistently.

Case 2.

On the other hand, if we start from imposing a more stringent condition on θ, that is,

$$u_t + uu_x \sim 0,\ \theta_t + u\theta_x = 0,$$

we have from the second equation

$$(\Delta u H + u_1)K' = 0$$

or

$$(1 - 2H)K' = 0.$$

This is satisfied if we define $H(0) = 1/2$. See [105, 106] for similar analyses.

Case 3.

$$u_t + uu_x = 0,\ \theta_t + u\theta_x = 0$$

The first of the equations was shown to lead to a contradiction [10].

4.5 Generalization of the Cole-Hopf Transform

In this section we consider a flow with finite total kinetic energy. For the Burgers equation (4.1) it is well known that the Cole-Hopf transform [95, 96, 97]:

$$u(x,t) = -2\nu\frac{\partial}{\partial x}\log\psi = -2\nu\frac{\psi_x}{\psi}$$

linearizes (4.1) to the diffusion equation

$$\frac{\partial\psi}{\partial t} = \nu\frac{\partial^2\psi}{\partial x^2}.$$

For some historical backgrounds on the Cole-Hopf transform, see e.g. [107, 108, 44].

The equation (4.2) for a passive scalar is already linear, but it is of interest to seek a similar transform which expresses its solution in a closed form.

We assume

$$\frac{\partial \phi}{\partial t} = \kappa \frac{\partial^2 \phi}{\partial x^2}, \tag{4.12}$$

and attempt to find a solution in the quotient form

$$\theta = \frac{\phi}{\psi}.$$

Then we find that

$$\phi_t = (\theta\psi)_t = 2\nu\psi_x\theta_x + \kappa\psi\theta_{xx} + \nu\theta\psi_{xx}.$$

Because $\phi_{xx} = \theta_{xx}\psi + 2\theta_x\psi_x + \theta\psi_{xx}$ and

$$\theta_{xx} = \frac{\phi_{xx}\psi - \phi\psi_{xx}}{\psi^2} - 2\frac{\phi_x\psi - \phi\psi_x}{\psi^3}\psi_x,$$

we obtain

$$\phi_t = \kappa\phi_{xx} + (\nu - \kappa)\left[2\frac{\psi_x\phi_x}{\psi} + \left(\frac{\psi_{xx}}{\psi} - 2\frac{\psi_x^2}{\psi^2}\right)\phi\right].$$

Therefore when $\nu = \kappa$ (i.e. $P_r = 1$) we may reduce the equation for the passive scalar to a heat diffusion equation (4.12). Note that u and θ, (or equivalently ψ and ϕ), can be chosen independently. In particular, for the special case $u = \theta$ we have $\phi = -2\nu\psi_x$ and recover the original Cole-Hopf transform.

In the general case $P_r \neq 1$, it is not known whether we may reduce (4.2) to a diffusion equation although it is known that (4.2) is regular for all time. To search for such a transformation left for future study. That might help in clarifying whether there is anomaly in passive scalar dissipation for the case of finite total energy and passive scalar variance.

4.6 Summary and Discussion

In this chapter we treat a steadily propagating solution of a passive scalar subject to Burgers equation. We have two results on this model.

First, there is anomaly in the dissipation of the passive scalar. In spite of its simplicity (after all, what we have solved is an ODE by a quadrature), it manifests a nontrivial behavior in its dissipation rate. Second, a lesson to be learned here is

that if we do not distinguish $\tanh^n \xi$ for different n, we would obtain a wrong answer for the dissipation rate. This suggests that Colombeau calculus plays an important role even for this simple example.

It may be in order to recall that in the case of 2D Navier-Stokes equations, the dissipation rate η of enstrophy is estimated from above [109] as $\eta \propto (\log Re)^{-1/2}$, where Re is the Reynolds number. In the large-Re limit, η decays to zero, but does so very slowly (as a transcendental function). In contrast, the decay of ϵ_θ with Prandtl number is much more rapid.

Dissipation anomaly is a subtle problem; a special care is required even in this linear, 1D model problem, let alone possible dissipation anomaly in the 3D Navier-Stokes equations for which we have only experimental or numerical evidence.

Chapter 5

Summary and Conclusions

The principal drive behind this work was the three-dimensional Navier-Stokes regularity problem. We have investigated the behavior of some of the quantities which must be bounded in order to guarantee global regularity. Building on the foundations of work carried out by others, most prominently for this thesis, Caffarelli, Kohn and Nirenberg, we have investigated the issue of regularity both numerically and analytically, formulating our own phenomenological theories and evaluating others already established.

In the second chapter, we carried out a comparison of the decaying Navier-Stokes and Burgers equations in three dimensions, beginning from identical initial conditions and subject to the same viscosity. Because the Burgers eqution are known to exhibit global regularity due to the maximum principle, this comparison charts the effect of nonlocality and incompressibility. By employing the Helmholtz-Hodge decomposition, we can split the Burgers equations up into incompressible (solenoidal) and compressible (potential) components.

We saw from the plots of energy and enstrophy that the incompressible term quickly becomes subserviant while the compressible term dominates, attaining a much higher peak enstrophy. The two terms become comparable at later times as the energy and enstrophy decay away. The Burgers equations clearly also attain a much larger peak value of enstrophy than the Navier-Stokes equations. Comparison of the fourier energy spectra reveals that the Burgers equations retain more excitations at higher wavenumbers. These observations all suggest that the Burgers equations, though known to be globally regular, behave far more singularly than the Navier-Stokes equations. We know, however, that the maximum principle bounds

the Burgers equations for all time. This seems to suggest that the Navier-Stokes equations should be globally regular (as is widely assumed in physical applications), albeit with sporadic intermittent events, despite the lack of mathematical verification.

Examination of the velocity PDFs confirmed the maximum principle in that higher amplitude excitations are prohibited for the Burgers equations, in contrast to those of the Navier-Stokes equations, which spread out, becoming increasingly Gaussian with time.

The maximum principle was originally attained by forming the local energy equation from the Burgers equation and bounding the rate of energy increase (see Introduction for sketch of proof). If the same procedure is attempted for the Navier-Stokes equations, we hit a road block in the form of the nonlocal pressure gradient term $-(\boldsymbol{u}\cdot\nabla)p$. This term precludes the possibility of bounding the rate of energy increase as it can be impartially positive or negative. Upon inspection of its PDF and joint PDFs with both energy and enstrophy, we see that they are basically symmetrical, with temporally rare random fluctuations which seem to have no correlation with either energy or enstrophy density. Our conclusion, therefore, was that the term $-(\boldsymbol{u}\cdot\nabla)p$ neither encourages nor stifles formation of singularity, it just invalidates the maximum principle.

To examine how this maximum principle breaks down, we investigated the three-dimensional Navier-Stokes equations with passive scalar θ initialized identical to the first component of velocity u_1, with $\kappa = \nu$. These are known as the quasi-4D (or 3.5D) Navier-Stokes equations. By studying the subesquent deviation of $(u_1 - \theta)^2$, we observed that the maximum of its spatial average occured between those of peak enstrophy and peak spatial average of squared passive scalar gradient. From an iso-surface visualisation of $(u_1 - \theta)^2$ with enstrophy, we saw a strong spatial and temporal correlation indicating that the maximum principle breaks down when the enstrophy becomes large (near-singular structure approached).

The performance of the established bounds for enstrophy growth (see introduction for derivation) were then evaluated. The method involves using a log-log plot after the application of the Cauchy-Schwartz and Gagliardo-Nirenberg inequalities to the enstrophy growth equation. This method was tested against numerical data for the 1D and 3D Burgers equations and the 3D and quasi-4D Navier-Stokes equations. It was found that for the 1D Burgers equation the exponent was 1, implying

that the bound is very accurate, almost an *equality*. For the 3D case, with exponent 0.7, the bounds over-estimate the situation slightly, but the discrepancy is not huge. In the case of 3D and quasi-4D Navier-Stokes equations, the exponent was observed as 0.4, revealing that the bounds greatly over-estimate the physical situation. Our conclusion was therefore that the bounds are less accurate in higher dimensions and for incompressible systems.

A possible reason for the same exponent in the 3D and quasi-4D Navier-Stokes equations may be due to the quasi-4D case being characteristically 3D, we would expect from our conclusion that in the case of genuine 4D Navier-Stokes equations, the bounds would be less accurate, with exponent < 0.7. Future work employing this analysis to the genuine 4D Navier-Stokes equations, under a range of different initial conditions would further clarify this hypothesis.

These results were also confirmed with other random, and also Taylor-Green initial data, suggesting that this is a non-specific law and may hold more generally. Further studies with a wide range of distinctly different initial conditions would be an excellent test of the universality of these exponents.

More intensive research into the breakdown of maximum principle (preferably at higher spatial resolutions) would help to illuminate a possible path to a solution of the Navier-Stokes regularity problem.

In the third chapter we estimated the local reynolds number $\delta(r)$ from CKN theory using numerical simulations of the forced Navier-Stokes equations in 3D at moderately high Reynolds numbers ($Re \approx 100$). We examined the dependence on the distance from the center point over a parabolic cylinder. The exponent r^4 were predicted earlier in the chapter and confirmed by the numerical results. The unexpected revelation, however, was that a positive exponent continues throughout the inertial subrange.

By CKN theory, a point is regular if near that point $\delta(r) \leq \epsilon_{CKN}$. This corresponds to a scaling of r^α where $\alpha > 0$ as $r \to 0$. Our results therefore imply that the flow is far from singularity at these points, some of which were chosen at points of local maximum $|\nabla \boldsymbol{u}|^2$. The analogous calculation for 1D Burgers equation also confirmed this theory, with an exponent of r^4 for small r, which decreases to r^3, becoming less regular as r increases.

The case of colliding orthogonal Lamb dipoles provided the opportunity to in-

vestigate $\delta(r)$ in regions of high vorticity. In this case a lower, but still positive, exponent r^1 is observed. From CKN theory this indicates that these points are less regular.

To quantify the transition between different exponents which is seen in the relationships between $\delta(r)$ and r, we introduced a cross-over scale $r_* \propto L \left(\frac{\overline{\|\nabla \boldsymbol{u}\|^2_{L^2}}}{\overline{\|\nabla \boldsymbol{u}\|^2_{L^\infty}}} \right)^{1/3}$, where $\|\nabla \boldsymbol{u}\|^2_{L^2} = \frac{1}{L^3} \int |\nabla \boldsymbol{u}|^2 \, d\boldsymbol{x}$, at which the CKN Reynolds number $\delta(r)$ changes its scaling behavior

$$\delta(r) \approx \begin{cases} \dfrac{4\pi}{3} \dfrac{r^4}{\nu^2} |\nabla \boldsymbol{u}|^2 (\boldsymbol{x}_0, t_0), & \text{as } r \to 0 \\ \dfrac{r}{\nu^2} \overline{\int_{\mathbb{R}^3} |\nabla \boldsymbol{u}|^2 \, d\boldsymbol{x}} & \text{as } r \to \infty. \end{cases}$$

where the bar denotes time-average.

This scale was then evaluated for the particular cases mentioned above. In addition, the exact solution of Burgers vortex in 2D verifies theories in a purely analytical way.

A method of quantitatively testing the β-model was then implemented. The analysis suggests that while the β-model may not be perfect, its qualitative prediction survives, irrespective of the validity of the underlying assumption of a fractal energy cascade.

On the basis of the mathematically well-established CKN local Reynolds number, the cross-over scale r_* offers a practical method of estimating and quantifying intermittency.

The use of larger numerical grids would enable better resolution of small scale, high Reynolds number events, resulting in greater accuracy. This in turn would facilitate the evaluation of CKN quantities at less regular locations, and yield scaling exponents for these interesting phenomena.

In the fourth chapter we considered the steady-state case of the 1D Burgers equation with associated passive scalar. For the passive scalar, we observe a dissipation anomaly, that is the average dissipation rate does not vanish as the Reynolds number approaches infinity. Instead it exhibits a pronounced dependence on the Prandtl number $P_r = \nu/\kappa$. Due to the nature of the problem, we were obliged to employ Colombeau calculus in order to obtain the correct dissipation rate. This rate ($\epsilon_\theta \propto 1/\sqrt{P_r}$) decays much faster with increasing P_r than the dissipation rate of enstrophy for the 2D Navier-Stokes equations ($\eta \propto 1/\sqrt{\log Re}$) in the limit of large

Re (small ν).

In the case of the 3D Navier-Stokes equations, the only information available on this topic is that of experimental or numerical data. Further analytical work on this problem may shed light on this subtle characteristic.

For the most part of this work, we were limited by spatial resolution and the associated time constraints to 256^3 numerical grids. Higher resolution numerical analysis of the regularity issues of the 3D Navier-Stokes equations discussed here (and elsewhere) would improve the level of knowledge greatly and allow us to delve into yet finer, more extreme structures within the flow field, with a view to finally establish whether these enigmatic equations do in fact admit singularities, or remain regular for all space and time.

Appendices

A: Cauchy formula for the Burgers equations

In the incompressible 3D Euler equations, vortex lines are material. In the 3D Burgers equations, vortex lines are still material but the first integrals should be modified. It is straightforward, but in view of the comparison of these two equations, it is best to state it here.

The vorticity equations read

$$\frac{\partial \boldsymbol{\omega}}{\partial t} + (\boldsymbol{u}\cdot\nabla)\boldsymbol{\omega} = (\boldsymbol{\omega}\cdot\nabla)\boldsymbol{u} - (\nabla\cdot\boldsymbol{u})\boldsymbol{\omega}. \tag{1}$$

Introducing a new variable

$$\tilde{\boldsymbol{\omega}}(\boldsymbol{a},t) = \boldsymbol{\omega}(\boldsymbol{a},t)\exp\left(\int_0^t (\nabla\cdot\boldsymbol{u})(\boldsymbol{a},t)dt'\right), \tag{2}$$

it satisfies

$$\frac{\partial \tilde{\boldsymbol{\omega}}}{\partial t} + (\boldsymbol{u}\cdot\nabla)\tilde{\boldsymbol{\omega}} = (\tilde{\boldsymbol{\omega}}\cdot\nabla)\boldsymbol{u}. \tag{3}$$

It follows from this

$$\tilde{\boldsymbol{\omega}}(\boldsymbol{a},t) = \tilde{\boldsymbol{\omega}}(\boldsymbol{a},0)\cdot\frac{\partial}{\partial \boldsymbol{a}}\boldsymbol{x}(\boldsymbol{a},t), \tag{4}$$

a generalized Cauchy formula. Because $\tilde{\boldsymbol{\omega}}$-lines are frozen, so are $\boldsymbol{\omega}$-lines. Noting that the Jacobian $J_{ij} = \frac{\partial x_i}{\partial a_j},\ (i,j=1,2,3)$ satisfies

$$\frac{D\boldsymbol{J}}{Dt} = \boldsymbol{V}\boldsymbol{J},\ \boldsymbol{V} = \nabla\boldsymbol{u}, \tag{5}$$

where $\boldsymbol{x} = a$ at $t = 0$. By Abel's formula

$$\frac{D}{Dt}\det\boldsymbol{J} = (\det\boldsymbol{J})\mathrm{tr}\left(\frac{D\boldsymbol{J}}{Dt}\boldsymbol{J}^{-1}\right), \tag{6}$$

we may write

$$\boldsymbol{\omega}(\boldsymbol{a},t) = \frac{\boldsymbol{J}(\boldsymbol{a},t)\cdot\boldsymbol{\omega}(\boldsymbol{a},0)}{|\det\boldsymbol{J}(\boldsymbol{a},t)|} \tag{7}$$

or, equivalently

$$\boldsymbol{\omega}(\boldsymbol{a},t) = \frac{\boldsymbol{\omega}(\boldsymbol{a},0)\cdot\frac{\partial}{\partial\boldsymbol{a}}\boldsymbol{x}(\boldsymbol{a},t)}{\left|\det\left(\frac{\partial\boldsymbol{x}}{\partial\boldsymbol{a}}\right)\right|}. \tag{8}$$

B: Burgers gauge

We have seen that even if we take a general velocity field which has both solenoidal and potential parts, under the dynamics of the Burgers equations the potential part dominates quickly. We may ask whether and how we can find a field whose solenoidal part solves the Navier-Stokes equations whilst the potential part solves the Burgers equations. This is readily done by choosing an appropriate gauge in the so-called impulse formalism [110].

$$\frac{\partial \boldsymbol{\gamma}}{\partial t} = \boldsymbol{u} \times \boldsymbol{\omega} + \nabla \Lambda + \nu \triangle \boldsymbol{\gamma}, \tag{9}$$

$$\frac{\partial \phi}{\partial t} = p + \frac{|\boldsymbol{u}|^2}{2} + \Lambda + \nu \triangle \phi. \tag{10}$$

where the two scalar fields are related by $\lambda = \Lambda + \boldsymbol{u} \cdot \boldsymbol{\gamma}$. If we choose these as follows, "Burgers gauge",

$$\Lambda = -p - \frac{|\boldsymbol{u}|^2 + |\nabla \phi|^2}{2}, \tag{11}$$

the potential part of $\boldsymbol{\gamma}$ solves the Burgers and the solenoidal part the Navier-Stokes equations.

C: Burgers equation with higher Reynolds number

As an illustration, we present energy spectra of the 3D Burgers equations at a spatial resolution of 256^3 with viscosity $\nu = 2.5 \times 10^{-3}$, for various instants of time.

The 3D Burgers spectra suffer from some truncation errors at high wavenumbers, as can be seen in Fig.1, nevertheless, this plot shows clearly that the Burgers equations (for which global regularity is well known) display far more singular behavior than the Navier-Stokes equations (for which global regularity is not known), whose energy spectra quickly decay to zero. Although this is not a mathematical proof, it gives us some insight into the question of regularity, suggesting that, given the contrast in behavior of the two systems, we would expect the Navier-Stokes equations to be globally regular.

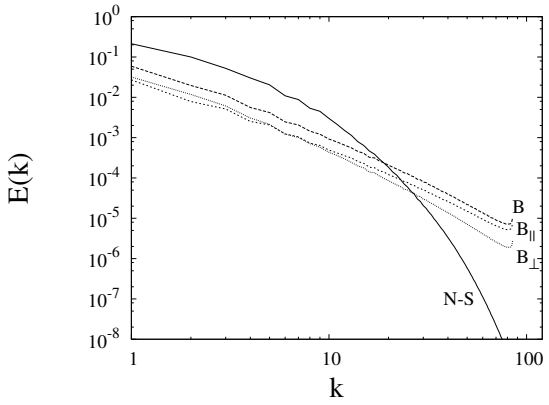

Figure 1: Energy spectra $E(k)$ of the Navier-Stokes equations at $t = 5$ (solid), with corresponding $E(k)$ (dashed), $E(k)^{\perp}$ (short-dashed) and $E(k)^{\parallel}$ (dotted) for the Burgers equations at the same time, all with viscosity $\nu = 2.5 \times 10^{-3}$. Symbols have the same meaning as in Fig.1.

D: Another initial condition for 1D Burgers equation

We test the bound (2.34) using another initial condition

$$u(x, 0) = -\sin x - \sin 2x. \tag{12}$$

As can be seen in Fig.2 Some deviation from (2.34) is noticeable at large amplitudes, while an overall scaling with $\alpha = 1$ works as an upper-bound.

E: Log-Poisson model

The Log-Poisson model has

$$\zeta_p = \frac{p}{9} + 2\left(1 - \left(\frac{2}{3}\right)^{p/3}\right)$$

for the scaling exponents. It follows that

$$\alpha = \lim_{p\to\infty} \frac{\zeta_p}{p} = 1/9 \approx 0.111,$$

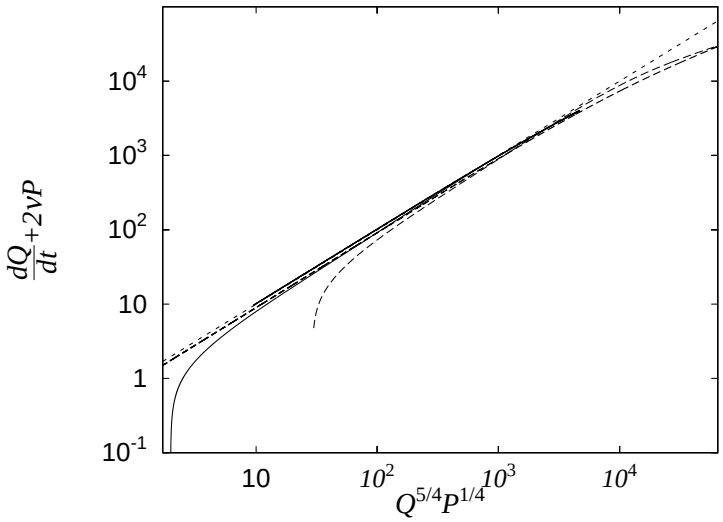

Figure 2: Enstrophy growth for the 1D Burgers equation, the initial conditions (12)(solid) and (2.33)(dashed). The dotted straight line denotes the bound (2.34).

and

$$1-\zeta_2 = 2\left(\frac{2}{3}\right)^{\frac{2}{3}} - \frac{11}{9} \approx 0.304 \neq \lim_{p\to\infty}\frac{\zeta_p}{p}.$$

This model is thus not consistent with the fundamental constraint (3.26).

Equivalently, in terms of $E(k) \propto k^{-q}$, $a = \frac{1-3\alpha}{3(1+\alpha)} = 1/5$ implies $q = \frac{5+9a}{3(1+a)} = \frac{17}{9} \approx 1.888$, whereas actually it has $\zeta_2 + 1 = \frac{29}{9} - 2\left(\frac{2}{3}\right)^{2/3} \approx 1.6959$.

Bibliography

[1] K. Ohkitani and M. Dowker, "Numerical study on comparison of Navier-Stokes and Burgers equations," Phys. Fluids **24**, 055113-1(2012).

[2] M. Dowker and K. Ohkitani "Intermittency and local Reynolds number in Navier-Stokes turbulence: a cross-over scale in the Caffarelli-Kohn-Nirenberg integral," preprint (2012).

[3] K. Ohkitani and M. Dowker, "Burgers equation with a passive scalar: Dissipation anomaly and Colombeau calculus," J. Math. Phys. **51**, 033101-1(2010).

[4] U. Frisch, *Turbulence: the legacy of AN Kolmogorov,* (Cambridge University Press, Cambridge, 1995).

[5] S.B. Pope, *Turbulent Flows,* (Cambridge University Press, New York, 2000).

[6] H. A. Rose and P. L. Sulem, "Fully developed turbulence and statistical mechanics," J. Phys. (Paris) **39**, 441(1978).

[7] U. Frisch, P.L. Sulem and M. Nelkin, "A simple dynamical model of intermittent fully developed turbulence," J. Fluid. Mech. **87**, 719(1978).

[8] P.L. Sulem and U. Frisch, "Bounds on energy flux for finite energy turbulence," J. Fluid Mech. **72**, 417(1975).

[9] J.F. Colombeau and A.Y. Le Roux, "The elastoplastic shock problem as an example of the resolution of ambiguities in the multiplication of distributions," J. Math. Phys. **30**, 2273(1989).

[10] J.F. Colombeau, "Multiplications of distributions in elasticity and hydrodynamics," J. Math. Phys. **29**, 315(1988).

[11] J.F. Colombeau, A.Y. Le Roux, A. Noussair and B Perrot, "Microscopic profiles of shock waves and ambiguities in multiplications of distributions," SIAM J. Numer. Anal. **26**, 871(1989).

[12] J.F. Colombeau, "Multiplication of distributions," Bull. Amer. Math. Soc. **23**, 251(1990).

[13] A.A. Kiselev and O.A. Ladyzhenskaya, "On existence and uniqueness of the solutions of the nonstationary problem for a viscous incompressible fluid," Izv. Akad. Nauk SSSR, Ser. Mat. **21**, 655(1957), [Am. Math. Soc. Transl. **24**, 79(1957)].

[14] J. Leray, "Essai sur le mouvement d'un liquide visqueux emplissant l'espace," Acta Math. **63**, 193 (1934). English translation: `http://www.math.cornell.edu/~bterrell/leray.html`.

[15] C.L. Fefferman, *The Millennium Prize Problems* (American Mathematical Society, Providence, RI, 2006), pp. 57-70.

[16] E. Hopf, "On the initial value problem for the basic equations of hydrodynamics," Math. Nachr. **4**, 213 (1951). English translation: `http://www.dam.brown.edu/people/menon/am224/hopf-NS.pdf`.

[17] V. Scheffer, "Hausdorff measure and the Navier-Stokes equations," Commun. Math. Phys. **55**, 97 (1977).

[18] L. Caffarelli, R. Kohn, and L. Nirenberg., "Partial regularity of suitable weak solutions of the Navier-Stokes equations," Commun. Pur. Appl. Math. **35**, 771 (1982).

[19] G. Gallavotti, "Some rigorous results about 3D Navier-Stokes," Text of two lectures delivered at NATO-ASI meeting "Turbulence in spatially ordered systems", Les Houches, 1992.

[20] J.D. Gibbon and C.R. Doering, "Intermittency in solutions of the three-dimensional Navier-Stokes equations," J. Fluid Mech. **478**, 227(2003).

[21] J.D. Gibbon and C.R. Doering, "Intermittency and regularity issues in 3D Navier-Stokes turbulence," Arch. Rational Mech. Anal. **177**, 115(2005).

[22] A. Cheskidov and R. Shvydkoy, "Euler equations and turbulence: analytical approach to intermittency," Arxiv preprint arXiv:1202.1460.

[23] C.R. Doering, "The 3D Navier-Stokes problem," Annu. Rev. Fluid Mech. **41**, 109(2009).

[24] J.D. Gibbon, "Regularity and singularity in solutions of the three-dimensional Navier-Stokes equations," Proc. R. Soc. London, Ser. A **466**, 2587(2010).

[25] C.R. Doering and J.D. Gibbon, *Applied Analysis of the Navier-Stokes Equations,* (Cambridge University Press, Cambridge, 1995).

[26] P. Constantin, *Navier-Stokes equations,* (University of Chicago Press, Chicago, 1988).

[27] C. Foias, O. Manley, R. Rosa and R. Temam *Navier-Stokes Equations and Turbulence,* (Cambridge University Press, Cambridge, 2001).

[28] G. Gallavotti, *Foundations of Fluid Dynamics* (Springer, Berlin, 2002).

[29] M. Arnold and W. Craig, "On the size of the Navier-Stokes singular set," Discrete Contin. Dyn. Syst. **28**, 3(2010).

[30] A. Biryuk and W. Craig, "Bounds on Kolmogorov spectra for the Navier-Stokes equations," Phys. D. **241**, 426(2011).

[31] T.Y. Hou and Z. Lei, "On the partial regularity of a 3D model of the Navier-Stokes equations," Commun. Math. Phys. Differ. Equ. **287**, 2(2009).

[32] S.I. Chernyshenko, P. Constantin, J.C. Robinson and E.S. Titi, "A posteriori regularity of the three-dimensional Navier-Stokes equations from numerical computations," J. Math. Phys. **48**, 6(2007).

[33] A. Pumir and E.D. Siggia, "Incipient singularities in the Navier-Stokes equations," Phys. Rev. Lett. **55**, 1749(1985).

[34] A. Pumir and E.D. Siggia, "Vortex dynamics and the existence of solutions to the Navier-Stokes equations," Phys. Fluids. **30**, 5(1987).

[35] A. Pumir and E.D. Siggia, "Finite-time singularities in the axisymmetric three-dimension Euler equations," Phys. Rev. Lett. **68**, 10(1992).

[36] K.R. Sreenivasan and C. Meneveau, "Singularities of the equations of fluid motion," Phys. Rev. A. **38**, 6287 (1988).

[37] G. Rosen, "Navier-Stokes initial value problem for boundary-free incompressible fluid flow," Phys. Fluids **12**, 2891(1970).

[38] J.G. Heywood, "Remarks on the possible global regularity of solutions of the three-dimensional Navier-Stokes equations," Pitman Res. Notes Math. Ser. **308**, 1(1994).

[39] C. Bardos, "Euler equation and burger equation - Relation with turbulence," in *Nonlinear Partial Differential Equations and Applications,* Lecture Notes in Mathematics Vol. 648 (Springer Verlag, Berlin, 1978).

[40] C. Bardos, "Equations de Navier-Stokes et modéle de la turbulence," J. Phys. (Paris), Colloq. **39**, C5-53(1978).

[41] C.V. Tran and D.G. Dritschel, "Energy dissipation and resolution of steep gradients in one-dimensional Burgers flows," Phys. Fluids **22**, 037102(2010).

[42] D. Ayala and B. Protas, "On maximum enstrophy growth in a hydrodynamics system," Physica D **240**, 1553(2011).

[43] K. Ohkitani, "A miscellany of basic issues on incompressible fluid equations," Nonlinearity. **21**, 1 (2008).

[44] F. Gesztesy and H. Holden, "The Cole-Hopf and Miura transformations revisited" in *Mathematical Physics and Stochastic Analysis: Essays in Honour of Ludwig Streit*, edited by S. Albeverio, P. Blanchard, L. Ferreira, T. Hida, Y. Kondratiev and R. Vilela Mendes (World Scientific, Singapore, 2000).

[45] T. Watanabe and T. Gotoh, "Statistics of a passive scalar in homogeneous turbulence," New J. Phys. **6**, 40(2004).

[46] Consider an equation which is *linear* in θ; $\frac{\partial \theta}{\partial t} + (\boldsymbol{u} \cdot \nabla)\theta = \nu \triangle \theta + f(\boldsymbol{x}, t)$ with a "forcing" $f(\boldsymbol{x}, t) = -\frac{\partial p}{\partial x}$, where $\boldsymbol{u}(\boldsymbol{x}, t)$ and $p(\boldsymbol{x}, t)$ are taken from the Naver-Stokes solutions. By a uniqueness argument, if $\theta = u_1$ at $t = 0$, then $\theta = u_1$ for all $t > 0$ as long as $\boldsymbol{u}$ remains smooth. If we drop "forcing" we obtain (2.19).

[47] B.B. Mandlebrot, "On the geometry of homogeneous turbulence, with stress on the fractal dimension of the iso-surfaces of scalars," J. Fluid Mech. **72**, 2(1975).

[48] L. Lu and C.R. Doering, "Limits on enstrophy growth for solutions of the three-dimensional Navier-Stokes equations," Indiana Univ. Math. J. **57**, 6(2008).

[49] P.E. Hamlington, J. Schumacher and W.J.A. Dahm, "Local and nonlocal strain rate fields and vorticity alignment in turbulent flows," Phys. Rev. E. **77**, 11(2008).

[50] P.E. Hamlington, J. Schumacher and W.J.A. Dahm, "Direct assessment of vorticity alignment with local and nonlocal strain rates in turbulent flows," Phys. Fluids. **20**, 111703(2008).

[51] J. Schumacher, B. Eckhardt and C.R. Doering, "Extreme vorticity growth in Navier-Stokes turbulence," Phys. Lett. A **374**, 861(2010).

[52] P. Orlandi and S.P. Sergio, "Vorticity dynamics in turbulence growth," Theor. Comput. Fluid Dyn. **24**, 247(2010).

[53] R.J. DiPerna and A.J. Majda, "Oscillations and concentrations in weak solutions of the incompressible fluid equations," Commun. Math. Phys. **108**, 667(1987).

[54] T. Gotoh, Y. Watanabe, Y. Shiga, T. Nakano, E. Suzuki, "Statistical properties of four-dimensional turbulence," Phys. Rev. E **75**, 016310(2007).

[55] E Suzuki, T. Nakano, N. Takahashi and T. Gotoh, "Energy transfer and intermittency in four-dimensional turbulence," Phys. Fluids **17**, 081702(2005).

[56] H. Dong and D. Du, "Partial regularity of solutions to the four-dimensional Navier-Stokes equations at the first blow-up time," Commun. Math. Phys.**273**, 785(2007).

[57] T. Miyazaki, W. Kubo, Y. Shiga, T. Nakano and T. Gotoh, "Classical and quantum turbulence," Physica D **239**, 14(2010).

[58] V. Scheffer, "The Navier-Stokes equations in space dimension four," Commun. Math. Phys. **61**, 41(1978).

[59] C. Gerhardt, "Stationary solutions to the Navier-Stokes equations in dimension four," Math. Z. **165**, 193(1979).

[60] H. Kim, "Existence and regularity of very weak solutions of the stationary Navier-Stokes equations," Arch. Ration. Mech. Anal. **193**, 117(2009).

[61] H. Liu, E. Tadmor and D. Wei, "Global regularity of the 4D restricted euler equations," Phys. D **239**, 1225(2010).

[62] The reason for this is that at $d = 4$ the Gagliardo-Nirenberg inequality

$$\int |\boldsymbol{\omega}|^4 d\boldsymbol{x} \leq c \left(\int |\nabla \times \boldsymbol{\omega}|^2 d\boldsymbol{x} \right)^{d/2} \left(\int |\boldsymbol{\omega}|^2 d\boldsymbol{x} \right)^{2(1-d/4)}$$

reduces to the Sobolev lemma. Hence no application of the Hölder inequality is possible, because P would get an exponent 1.

[63] C.R. Doering and J.D. Gibbon, "Bounds on moments of the energy spectrum for weak solutions of the three-dimensional Navier-Stokes equations," Physica D **165**, 163(2002).

[64] P. Constantin, E. Weinan and E.S. Titi, "Onsager's conjecture on the energy conservation for solutions of Euler's equation," Commun. Math. Phys. **165**, 207(1994).

[65] G.L. Eyink, "Energy dissipation without viscosity in ideal hydrodynamics I. Fourier analysis and local energy transfer," Physica D **78**, 222(1994).

[66] E. Kim, H. Liu and J. Anderson, "Intermittency and self-organization in turbulent flows," Phys. Scripta **142** 014053 (2010).

[67] T. Y. Hou, Z. Lei and C. Li, "Global regularity of the 3D axi-symmetric Navier-Stokes equations with anisotropic data," Commun. Part. Diff. Eq.**33**, 1622 (2008).

[68] T. Y. Hou, C. Li, Z. Shi, S. Wang and X. Yu. "On singularity formation of a nonlinear nonlocal system," Arch. Rational Mech. Anal. **199**, 117 (2011).

[69] J.C. Robinson, and W. Sadowski, "Decay of weak solutions and the singular set of the three-dimensional Navier-Stokes equations," Nonlinearity **20**, 1185(2007).

[70] I. Kukavica, "The fractal dimension of the singular set for solutions of the Navier-Stokes system," Nonlinearity **22**, 2889(2009).

[71] W.D. Henshaw, H.O. Kreiss and L.G Reyna, "Smallest scale estimates for the Navier-Stokes equations for incompressible fluids," Arch. Rat. Mech. Anal. **112**, 21 (1990).

[72] W.D. Henshaw, L.G Reyna and H.O. Kreiss, "On the smallest scale for the incompressible Navier-Stokes equations," Theor. Comput. Fluid Dyn. **1**, 65 (1989).

[73] G. Paladin and G. Vulpiani, "Degrees of freedom of turbulence," Phys. Rev. A **35**, 1971(1987).

[74] D. Ruelle, "Large volume limit of the distribution of characteristic exponents in turbulence," Commun. Math. Phys. **87**, 287(1982).

[75] Z.S. She and E. Leveque, "Universal scaling laws in fully developed turbulence," Phys. Rev. Lett. **72**, 336(1994).

[76] In the phenomenology, the spatial scale is taken in the longitudinal, say, in x-direction. By definition, we have $\lim_{r\to 0}\frac{\delta u(r)}{r} = \frac{\partial u}{\partial x}$, where the mathematical limit $r \to 0$ physically means $r \to r_{\min}$ in developed turbulence.

[77] If $\alpha = 0$, that would imply $\|\nabla \boldsymbol{u}\|_{L^\infty} = \infty$, which contradicts with the regularity of the Navier-Stokes flows. If $\alpha = \infty$, that would imply $\|\nabla \boldsymbol{u}\|_{L^\infty} = 0$, which is also absurd. The other possibility, α is indeterminate, is at variance with the assumption 2).

[78] B. Lashermes, P. Abry and P. Chainais, "New Insights into the estimation of scaling exponents," Int. J. of Wavelets, Multiresolution and Information Processing, **2**, 497(2004).

[79] J.D. Gibbon, "A hierarchy of length scales for weak solutions of the three-dimensional Navier-Stokes equations," to appear in Comm. Math. Sci.

[80] K.R. Sreenivasan, "An update on the energy dissipation rate in isotropic turbulence," Phys. Fluids **10**, 528(1998).

[81] K.R. Sreenivasan and P. Kailasnath, "An update on the intermittency exponent in turbulence," Phys. Fluids A **5**, 512(1993).

[82] I. Hosokawa and K. Yamamoto, "Intermittency of dissipation in a directly simulated fully-developed turbulence," Phys. Fluids A **59**, 401(1989).

[83] D.A. Donzis, K.R. Sreenivasan and P.K. Yeung, "Some results on the Reynolds number scaling of pressure statistics in isotropic turbulence," J. Phys. Soc. Jpn. **241**, 164(2012).

[84] D.A. Donzis, P.K. Yeung and K.R. Sreenivasan, "Dissipation and enstrophy in isotropic turbulence: Resolution effects and scaling in direct numerical simulations," Phys. Fluids **20**, 045108(2008).

[85] D.A. Donzis and K.R. Sreenivasan, "Short-term forecasts and scaling of intense events in turbulence," J. Fluid Mech. **647**, 13(2010).

[86] P.K. Yeung, D.A. Donzis and K.R. Sreenivasan, "Dissipation, enstrophy and pressure statistics in turbulence simulations at high Reynolds numbers," J. Fluid Mech. to appear (2012).

[87] R.M. Kerr, M. Meneguzzi and T. Gotoh, "An inertial range crossover in structure functions," Phys. of Fluids **13**, 1985(2001).

[88] S. Almalkie and S.M. de Bruyn Kops, "Energy dissipation rate surrogates in incompressible Navier-Stokes turbulence," J. Fluid Mech. **697**, 204(2012).

[89] P. Orlandi and G. F. Carnevale, "Nonlinear amplification of vorticity in inviscid interaction of orthogonal lamb dipoles," Phys. Fluids. **19**, 1 (2007).

[90] A. Cheskidov and R. Shvydkoy, "A unified approach to regularity problems for the 3D Navier-Stokes and Euler equations: the use of Kolmogorov's dissipation range," Arxiv preprint arXiv:1102.1944.

[91] A Cheskidov, S. Friedlander and R. Shvydkoy, "A continuous model for turbulent energy cascade," Arxiv preprint arXiv:1112.5376.

[92] J.M. Burgers, "Mathematical examples illustrating relations occurring in the theory of turbulent motion," Trans. Roy. Neth. Acad. Sci. Amsterdam, Phys.-Sci.1 **17**, 1(1939).

[93] J.M. Burgers, "A mathematical model illustrating the theory of turbulence," Adv. Appl. Mech. **1**, 171(1948).

[94] B.K. Shivamoggi, "Passive Scalar Advection in Burgers Turbulence: Mapping-Closure Model," Intern. J. Theor. Phys. **43**, 2081(2004).

[95] J.D. Cole, "On a quasi-linear parabolic equation occurring in aerodynamics," Quart. Appl. Math. **9**, 225(1951).

[96] A.R. Forsyth, *Theory of Differential Equations, Part IV Partial Differential Equations (Vol. VI),* (Cambridge University Press, Cambridge, 1906).

[97] E. Hopf, "The partial differential equation $u_t + uu_x = \mu u_{xx}$," Commun. Pure Appl. Math. **3**, 201(1950).

[98] H. Bateman, "Some recent researches on the motion of fluids," Mon. Weather Rev. **43**, 167(1915).

[99] S. Moriguchi, K. Udagawa and S. Hitotsumatsu, *Sugaku Koshiki (Mathematical Foumulae) II*, (Iwanami Shoten, Tokyo, 1957).

[100] A. Gsponer, "Colombeau generalized functions in classical electrodynamics," Eur. J. Phys. **30**, 109(2009).

[101] R. Steinbauer and J.A. Vickers, "The use of generalised functions and distributions in general relativity," Class. Quantum Grav. **23**, R91(2006).

[102] R.S. Baty, F. Farassat and D.H. Tucker, "Nonstandard analysis and jump conditions for converging shock waves," J. Math. Phys. **49**, 063101-1(2008).

[103] C.O.R. Sarrico, "Distributional products and global solutions for nonconservative inviscid Burgers equation," J. Math. Anal. Appl. **281**, 641(2003).

[104] C.O.R. Sarrico, "New solutions for the one-dimensional nonconservative inviscid Burgers equation," J. Math. Anal. Appl. **317**, 496(2006).

[105] M. Oberguggenberger, "Hyperbolic systems with discontinuous coefficients: generalized solutions and a transmission problem in acoustics," J. Math, Anal. Appl. **142**, 452(1989).

[106] M. Oberguggenberger, "Case study of a nonlinear, nonconservative, nonstrictly hyperbolic system," Nonlinear Anal. Theory, Methods Appl. **19**, 53(1992).

[107] S.H. Benton, "Book Review on *Generalized solutions of Hamilton-Jacobi equations,* P.L. Lions," Bull. Amer. Math. Soc. **9**, 252(1983).

[108] A. Biryuk, "Note on the transformation that reduces the Burgers equation to the heat equation," preprint (2004), `http://www.ma.hw.ac.uk/~kuksin/students/bir.ps`

[109] C.V. Tran and D.G. Dritschel, "Vanishing enstrophy dissipation in two-dimensional Navier-Stokes turbulence in the inviscid limit," J. Fluid Mech. **559**, 107(2006).

[110] G. Russo and P. Smereka, Impulse formulation of the Euler equations: general properties and numerical methods," J. Fluid Mech. **391**, 189(1991).